arXiv:0710.5707v1 [astro-ph] 30 Oct 2007

The VSOP 5 GHz Active Galactic Nucleus Survey: V. Imaging Results for the Remaining 140 sources

R. Dodson[1,2], E. B. Fomalont[3], K. Wiik[4,1], S. Horiuchi[5,6,7,8], H. Hirabayashi[1,9], P. G. Edwards[10,1], Y. Murata[1,9], Y. Asaki[1,9], G. A. Moellenbrock[1,11], W. K. Scott[12], A. R. Taylor[12] L. I. Gurvits[13], Z. Paragi[13,14], S. Frey[15,14], Z.-Q. Shen[16,1], J. E. J. Lovell[10,1,17], S. J. Tingay[6,7,18], M. J. Rioja[2], S. Fodor[6,19], M. L. Lister[20], L. Mosoni[21,15], G. Coldwell[22], B. G. Piner[19], J. Yang[13,16]

ABSTRACT

In February 1997, the Japanese radio astronomy satellite HALCA was launched to provide the space-bourne element for the VLBI Space Observatory Programme (VSOP) mission. Approximately twenty-five percent of the mission time was dedicated to the VSOP Survey of bright compact Active Galactic Nuclei (AGN) at 5 GHz. This paper, the fifth in the series, presents images and models for the remaining 140 sources not included in Paper III, which contained 102 sources. For most sources, the plots of the (u,v) coverage, the visibility amplitude versus (u,v) distance, and the high resolution image are presented. Model fit parameters to the major radio components are determined, and the brightness temperature of the core component for each source is calculated. The brightness temperature distributions for all of the sources in the VSOP AGN survey are discussed.

Subject headings: galaxies: active — radio continuum: galaxies — surveys

---

[1] Institute of Space and Astronautical Science, Japan Aerospace Exploration Agency, 3-1-1 Yoshinodai, Sagamihara, Kanagawa 229-8510, Japan

[2] Observatorio Astronómico Nacional, Apartado 112, E-28803, Alcala de Henares, España

[3] National Radio Astronomy Observatory, 520 Edgemont Road, Charlottesville, VA 22903, USA

[4] Tuorla Observatory, University of Turku, Väisäläntie 20, FIN-21500 Piikkiö, Finland

[5] National Astronomical Observatory, 2-21-1 Osawa, Mitaka, Tokyo 181-8588, Japan

[6] Jet Propulsion Laboratory, 4800 Oak Grove Drive, Pasadena, CA 91109, USA

[7] Centre for Astrophysics and Supercomputing, Swinburne University of Technology, P.O. Box 218, Hawthorn, Vic. 3122, Australia

[8] Canberra Deep Space Communication Complex, PO Box 1035, Tuggeranong, ACT 2901, Australia

[9] Department of Space and Astronautical Science, School of Physical Sciences, The Graduate University for Advanced Studies, 3-1-1 Yoshinodai, Sagamihara, Kanagawa 229-8510, Japan

[10] Australia Telescope National Facility, Commonwealth Scientific and Industrial Research Organization, P. O. Box 76, Epping NSW 2122, Australia

[11] National Radio Astronomy Observatory, P.O. Box 0, Socorro, NM 87801, USA

[12] Physics and Astronomy Department, University of Calgary, 2500 University Dr. NW, Calgary, Alberta, Canada, T2N 1N4

[13] Joint Institute for VLBI in Europe, P.O. Box 2, 7990 AA, Dwingeloo, Netherlands

[14] MTA Research Group for Physical Geodesy and Geodynamics, P.O. Box 91, H-1521 Budapest, Hungary

[15] FÖMI Satellite Geodetic Observatory, P.O. Box 585, H-1592, Budapest, Hungary

[16] Shanghai Astronomical Observatory, Chinese Academy of Sciences, 80 Nandan Lu, Shanghai 200030, China

[17] School of Mathematics and Physics, University of Tasmania, Private Bag 21, Hobart, Australia

[18] Department of Imaging and Applied Physics, Curtin University of Technology, Perth, Australia.

[19] Physics Department, Whittier College, 13406 East Philadelphia, P.O. Box 634, Whittier, CA 90608-4413, USA

[20] Department of Physics, Purdue University, West Lafayette, IN 47907, USA

[21] MTA Konkoly Observatory, P.O. Box 67, H-1525, Budapest, Hungary

[22] Observatorio Astronómico de la Universidad Nacional

1. Introduction

The radio astronomy satellite HALCA (Highly Advanced Laboratory for Communications and Astronomy) was launched by the Institute of Space and Astronautical Science in February 1997 to participate in Very Long Baseline Interferometry (VLBI) observations with arrays of ground radio telescopes. HALCA provides the longest baselines of the VSOP, an international endeavor that has involved over 28 ground radio telescopes, five tracking stations and three correlators (Hirabayashi et al. 1998, 2000a). HALCA was placed in an orbit with an apogee height above the Earth's surface of 21,400 km, a perigee height of 560 km, and an orbital period of 6.3 hours.

During the seven years of HALCA's mission lifetime, about 75% of observing time was used for projects selected by international peer-review from open proposals submitted by the astronomical community in response to Announcements of Opportunity. This part of the mission's scientific programme constituted the General Observing Time (GOT). The remaining observing time was devoted to a mission-led survey of active galactic nuclei at 5 GHz: the VSOP Survey Program. The major goal of the Survey was to determine the statistical properties of the submilliarcsecond structure of a complete sample of AGNs. (Hirabayashi et al. 2000b; Fomalont et al. 2000a). Following the end of the formal international mission period in February 2002, the Japanese-dominated effort continued survey observations until October 2003, when HALCA lost its attitude control capability. This occurred well after the end of the original planned mission lifetime.

This paper is the fifth in the series of VSOP Survey related papers. Scott et al. (2004) (henceforth P-III) contains the results for 102 sources which were observed and reduced before 2001 October. Horiuchi et al. (2004) (henceforth P-IV) analyzed the cumulative visibilities of those sources to obtain the 'typical source structure'. This paper contains the additional 140 survey sources which were successfully observed by VSOP and completes the survey programme observing results. The brightness temperature properties of the entire sample of sources are discussed.

2. The Observations

The VSOP mission and the 5 GHz AGN Survey are fully discussed in Hirabayashi et al. (1998); Fomalont et al. (2000b); Hirabayashi et al. (2000a,b). Briefly, in order to be included in the VSOP Survey, a source was required to have:

- a total flux density at 5 GHz, $S_5 \geq 5.0$ Jy

or

- a total flux density at 5 GHz, $S_5 \geq 0.95$ Jy and
- a spectral index $\alpha \geq -0.45$ ($S \propto \nu^{\alpha}$) and
- a galactic latitude $|b| \geq 10°$.

The finding surveys from which sources were selected were primarily the Green Bank GB6 Catalog for the northern sky (Gregory et al. 1996), and the Parkes-MIT-NRAO (PMN) Survey (Lawrence et al. 1986; Griffith & Wright 1993) for the southern sky. The 402 sources satisfying these criteria comprise the VSOP source list (Hirabayashi et al. 2000b).

As this source list was compiled from single dish catalogues, some of the selected sources would not be detectable by HALCA due to insufficient correlated flux density on baselines longer than about 1000 km. Therefore, sources with declination $> -44°$ were observed in a VLBA pre-launch survey (VLBApls, Fomalont et al. 2000b) and a cutoff criterion, a minimum flux density of 0.32 Jy at 140 Mλ, was established for inclusion of a source in the VSOP Survey (Fomalont et al. 2000a). For sources south of $-44°$ this cutoff could not be determined, so all sources were included for HALCA observations. We find that 14 of these 24 southern sources observed have no detectable flux density on baselines to HALCA. Of the 402 sources in the complete sample, 294 were selected for VSOP observations, and this sample is designated as the VSOP Source Sample (VSS) (Hirabayashi et al. 2000b; Edwards et al. 2002).

Observations of the VSS began in August 1997, with the final observations being made in October 2003 when a second of the four HALCA momentum wheels became non-functional. Despite heroic attempts to heat up and free this reaction wheel through out 2004 no further observations were possible. Of the VSS sample of 294 sources all but 29 were observed. Details of the final status, the latest values of total density flux at 5 GHz,

---

de Córdoba, Argentina

the redshift, relevant references, best fit (or lower limit) observer frame brightness temperatures of the core, detected area, and flux density on the longest baselines, can be found in Table 1.

A typical VSOP Survey observation used ∼3 ground telescopes and HALCA, co-observing for up to ∼6 hours. Ground radio telescopes that made the largest contributions to the Survey Program observations include the VLBA (USA), Mopra (Australia), Hartebeesthoek (South Africa), Sheshan (China), Hobart (Australia), Kashima (Japan), Usuda (Japan), Ceduna (Australia), Kalyazin (Russia), Noto (Italy). Other participants were the Green Bank 43 m (USA), ATCA (Australia), Effelsberg (Germany), Arecibo (Puerto Rico), Torun (Poland), Onsala (Sweden), VLA (USA), Jodrel Bank Mk2 (UK) and Medicina (Italy). Further details are available in Dodson et al. (2006).

The VSOP survey observations were made at 5 GHz, with two left-circularly polarized 16 MHz IF bandwidths, sampled with two bits (Hirabayashi et al. 2000a). GOT observations of survey sources which were made with a similar configuration, were also included (see P-III for discussion of this). Data were usually correlated at either the DRAO Penticton correlator (Carlson et al. 1999) or the NAOJ Mitaka correlator (Shibata et al. 1998), with one non-GOT experiment processed at the Socorro correlator (Napier et al. 1994) along with two dozen GOT extractions (see Hirabayashi et al. 2000b; Scott et al. 2004, for details) and a test experiment in the data presented here. After correlation, the data were sent to ISAS for distribution to the Survey Reduction Team members. The subset of those members who contributed the reductions that appear in this paper are represented in the author list.

3. Data Reduction

Analysis of the data has been described elsewhere (Lovell et al. 2004) and hence will only be briefly outlined here. The data were imported into AIPS, amplitude calibrated (with the measured or expected system temperature and, if needed, the autocorrelation normalised) then fringe fitted. A check of the amplitude calibration of the ground telescopes was made by observing a nearby calibrator source for about five minutes during the experiment. Because HALCA could not slew quickly between sources, its amplitude calibration could not be checked using a bright astronomical source. It was found, however, to be quite stable. Nevertheless, the amplitude calibration was entirely derived from the measured or expected gains for both HALCA and a number of ground antennae, which can be very uncertain. In P-III, great effort was spent in measuring an absolute correction for the flux scale of the survey, in comparison with that of the VLBApls. In the dataset presented here, we have fewer GOTs and a smaller overlap with the VLBApls, so such an approach was not possible. Therefore we have assumed that the same correction (that the survey experiments underestimate the flux densities by a factor of 0.83 ± 0.05, compared to the VLBApls) can be made for these experiments. The amplitude scale errors were estimated as 20%, via the same comparison. After satisfactory delay and rate calibration, the data for all spectral channels were summed to a single channel per 16 MHz sub-band (i.e. two) and exported to DIFMAP (Shepherd 1997) for self calibration and model fitting. Scripts were used as much as possible to ensure that the methods were standardized.

The results of, and supporting documentation for, the data reduction can be found on the project web site (http://www.vsop.isas.jaxa.jp/survey). The raw and calibrated data are available from ISAS on request.

Most VSS sources have been imaged with previous ground VLBI observations (including the VLBApls, which was specifically designed to add the lower resolution data to the VSOP Survey), and consistency of the VSOP image with these other images was used to constrain the cleaning and modeling. Where no supporting information was available, the models are relatively conservative.

For the entire VSOP survey programme, 265 of the 294 sources were observed. The observations that are reported in this paper are listed in Table 2, which includes source names, experiment code, Ground Radio Telescopes, Tracking stations and Correlator used, time over which fringes were detected and the optical ID and redshift. For fifty of the observed sources, fringes to the spacecraft were not detected. Many of the sources were significantly resolved on shorter ground-only baselines, so that the lack of space fringes (RMS detection is typically 0.1 Jy) is consistent with the resolving structure seen on shorter baselines. However, for twenty three of the observed sources where space fringes were not detected, ground observations suggested that the space baselines (typically greater than 150 Mλ) should have been detected. These observations are not included in the table of results, since the ground-only data provides no additional information about the source structure than is published elsewhere.

4. The Results

4.1. The (*u*,*v*) Coverage, Visibility Amplitudes and Images

The graphical results for most of the 140 additional survey sources are given in Fig. 1, which shows the (*u*,*v*) coverage, the visibility amplitude versus projected (*u*,*v*) distance, and the image displayed in contour form, with one row per source. The (*u*,*v*) distance is plotted in Mλ, the flux density in janskys, and the image in milliarcseconds (mas). The J2000 name of the source is listed at the top left of each row, followed by the experiment name and the observation date. The peak brightness (P) in janskys per beam appears above the image plot, followed by the noise level (σ), and the beam (B) major and minor axes and the major axis position angle. The image σ is estimated from a Gaussian fit to the pixel flux density distribution, but in a few cases had to be manually increased due to high sidelobes in the image. The lowest contours are at -3 (dashed line) and 3 (solid line) times σ, doubling thereafter. The images presented are all made with uniform weighting, which highlights the highest resolution structure. The weighting scheme for each source was selected to give the clearest image. Further details are to be found on the VSOP Survey web site. The (*u*,*v*) coverage among the sources varies considerably, and this had significant impact on the quality, resolution and dynamic range of the images. For sources which were so heavily resolved that no space fringes are detected and with limited ground baseline coverage, no graphical results are shown, although the indication of overall angular size is still presented in Table 3. Sources for which no conclusions could be drawn (J1218$-$4600, J1424$-$4913 and J2358$-$1020) are not included.

During deconvolution we cross-checked our images with any other ground-based images of the source available, usually the VLBA Pre-Launch Survey (Fomalont et al. 2000b). Although most AGNs are variable with time and frequency, these other images provided reasonable constraints to the VSOP source images, for example, the source extent and component locations. The space baselines have considerably higher noise compared to those on the ground, because of the higher system temperature and smaller size of the HALCA antenna. Therefore the space data were up-weighted to approximately the same significance as the ground data, in order to emphasize the highest resolution structure in the source. This was typically a factor of ten to twenty.

The VSOP data indicated the strength and approximate angular size of a core component, even if, in some cases, most of the most extended emission, shown with lower-resolution images, was resolved out in the VSOP data. In general, the Survey datasets have a typical image fidelity of 20:1, and features less than 5% of the peak brightness should be treated with caution.

4.2. Model-Fitting and Brightness Temperature Determination

Once we obtained the best image for a source, consistent with the quality and quantity of the (*u*,*v*) coverage, we estimated the parameters for the major components of the source structure by Gaussian fitting: the integrated flux density, the centroid position and the major, minor axis and orientation of the major axis. These parameters are listed in Table 3. In all cases, the radio core could be identified (it was usually the most compact component and often at one edge of the radio emission). Occasionally, high resolution ground images at 15 and 23 GHz were also used to identify the location of the core. The radio core component is listed as the first component for sources which contain several components.

The brightness temperature of a component in the observer's frame is given by:

$$T_b = \frac{S\lambda^2}{2k_b\Omega} \tag{1}$$

where S is the component flux density at wavelength λ, k_b is Boltzmann's constant, and $\Omega \approx$

$1.13 \cdot (\theta_{\rm maj})(\theta_{\rm min})$ is the (Gaussian) weighted solid angle subtended by the component (which we have expressed in terms of the full width at half maximum of the component major and minor axes). To convert to brightness temperature in the source frame, equation (1) is multiplied by $(1+z)$, where z is the source redshift.

For the radio core only, we carefully determined the best-fit angular size and its allowable range. Although several quasi-analytical methods are available (eg. Difmap: Shepherd (1997), DIFWRAP: Lovell et al. (2000)), we relied on the ad-hoc method of varying critical parameters and estimating the range of angular size and flux density for each core component that is consistent with the data and its scatter (cf Lovell et al. (2000)). Two brightness temperatures are given for the radio cores in Table 3. First is the measured brightness temperature in the observer's frame, assuming that the core is a Gaussian-shaped component of the specified parameters. Sources for which only lower limits could be derived (i.e. unresolved sources) are marked with a >. The second brightness temperature is the lower limit of the brightness temperature (using the maximum angular size) converted to the *source frame*. If no redshift is available, zero redshift is assumed. These values are the lowest possible temperature compatible with the data. We list these as we feel that these are a more useful value than upper limits or best fits which depend critically on the interpretation of the very highest resolution data, which have the highest noise and the most sparse coverage.

4.3. Discussion of the Brightness Temperature Distributions

Histograms depicting the brightness temperature distribution in both the source and observer's frame for the sources presented here are shown in Fig. 2. Here we have used the values for the best fits to the models (following the style of P-III), rather than using the lower limits, in order to combine both datasets. (Sources with no measured redshift are not included in the plot of source-frame brightness temperatures.)

Most cores have $T_b > 10^{11}$ K, with approximately 56% of the sources having a measured brightness temperature in excess of 10^{12} K in the source frame, and approximately 30% of the sources having a measured brightness temperature greater than 10^{12} K in the observer's frame.

We find that overall, the mean brightness temperatures in our data are slightly lower than those in P-III. This could be expected, given that our data include many more of the weaker sources (the median total flux density of sources in this paper is less than half of those in P-III), and a significant number with no space fringes, none of which were included in P-III.

Comparing this result with other similar datasets (Tingay et al. 2001; Kovalev et al. 2005) we note that, as discussed in P-III, the distribution in Tingay et al. (2001) matches the one presented here once corrected by the factor $(1+z)^{1/2}/0.56$. This factor comes from the corrections for changing their results from an optically thick core model to a Gaussian, and from co-moving frame to the source frame. The distribution presented in Kovalev et al. (2005) is from VLBA observations at 15 GHz. They find also a median value of 10^{12}K, but the distribution towards 10^{13} and beyond is largely made up of lower limits, rather than actual measurements as we have here. We have compared the T_b for the source in common with Kovalev et al. (2005) by selecting the data with the closest observation dates. The T_b in the VSS tend to be higher, as expected since the majority of the brightness temperatures in Kovalev et al. (2005) are lower limits, with a median ratio of 2.4. Detailed comparison of individual sources, in particular those with very different T_b, will be presented in a future paper (Gurvits et al. in prep.).

When looking at individual sources, we believe that the most useful number that can be provided is the lower limit to the brightness temperatures, which is that which *must* be generated by any proposed model or theory, rather than the brightest possible which *could* be required by any proposed model. The former will not produce the highest measured temperatures, nor the most extended distribution. However, it will provide limits and distributions which must be achieved or exceeded. To probe the distribution of brightness temperatures, we prefer the approach taken in P-IV, where a cumulative visibility distribution was produced from all sources and a measurement of typical core sizes was fitted to these data. By this approach the very high errors at the extremes have reduced contributions.

4.4. Comments on Individual Sources

Survey sources that were not successfully scheduled are included in Table 1 with references (where they exist) to other VLBI observations marked with a † on the experiment name.

The complete list of VSOP Survey observations is presented in Table 2. In addition, short notes on the sources are given. A general comparison is made with VLBI images from other observations, primarily the VLBApls (Fomalont et al. 2000b), U. S. Naval Observatory Database (USNO) (Fey, Clegg, & Fomalont 1996; Fey & Charlot 1997, 2000), a space VLBI Survey of Pearson-Readhead sources (VSOPPR) (Lister et al. 2001), the VLBA 2 cm Survey (VLBA2cm1) (Kellermann et al. 1998; Zensus et al. 2002; Kellermann et al. 2004; Kovalev et al. 2005), MOJAVE (Lister & Homan 2005) and VLBA2cm2 (Gurvits et al. in prep.), results from VSOP observations of southern sources (VSOPsth) (Tingay et al. 2002), and the VLBA Calibrator Survey (VCS) (Beasley et al. 2002). Any significant differences are noted. The largest linear extent, or upper limit, is given.

J0013+4051 — The core is < 0.2 mas in size, with extended emission to the north-west as observed in other VLBA images.

J0105+4819 — The core is 0.2 mas in size. The more extended emission in other VLBA images that surrounds the core is undetected with the VSOP data.

J0108+0135 — The core is 0.2 mas in size and the location of the extended component is in agreement with other VLBA images.

J0116−1136 — Not detected on space baselines. The VSOP ground-only image and other VLBA images give a core size of about 0.5 mas in size.

J0121+0422 — The core is 0.4 mas in size. There is faint radio emission to the east, also seen with 15 GHz VLBA observations (Kellermann et al. 2004)

J0125−0005 — The core is 0.3 mas in size and there is extended emission to the west.

J0141−0928 — Redshifts of both 0.733 and 0.44 have been reported (Stocke and Rector 1997). The core is 0.4 mas in size and nearly circular (Beasley et al. 2002)

J0149+0555 — The core is 0.4 mas in size and the extended emission is similar to that seen with other VLBA images (Beasley et al. 2002)

J0152+2207 — The core is 0.4 mas in size and extended to the north. A faint extended component to the north, seen with other VLBA images, is present. (Fomalont et al. 2000b; Kellermann et al. 2004)

J0204+1514 — The core is < 0.2 mas in size. The faint emission to the south-east is in the opposite direction of most of the jet emission, but the source structure evolution is complicated.

J0204−1701 — The core is 0.6 mas in size and there is an extended component to the south.

J0217+0144 — The core is unresolved, < 0.1 mas in size. The faint extended structure from lower resolution VLBA images is not detected.

J0224+0659 — The core is 0.3 mas in size. Emission to the west is also detected.

J0231+1322 — The core is about 0.4 mas in size. Faint emission to the north-east is also detected.

J0237+2848 — The core is < 0.2 mas in size. Very extended emission to the north is detected.

J0239+0416 — The core is < 0.2 mas in size. Extended emission to the north-west is detected.

J0242+1101 — The core is < 0.2 mas in size. The emission to the south-east is clearly extended.

J0253−5441 — The core is 0.3 mas in size, in agreement with Ojha et al. (2005). The fainter component to the west is too weak to be detected by VSOP.

J0259+0747 — The core is 0.8 mas in size. The faint emission 3 mas to the south, seen in VLBA images, is not detected.

J0303−6211 — The core is 0.6 mas in size, extended east-west. There is a faint component 1.5 mas to the east.

J0309−6058 — Two small-diameter components, separated by 0.5 mas, are detected. The component to the north-east has the higher brightness temperature and is assumed to be the core.

J0312+0133 — The core is < 0.2 mas in size. Faint emission to the east, seen with the VLBA, is just detected with VSOP.

J0321+1221 — The core is < 0.15 mas in size. The extended component seen by VSOP is the inner part of a 20 mas jet seen by the VLBApls.

J0336+3218 — The core is 0.4 mas in size. Because of the lack of short spacings, none of the extended structure is detected by VSOP.

J0339−0146 — The core is 0.2 mas in size. The extended emission to the north-east is seen with other VLBA images.

J0359+5057 — The core is about 1.0 mas in size. The extended emission to the north-east, which extends 20 mas from the core in the VLBA images, is just detected by VSOP.

J0402−3147 — The core is 0.3 mas in size. The faint emission to the west is seen by the VLBApls.

J0403+2600 — The core is 0.35 mas in size. The extended emission to the west seen by the VLBApls is detected with VSOP. The model does not include the emission 15 mas to the north.

J0406−3826 — The core is < 0.25 mas in size. The faint component to the west is found in the VLBApls, although the VCS image at 8 GHz has the fainter component to the east. This source is one of the most extreme of the Intra Day Variable sources (Kedziora-Chudczer et al. 1997).

J0414+0534 — A gravitationally lensed object with two major emission centers separated by 400 mas (Fomalont et al. 2000b). No image is shown, but the model fit of the Shanghai to Kashima baseline (20 Mλ) suggests a size of 1.6 mas for the more compact (probably southern) component.

J0416−1851 — The core is 0.5 mas in size. However, the flux density is about a factor 5 to 10 less than seen by other VLBI observations.

J0424+0036 — The core is 0.2 mas in size. The faint emission to the north is associated with more extensive emission seen in other VLBA images.

J0424−3756 — The core is 0.5 mas in size. The faint, extended component to the east is observed in other VLBA images.

J0428−3756 — The core is < 0.5 mas in size. The faint, extended component to the east is observed in the VLBApls.

J0433+0521 — The VSOP observations suggest that the core is < 0.3 mas in size. Only some of the extended structure to the west is imaged with VSOP.

J0437−1844 — The core is 0.7 mas in size and the extended emission to the north-west is observed with other VLBA images. The space baselines are short, so the angular resolution is relatively low.

J0442−0017 — Not detected on space baselines and no image is shown. The approximate size is 1.1 mas.

J0449+1121 — The VSOP data are consistent with a core < 0.2 mas in size and extended emission to the east.

J0450−8101 — The core is < 0.2 mas in size. There is extended emission on both sides of the core.

J0508+8432 — A redshift of 0.112 was initially reported for this object, but subsequently an absorption system at 1.34 places a lower limit on the redshift (Stocke and Rector 1997). The core is 0.35 mas in size.

J0509+0541 — The core is < 0.4 mas in size. The extended emission to the south and east is seen in the VLBApls.

J0513−2159 — The core is 1.1 mas in size with no detection on space baselines. No image is given.

J0522−3627 — The brightest component is identified as the core and is 0.4 mas in size. Most of the extended emission is to the north-west, with fainter emission to the south-east which is identified as the core in Tingay & Edwards (2002). This component is < 0.2 mas in size.

J0530+1331 — The space baselines suggest that the core component lies at the extreme south-west of the emission, and contains about 0.22 Jy within a size < 0.3 mas. Only a small part of the extended emission is contained in the other two model components.

J0541−0541 — The core is 1.2 mas in size, with no detection on space baselines. No image is given.

J0607+6720 — The emission is about 0.6 mas in size. It is best fit by two small components each with a size < 0.2 mas.

J0614+6046 — The core is 0.25 mas in size.

J0626+8202 — The core is 0.3 mas in size. The extended emission is complex and approximated by the additional two components. This source shows very interesting sub-mas structure.

J0646+4451 — The core is identified with the fainter component to the west, based on the extended structure from VLBA images. The core is < 0.2 mas in size.

J0648−3044 — The core is 0.4 mas in size. There is extended emission to the east, in agreement with other VLBA images.

J0713+4349 — The space baselines suggest a core component of 0.20 Jy with a size < 0.2 mas. No image is given since there is little ground baseline data.

J0739+0137 — The core is 0.2 mas in size. There is extended emission to the north-west.

J0743−6726 — The core is 0.7 mas in size. There is a slightly extended component 29 mas to the east. This structure agrees with Ojha et al. (2005).

J0745+1011 — The core is 0.4 mas in size. There is emission both north and south of the core. The VLBA images show that the source structure is variable and changes with frequency.

J0750+1231 — The core is 0.6 mas in size. There is extended emission to the east.

J0808+4950 — The core is 0.15 mas in size. Most of the extended emission is to the south-east, as seen in other VLBA images.

J0820−1258 — The core is $<$ 0.3 mas in size. There is extended emission to the east.

J0825+0309 — The core is $<$ 0.1 mas in size. There is limited data so the faint extended emission to the north, seen in other VLBA images, is not present.

J0831+0429 — The core is 0.5 mas in size. There is extended emission to the east.

J0842+1835 — The southern, fainter component is the core with an angular size 0.3 mas. The northern component is only the inner part of the jet emission which extends over 10 mas from the core.

J0854+5757 — The core is 0.3 mas in size. Most of the extended emission is south of the core, with a hint of emission to the north.

J0909+4253 — The core is $<$ 0.15 mas in size. There is extended emission to the south.

J0921−2618 — Not detected on space baselines and no image is given. The approximate angular size of the emission is 0.9 mas in position angle $-17°$, which agrees with the VLBApls results.

J0948+4039 — The core is 0.15 mas in size. There is extended emission to the south-east.

J0956+2515 — The core is $<$ 0.2 mas in size. The extended emission, some of which overlaps the core, lies to the west.

J0958+4725 — The core is 0.3 mas in size. There is no significant extended emission.

J0958+6533 — The core is $<$ 0.2 mas in size. There is extended emission to the north-west which agrees with Beasley et al. (2002).

J1014+2301 — No detection on space baselines. No image is shown and the size of the emission of 0.8 mas.

J1035−2011 — The core is $>$ 0.15 mas in size. The faint extended emission is not detected in these observations.

J1041+0610 — The core is 0.5 mas in size. There is extended emission to the south-east.

J1048−1909 — The core is $<$ 0.1 mas in size. There is extended emission to the south.

J1051+2119 — The core is 0.2 mas in size. There is extended emission to the east.

J1051−3138 — The core is $<$ 0.2 mas in size. There is extended emission near and south-west of the core.

J1058+1951 — The source contains 0.07 Jy at 180 Mλ north-south, which is consistent with the VLBApls, with 0.4 Jy in a 0.9 mas north-south component.

J1058−8003 — The core is 0.4 mas in size. There is no indication of extended emission.

J1118−4634 — The core of 0.27 Jy is 0.7 mas in size. The total flux density is about 1.0 Jy (Tingay et al. 2003), hence there may be additional extended emission.

J1125+2610 — The core is 0.8 mas in size, elongated in the direction of the more extended emission seen by the VLBApls.

J1127−1857 — The core is $<$ 0.2 mas in size. There is extended emission to the south.

J1130−1449 — The core is $<$ 0.2 mas in size. There is extended emission to the east. See Tingay et al. (2002).

J1150−0023 — No detection on space baselines and no image is given. The core region contains about 0.13 Jy in a component $<$ 0.6 mas. See VLBApls for a model of the extended emission.

J1153+4931 — No detection on space baselines and no image is given. The core emission is about 2.5 mas in the north-south direction. This does not agree with the VLBApls data.

J1153+8058 — The core is 0.3 mas in size. There is faint emission south of the core.

J1159+2914 — The core is 0.3 mas in size. There is extended emission to the north-east.

J1218−4600 — No detectable flux density on ground baselines greater than $\sim$ 100 Mλ. Hence, there is no image and model.

J1224+0330 — The core is $<$ 0.25 mas in size. There is extended emission to the west.

J1224+2122 — The core is $<$ 0.4 mas in size. There is extended emission to the north.

J1257−3155 — The core is $<$ 0.3 mas in size in the position angle of the extended emission seen by the VLBApls. There is a possible amplitude scaling error, so the core flux density may be a factor of two higher.

J1305−1033 — The core is < 0.2 mas in size. No additional structure is seen with VSOP because of lack of short spacings.

J1316−3338 — The core is 0.3 mas in size. There is extended structure to the south-west and west.

J1351−1449 — Not detected on space baselines. No image is given. The core size is 1.0 mas.

J1357+1919 — We believe that the northern most component is the core with a size of 0.7 mas. The component 2 mas south-east has a higher brightness temperature, but is probably a bright spot of the jet. More extended emission occurs further to the south-east.

J1405+0415 — The structure seen in the image with the full VSOP GOT 5-GHz data (Yang et al. 2006) is consistent with our result: the jet is extended ~15 mas to the West.

J1415+1320 — The core is 0.4 mas in size. There is extended emission at the same position as the core, and also to the north-west.

J1424−4913 — No detectable flux density on global baselines, greater than $\sim 140\,\mathrm{M}\lambda$.

J1427−4206 — The core is 0.25 mas in size. There is extended emission to the north and east (Tingay et al. 2002).

J1436+6336 — The core is < 0.25 mas in size. There is a stronger component north of the core, and weaker emission to the south (VLBApls).

J1504+1029 — The core is < 0.2 mas in size. There is extended emission to the east.

J1516+0015 — The core is < 0.2 mas in size. Only space baselines are available, hence none of the extended structure (to the north-west) is seen.

J1522−2730 — The core is 0.25 mas in size. There is extended structure to the west.

J1550+0527 — The core is < 0.1 mas in size. There is extended structure to the north.

J1557−0001 — The core is 0.20 mas in size. No other significant extended structure is seen with VSOP.

J1602+3326 — The core is < 0.2 mas in size. There is extended emission somewhat south-east of the core, but it is poorly defined because of the lack of short spacings.

J1608+1029 — The core is 0.5 mas in size. There is extended emission to the north-west.

J1625−2527 — The core is 0.5 mas in size. There is no significant extended structure.

J1647−6437 — The core is 0.9 mas in size. There is little (u,v)coverage, but no significant extended structure is seen.

J1658+4737 — Only space baselines. The core is 0.3 mas in size. The large scale emission to the north is not seen.

J1726−6427 — There are no detections on space baselines, and no image is given. The Hartebeesthoek–Hobart baseline (145 $\mathrm{M}\lambda$) detects only 0.04 Jy.

J1743−0350 — The core is < 0.15 mas in size and contains about 20% of the emission. The extended emission is somewhat south and east of the core.

J1744−5144 — There are no detections on space baselines, and no image is given. The Hartebeesthoek–Hobart baseline (145 $\mathrm{M}\lambda$) detects only 0.07 Jy.

J1753+4409 — There are only space baselines and no image is given. The core is < 0.15 mas in size.

J1809−4552 — The core is 0.5 mas in size and extended in PA −64°.

J1824+1044 — The core is 0.15 mas in size and there is some extended structure to the north.

J1837−7108 — The core is 0.2 mas in size and there is extended structure. We model this as to the south, however there is some ambiguity as to whether it is actually to the south or the north.

J1842+7946 — There are no detections on space baselines. The image and model show a core 0.3 mas in size and extended emission to the north-west up to 5 mas away.

J1911−2006 — The core is < 0.2 mas in size. The flux density in the extended emission is higher and closer to the core than that in the VLBApls.

J1912−8010 — There are no detections on space baselines and no image is given. The core is 0.6 mas in size, in general agreement with Ojha et al. (2005).

J1925+2106 — The core is 0.5 mas in size. There is extended emission to the west.

J1927+7358 — Lister et al. (2001) show the complete VSOP image. With more limited data, we assume that the core is the component at the northern edge of the source (component D in Lister et al.). Its flux density is 0.4 Jy with an angular size < 0.4 mas. Only the two other components just south of the core are listed in our table. The extended emission to the south is not included.

J1932−4546 — There are no detections on space baselines and no image is given. Hartebeesthoek–Hobart at 140 $\mathrm{M}\lambda$ has 0.1 Jy correlated flux density. If one assumes a total flux density of 0.74 Jy (Tingay et al. 2003) in a circular Gaussian, the core size is 1.1 mas.

J1937−3958 — The core is 0.3 mas in size. There are no baselines less than 120 Mλ so the extended structure seen with the VLBApls is not present.

J1939−6342 — Ojha et al. (2004) shows two components, separated by 40m̃as. The source is not detected on space baselines and no image is given. Hartebeesthoek–Hobart at 140 Mλ has 0.1 Jy correlated flux density. If one assumes a total flux density of 1.0 Jy in the core component (the western of the 40-mas double), the core angular size is 1.1 mas.

J1940−6907 — There are no detections on space baselines. One component fit to the sparse ground data suggest a core size of 0.9 mas.

J1955+5131 — The core is 0.3 mas in size. There is extended emission toward the north-west.

J2009−4849 — There are no detections on space baselines. The core is 1.2 mas in size. The faint component to the west seen by Ojha et al. (2005) is below the VSOP detection level.

J2011−1546 — The core is $<$ 0.3 mas in size. There is a component just north of the core and a more extended component 2 mas north of the core.

J2123+0535 — The core is 0.3 mas in size. There is extended emission to the north-east.

J2139+1423 — The core is $<$ 0.3 mas in size. There is extended emission slightly to the east and to the south.

J2148+0657 — The core is 0.9 mas in size with no indication of more compact emission. There is faint extended emission to the south-east.

J2151+0552 — The core is $<$ 0.3 mas in size. There is extended emission over the core and to the west.

J2152−7807 — There are no detections on space baselines. The sparse data suggest a component of 0.9 mas in size, elongated in position angle 33°.

J2207−5346 — The core component is 0.15 mas in size. There is extended emission towards the east.

J2218−0335 — The core component is 1.3 mas in size. Any compact core in this source is less 0.1 Jy.

J2232+1143 — The core component is 0.4 mas in size. The complicated emission extends well to the south.

J2236+2828 — The core component is 0.5 mas in size. Any further compact component is less than 0.3 Jy.

J2239−5701 — There are no detections on space baselines and no image is given. Hartebeesthoek–Hobart at 140 Mλ has 0.4 Jy correlated flux density. If one assumes a total flux density of 0.7 Jy (Tingay et al. 2003) in a circular Gaussian, the core size is 0.6 mas.

J2246−1206 — The core component is $<$ 0.2 mas in size. There is extended emission to the north.

J2258−2758 — The core component is 0.2 mas in size. There is extended emission to the south and east.

J2336−5236 — There are no detections on space baselines and no image is given. Hartebeesthoek–Hobart at 140 Mλ has 0.15 Jy correlated flux density. If one assumes a total flux density of 1.63 Jy (Tingay et al. 2003) in a circular Gaussian, the core size is 1.2 mas.

J2357−5311 — The core component is 0.3 mas in size. There is extended emission to the south-west, in agreement with the lower resolution image of Shen et al. (1998).

J2358−1020 — There are space fringes implying a core component of 0.2 Jy within 0.2 mas. The ground data has amplitude scaling errors, so there is no image nor model.

5. Summary and Discussion

We have presented images, models and comments of the 140 sources which were observed as part of the VSOP Survey project that were not covered in P-III. We have combined the brightness temperature measurements and limits found for the entire sample to produce the T_b distribution for the VSS.

We find that about half of the AGN sample of sources reported upon in this paper have significant radio emission in the core component, with $T_b \geq 10^{12}$ K in the source frame. Since the maximum brightness temperature one is able to determine using only ground-based arrays is of the order of 10^{12} K, our results confirm the necessity of using space VLBI to explore the extremely high brightness temperature regime. In addition, our Survey results clearly show that by using space VLBI with higher sensitivity, and somewhat higher resolution, the radio cores of many AGN can be successfully imaged.

Because of the variability of many of the sources in the Survey sample, detailed spectral indices of the core components are difficult to determine.

However, many of the sources were observed with the VLBA at 15 GHz as part of the VLBA2cm2 survey, and the spectral properties of the cores will be reported elsewhere (Gurvits et al. in prep.).

It was not possible to slew the HALCA satellite during the observing runs, therefore HALCA was not able to participate in scans of fringe finders, or flux calibrators. It is the absence of these which forces us to label a number of experiments with no space fringes as failures, when it could be the effects of the source structure. The design of VSOP-2 will allow fringe checks, and also phase referencing experiments, to be performed (Hirabayashi 2000c).

The completion of this survey has been a Quixotic endeavor, and possibly: “vino a dar en el más estraño pensamiento que jamás dio loco en el mundo; y fue que le pareció convenible y necesario, así para el aumento de su honra como para el servicio de su república, hacerse caballero andante” (Cervantes 1605).

We gratefully acknowledge the VSOP Project, which is led by the Institute of Space and Astronautical Science of the Japan Aerospace Exploration Agency, in cooperation with many organizations and radio telescopes around the world. RD, KJW, GAM and JEJL acknowledge support from the Japan Society for the Promotion of Science. RD acknowledges support as a Marie-Curie fellow via EU FP6 grant MIF1-CT-2005-021873. ZS acknowledges support from NNSFC (10573029 and 10625314). WKS wishes to acknowledge support from the Canadian Space Agency. SH acknowledges support through an NRC/NASA-JPL Research Associateship. SF, ZP and LM acknowledge the OTKA T046097 grant received from the Hungarian Scientific Research Fund. SF and GC acknowledge the ASTRON and JIVE summer studentship programme. JY acknowledges the CAS-UNAW cooperation programme in Radio Astronomy. This research has made use of data from the University of Michigan Radio Astronomy Observatory (UMRAO) which is supported by funds from the University of Michigan and the NSF, the United States Naval Observatory (USNO) Radio Reference Frame Image Database (RRFID), and the NASA/IPAC Extragalactic Database (NED) which is operated by the Jet Propulsion Laboratory, California Institute of Technology, under contract with the National Aeronautics and Space Administration. The NRAO is a facility of the National Science Foundation, operated under cooperative agreement by Associated Universities, Inc. The Australia Telescope Compact Array is part of the Australia Telescope which is funded by the Commonwealth of Australia for operation as a National Facility managed by CSIRO. Meetings of the VSOP Survey Working Group were supported by EC FP6 Integrated Infrastructure Initiative, RadioNet (contract RII3-CT-2003-505818), JIVE and the OAN.

REFERENCES

Beasley, A. J., Gordon, D., Peck, A. B., Petrov, L., MacMillan, D. S., Fomalont, E. B., Ma, C., 2002, ApJS, 141, 13

Carlson, B. R., Dewdney, P. E., Burgess, T. A., Casorso, R. V., Petrachenko, W. T., & Cannon, W. H. 1999, PASP, 111, 1025

Cervantes, M., 1605, “El ingenioso hidalgo don Quijote de la Mancha”

Dodson, R., et al., 2006, Proceedings of Science, PoS(8thEVN), 070

Edwards, P. G., Hirabayashi, H., Fomalont, E. B., Gurvits, L. I., Horiuchi, S., Lovell, J. E. J., Moellenbrock, G. A., Scott, W. K. 2002, 8th Asian-Pacific Regional Meeting, Volume II 375

Fey, A. L., Clegg, A. W., & Fomalont, E. B. 1996, ApJS, 105, 299

Fey, A. L., & Charlot, P. 1997, ApJS, 111, 95

Fey, A. L., & Charlot, P. 2000, ApJS, 128, 17

Fomalont, E., et al. 2000a, in Proceedings of the VSOP Symposium, January 2000, Astrophysical Phenomena Revealed by Space VLBI, ed H. Hirabayashi, P. G. Edwards, & D. W. Murphy (Sagamihara: The Institute of Space and Astronautical Science), 167

Fomalont, E. B., Frey, S., Paragi, Z., Gurvits, L. I., Scott, W. K., Taylor, A. R., Edwards, P. G., & Hirabayashi, H. 2000b, ApJS, 131, 95

Gregory, P. C., Scott, W. K., Douglas, K., & Condon, J. J. 1996, ApJS, 103, 427

Greisen, E. W. 1988, in Acquistion, Processing and Archiving of Astronomical Images, ed. G. Longo & G. Sedmak (Napoli: Osservatorio Astronomico di Capodimonte), 125

Griffith, M. R., & Wright, A. E. 1993, AJ, 105, 1066

Hirabayashi, H., et al. 1998, Science, 281, 1825 (erratum 282, 1995)

Hirabayashi, H., et al. 2000a, PASJ, 52, 6, 955

Hirabayashi, H., et al. 2000b, PASJ, 52, 6, 997 (Paper I)

Hirabayashi, H. 2000c, Adv. Space Res., 26, 751

Horiuchi et al, 2004, ApJ, 616, 110 (Paper IV)

Gurvits, L. et al. , in preparation, (Paper VI)

Kedziora-Chudczer L., Jauncey D. L., Wieringa M. H., Walker M. A., Nicolson G. D., Reynolds J. E., Tzioumis A. K., 1997, ApJ, 490, L9

Kellermann, K. I. & Pauliny-Toth, I. I. 1969, ApJ, 155, L71

Kellermann, K. I., Vermeulen, R. C., Zensus, J. A., & Cohen, M. H. 1998, AJ, 115, 1295

Kellermann, K. I., et al. 2004, ApJ, 609, 539

Kovalev, Y. Y. et al. , 2005, AJ, 130, 2473

Lawrence, C. R., Bennet, C. L., Hewitt, J. N., Langston, G. I., Klotz, S. E., Burke, B. F., & Turner, K. C. 1986, ApJS, 61, 105

Lister, M. L., Tingay, S. J., Murphy, D. W., Piner, B. G., Jones, D. L. & Preston, R. A. 2001, ApJ, 554, L948

Lister, M. L., & Homan, D. C. 2005, AJ, 130, 1389

Lovell J., et al., 2000, in Proceedings of the VSOP Symposium, January 2000, Astrophysical Phenomena Revealed by Space VLBI, ed H. Hirabayashi, P. G. Edwards, & D. W. Murphy (Sagamihara: The Institute of Space and Astronautical Science), 301

Lovell, J., et al, 2004, ApJS, 155, 27 (Paper II)

Napier, P. J., Bagri, D. S., Clark, B. G., Rogers, A. E. E., Romney, J. D., Thompson, A. R., & Walker, R. C. 1994, IEEE Proc. 82, 658

Pearson, T. J. & Readhead A. C. S., 1988, ApJ, 328, 114

Ojha, R. Fey, A., Johnston, K., Jauncey, D., Reynolds, J., Tzioumis, A., Quick, J., Nicolson, G., Ellingsen, S., Dodson, R., McCulloch P. 2004 AJ, 127, 3609

Ojha, R., Fey, A., Charlot, P.,Jauncey, D.,Johnston, K., Reynolds, J., Tzioumis, A., Quick, J. Nicolson, G., Ellingsen, S., McCulloch, P., Koyama, Y., 2005 AJ, 130, 2529

Scott, W. K., et al, 2004, ApJS, 155, 33 (Paper III)

Shen, Z.-Q., et al., AJ, 1998, 115, 1357

Shepherd, M. C. 1997, in ASP Conf. Ser. 125, Astronomical Data Analysis Software and Systems VI, ed J. A. Zensus, G. B. Taylor, & J. M. Wrobel (San Francisco: ASP), 77

Shibata, K. M., Kameno, S., Inoue, M., & Kobayashi, M. 1998, in ASP Conf. Ser. 144, Radio Emission from Galactic and Extragalactic Compact Radio Sources, ed J. A. Zensus, G. B. Taylor, & J. M. Wrobel (San Francisco: ASP), 397

Stocke, J. T. and Rector, T. A., 1997, ApJL, 489, L17

Tingay, S. J. et al. , 2001, ApJ, 549, L55

Tingay, S. J. et al. , 2002, ApJ Suppl, 141, 311

Tingay, S. J., & Edwards, P. G. 2002, AJ, 124, 652

Tingay, S. J. et al. , 2003, Pub. Astron. Soc. Japan, 55, 351

Véron-Cetty, M.-P. & Véron, P. 2006, A&A, 445, 773

Zensus, J. A., Ros, E., Kellermann, K. I., Cohen, M. H., Vermeulen, R. C., & Kadler, M. 2002, AJ, 124, 662

Yang J., Gurvits L., Lobanov A., Frey S., Hong X., 2006, Proceedings of Science, PoS (8thEVN), 086

This 2-column preprint was prepared with the AAS LaTeX macros v5.2.

TABLE 1
VSOP AGN SURVEY SOURCE LIST

(1) IAU Name	(2) S_5 [Jy]	(3) ID	(4) z	(5) Exp	(6) Paper	(7) T_b [10^{12} K]	(8) area [mas^2]	(9) Jy – Mλ
J0006−0623	2.69†	G	0.347*	vs03t	III	>0.5	0	0.52 – 380
J0013+4051	1.0	G	0.256	vs13a	V	1.3	0.01	0.23 – 460
J0019+7327	0.78*	QSO	1.781	vs07a	III	>0.2	0	0.12 – 420
J0042+2320	1.6	VisS		vs07u	III	0.3	0.04	0.19 – 460
J0050−0929	1.9	QSO		vs06i†	1,2			–
J0105+4819	1.1	RadioS		vs08q	V	0.3	0.04	0.13 – 540
J0106−4034	3.40†	QSO	0.584	vs03s	III	>3.8	0	1.36 – 500
J0108+0135	3.60*	QSO	2.107	vs02t	V	1.7	0.04	0.54 – 500
J0115−0127	0.91†	QSO	1.365	vs07t	III	0.2	0.06	0.30 – 500
J0116−1136	0.89†	QSO	0.672	vs06h	V	0.2	0.16	0.63 – 180
J0121+1149	1.1	QSO	0.570	vs08p	III	0.3	0.45	0.30 – 500
J0121+0422	1.45†	QSO	0.637	vs05y	V	0.8	0.04	0.52 – 260
J0125−0005	1.48†	QSO	1.070	vs05x	V	0.3	0.09	0.23 – 460
J0126+2559	1.4	QSO	2.370	vs08o	III	>0.0	0	0.88 – 220
J0132−1654	1.2	QSO	1.020	vs08c†	1,6			–
J0136+4751	2.06*	QSO	0.859	vs03r	III	4.3	0.02	1.25 – 500
J0137−2430	1.6	QSO	0.835	vs07s†				–
J0141−0928	1.2	QSO	0.733*	vs10i	V	0.5	0.12	0.35 – 420
J0149+0555	1.40†	QSO	2.345	vs06z	V	1.9	0.03	0.63 – 300
J0152+2207	1.1	QSO	1.320	vs08n	V	0.4	0.04	0.12 – 500
J0202−7620	1.0	QSO	0.389	vs11l†	6			–
J0204+1514	2.72*	QSO	0.405*	vs03i	V	2.6	0.04	1.01 – 460
J0204−1701	1.06†	QSO	1.740	vs08b	V	0.2	0.18	0.19 – 420
J0205+3212	1.0	QSO	1.466	vs12c†	1,2			–
J0210−5101	3.02†	QSO	0.999*	vs03a	III	0.5	0.08	0.43 – 420
J0217+7349	3.10*	QSO	2.367	vs02o	III	0.5	0.04	0.18 – 540
J0217+0144	0.94†	QSO	1.715	vs07r	V	>1.2	0	0.35 – 420
J0224+0659	0.56†	QSO	0.511*	vs12b	V	0.2	0.09	0.27 – 420
J0226+3421	1.7	QSO	2.910	vs05o†	1			–
J0231+1322	2.4	QSO	2.065	vs04l	V	0.4	0.16	0.20 – 420
J0237+2848	2.24*	QSO	1.207	vs02s	V	>0.7	0	0.68 – 500
J0239+0416	0.58†	QSO	0.978	vs11i	V	0.5	0.04	0.12 – 500
J0242+1101	1.6	QSO	2.694*	vs05w	V	0.7	0.04	0.29 – 460
J0251+4315	1.25*	QSO	1.310	vs07q	III	0.2	0.16	0.22 – 540
J0253−5441	0.88*	QSO	0.537	vs09o	V	0.5	0.09	0.36 – 460
J0259+0747	0.62*	QSO	0.893	vs12a	V	0.1	0.16	0.22 – 460
J0303−6211	2.36†	QSO		vs04v	V	0.4	0.24	0.28 – 420
J0309−6058	1.60†	QSO		vs08u	V	0.9	0.01	0.45 – 460
J0312+0133	0.32†	QSO	0.664	vs11z	V	1.1	0.01	0.26 – 420
J0319+4130	23.20*	G	0.018*	vs01c	III	0.1	0.64	0.23 – 420
J0321+1221	1.6	QSO	2.670	vs07p	V	>0.5	0	0.44 – 380
J0334−4008	2.6	QSO	1.445*	vs04b	III	>0.6	0	0.19 – 460
J0336+3218	1.80*	QSO	1.259	vs05f	V	0.1	0.16	0.19 – 300
J0339−0146	1.72*	QSO	0.852	vs03q	V	1.5	0.04	0.79 – 340
J0348−2749	0.79†	QSO	0.987	vs08m	III	1.1	0.03	0.38 – 420
J0359+5057	2.55*	QSO		vs01i	V	0.2	0.55	0.16 – 380
J0402−3147	1.0	QSO	1.288	vs11y	V	0.3	0.09	0.40 – 180
J0403+2600	1.0	QSO	2.109	vs11x	V	0.3	0.09	0.28 – 340

TABLE 1—*Continued*

(1) IAU Name	(2) S_5 [Jy]	(3) ID	(4) z	(5) Exp	(6) Paper	(7) T_b [10^{12} K]	(8) area [mas^2]	(9) Jy – Mλ
J0403−3605	1.64†	QSO	1.417	vs03z	III	0.8	0.1	0.70 – 500
J0405−1308	2.54†	QSO	0.571	vs03e	III	1.0	0.04	0.42 – 420
J0406−3826	1.18†	QSO	1.285	vs07o	V	1.3	0.04	0.45 – 500
J0407−1211	1.8	QSO	0.574	vs06q†	1			–
J0414+0534	0.65†	G	2.639	vs13b	V	0.0	2.56	0.11 – 20
J0416−1851	1.3	QSO	1.536	vs08a	V	0.0	0.25	0.10 – 180
J0423−0120	2.99†	QSO	0.915	vs02g	III	1.9	0.09	1.35 – 340
J0424+0036	0.54*	QSO	0.310*	vs07z	V	1.0	0.04	0.40 – 380
J0424−3756	1.39†	QSO	0.782	vs06y	V	1.8	0.05	0.56 – 260
J0428−3756	0.91†	QSO	1.112	vs05e	V	0.2	0.16	0.49 – 180
J0433+0521	5.54*	G	0.033*	vs02n	V	>0.2	0	0.55 – 380
J0437−1844	0.90†	QSO	2.702	vs09m	V	0.1	0.49	0.31 – 180
J0440−4333	3.05†	QSO	2.852	vs01r	III	1.7	0.04	0.48 – 500
J0442−0017	1.63†	QSO	0.844	vs03h	V	0.1	1.21	0.27 – 140
J0449+1121	1.21*	G	1.207*	vs10h	V	>1.4	0	0.90 – 180
J0450−8101	0.86†	QSO	0.444*	vs08l	V	2.2	0.01	0.90 – 500
J0453−2807	1.63†	QSO	2.560	vs04g	III	1.1	0.02	0.29 – 420
J0457−2324	1.60†	QSO	1.003	vs05n	III	1.4	0.16	3.45 – 140
J0459+0229	1.7	QSO	2.384	vs05m†	1			–
J0501−0159	1.17†	QSO	2.291	vs02z	III	0.2	0.2	0.17 – 540
J0503+0203	2.1	QSO	0.585*	vs04a†	1			–
J0508+8432	1.1	QSO		vs11h	V	0.2	0.08	0.18 – 340
J0509+0541	0.65†	VisS		vs11w	V	>0.1	0	0.25 – 140
J0513−2159	1.3	QSO	1.296	vs09l	V	0.1	0.33	0.40 – 180
J0522−3627	7.61*	G	0.055*	vs01j	V	0.4	0.08	0.25 – 380
J0525−4557	1.9	QSO	1.479	vs06a†				–
J0530+1331	1.97*	QSO	2.070	vs01o	V	0.5	0.04	0.21 – 500
J0538−4405	2.17†	QSO	0.892	vs02c	III	0.8	0.04	0.29 – 500
J0539−2839	1.64†	QSO	3.104	vs10g	III	3.5	0.02	0.29 – 500
J0541−0541	1.50†	QSO	0.839	vs07y	V	0.0	1.44	0.14 – 140
J0542+4951	8.15*	QSO	0.545	vs01p	III	>0.1	0	0.13 – 540
J0555+3948	6.03*	QSO	2.363	vs01n	III	1.6	0.16	0.41 – 460
J0607+6720	1.0	QSO	1.970	vs11v	V	>0.6	0	0.34 – 380
J0607−0834	2.15†	QSO	0.872	vs03p	III	1.2	0.03	0.69 – 420
J0609−1542	3.82†	QSO	0.324	vs02a	III	>3.8	0	1.74 – 420
J0614+6046	1.1	QSO	2.702	vs10f	V	0.3	0.09	0.29 – 340
J0626+8202	1.0	QSO	0.710	vs11u	V	0.5	0.03	0.18 – 500
J0635−7516	6.43†	QSO	0.651	vs01t	III	0.7	0.28	0.40 – 530
J0644−3459	1.0	QSO	2.165	vs10e†	1			–
J0646+4451	1.7	QSO	3.408	vs05l	V	>0.8	0	0.56 – 500
J0648−3044	1.0	QSO	1.153	vs11t	V	0.2	0.16	0.24 – 340
J0713+4349	1.42*	QSO	0.518*	vs06p	V	>0.3	0	0.22 – 300
J0714+3534	1.04*	QSO	1.620	vs09k	III	0.1	0.35	0.14 – 460
J0738+1742	1.23*	QSO	0.424*	vs05d	III	0.8	0.04	0.33 – 460
J0739+0137	1.87†	QSO	0.191	vs05c	V	0.8	0.04	0.51 – 340
J0741+3112	3.96*	QSO	0.631*	vs02k	III	1.1	0.16	0.25 – 540
J0743−6726	1.11†	QSO	1.510	vs04u	V	0.1	0.49	0.19 – 180
J0745+1011	3.35*	G	2.624*	vs02j	V	0.5	0.08	0.53 – 340

TABLE 1—*Continued*

(1) IAU Name	(2) S_5 [Jy]	(3) ID	(4) z	(5) Exp	(6) Paper	(7) T_b [10^{12} K]	(8) area [mas^2]	(9) Jy – Mλ
J0745−0044	2.0	QSO	0.994	vs04f†	1			–
J0748+2400	1.2	QSO	0.409*	vs10d	III	>0.2	0	0.46 – 420
J0750+1231	1.9	QSO	0.889	vs04k	V	0.3	0.18	0.41 – 300
J0808+4950	0.54*	QSO	1.432	vs09j	V	0.9	0.04	0.40 – 500
J0811+0146	0.91†	QSO	1.148*	vs07n	III	0.4	0.12	0.32 – 420
J0815+3635	1.0	QSO	1.025	vs10c†	1			–
J0818+4222	1.03*	QSO	0.530*	vs06g	III	1.2	0.02	0.45 – 500
J0820−1258	0.63*	QSO		vs11s	V	>0.2	0	0.27 – 180
J0824+5552	1.2	QSO	1.417	vs09i	III	0.5	0.08	0.30 – 460
J0824+3916	1.0	QSO	1.216	vs10b†	1,3			–
J0825+0309	1.58*	QSO	0.506*	vs05v	V	>4.5	0	1.02 – 300
J0831+0429	1.07*	QSO	0.174*	vs05k	V	0.1	0.25	0.24 – 220
J0836−2016	2.6	QSO	2.752	vs02y	III	0.1	0.8	0.50 – 220
J0840+1312	1.3	QSO	0.684	vs09h†	1			–
J0841+7053	2.04*	QSO	2.218	vs04e	III	>0.1	0	0.24 – 540
J0842+1835	1.0	QSO	1.272	vs10a	V	>0.1	0	0.34 – 300
J0854+5757	1.13*	QSO	1.322	vs09z	V	0.5	0.06	0.21 – 500
J0854+2006	1.81*	QSO	0.306*	vs03y	III	>0.1	0	0.31 – 460
J0903+4651	1.34*	QSO	1.462	vs09g	III	0.2	0.09	0.23 – 540
J0909+0121	1.0	QSO	1.018	vs11r	III	0.6	0.08	0.47 – 420
J0909+4253	1.5	QSO	0.670*	vs07m	V	>0.8	0	0.39 – 540
J0920+4441	1.2	QSO	2.180	vs07x	III	>0.1	0	0.33 – 500
J0921−2618	1.72†	QSO	2.300	vs04s	V	2.1	0	1.30 – 140
J0921+6215	1.5	QSO	1.446	vs06f†	1,5			–
J0927+3902	11.27*	QSO	0.698	vs01f	III	2.0	0.25	0.91 – 500
J0948+4039	2.08†	QSO	1.252	vs05u	V	>1.6	0	0.61 – 460
J0956+2515	1.3	QSO	0.712	vs07l	V	>0.5	0	0.54 – 380
J0958+4725	1.3	QSO	1.873	vs07k	V	1.1	0.09	0.83 – 340
J0958+6533	0.47*	QSO	0.368*	vs08k	V	1.7	0.01	0.33 – 540
J1014+2301	1.1	QSO	0.565	vs11g	V	0.1	0.64	0.56 – 140
J1035−2011	1.05†	QSO	2.198	vs11f	V	>0.8	0	0.33 – 460
J1037−2934	1.37†	QSO	0.312	vs05t	III	0.3	0.15	0.16 – 380
J1041+0610	1.74†	QSO	1.265	vs05j	V	0.3	0.1	0.44 – 300
J1044+8054	1.1	QSO	1.260	vs11e†	1			–
J1048−1909	1.1	QSO	0.595	vs11d	V	>3.3	0	0.67 – 540
J1048+7143	2.4	QSO	1.150	vs04j	III	2.2	0.03	1.32 – 500
J1051+2119	1.3	QSO	1.300	vs07j	V	0.4	0.04	0.33 – 300
J1051−3138	0.54†	QSO	1.429	vs09y	V	>0.2	0	0.17 – 460
J1058+0133	2.56†	QSO	0.888	vs02l	III	2.3	0.04	0.67 – 460
J1058+1951	1.7	QSO	1.110	vs06x	V	>0.0	0	0.04 – 380
J1058−8003	2.14†	QSO		vs05h	V	2.4	0.08	1.51 – 500
J1107−4449	2.93†	QSO	1.598	vs02v	III	0.4	0.28	0.16 – 460
J1118−4634	1.81†	QSO	0.713	vs05z	V	0.0	0.49	0.09 – 180
J1118+1234	2.0	QSO	2.118	vs05s	III	>0.3	0	0.51 – 500
J1125+2610	1.1	QSO	2.341	vs09f	V	0.2	0.08	0.19 – 300
J1127−1857	1.71†	QSO	1.048	vs07i	V	3.9	0.01	0.61 – 460
J1130−1449	4.15*	QSO	1.187	vs01z	V	0.8	0.16	0.56 – 380
J1146−2447	1.35†	QSO	1.940	vs06w	III	0.1	0.15	0.25 – 540

TABLE 1—*Continued*

(1) IAU Name	(2) S_5 [Jy]	(3) ID	(4) z	(5) Exp	(6) Paper	(7) T_b [10^{12} K]	(8) area [mas^2]	(9) Jy – Mλ
J1147−0724	1.2	QSO	1.342	vs09x	III	0.3	0.15	0.84 – 340
J1147−3812	2.59†	QSO	1.048	vs04d	III	1.8	0.04	0.90 – 420
J1150−0023	1.71†	QSO	1.980	vs05r	V	>0.0	0	0.16 – 140
J1153+4931	1.35*	G	0.334	vs09w	V	0.0	4.2	0.04 – 100
J1153+8058	1.4	QSO	1.250	vs06v	V	0.6	0.09	0.44 – 380
J1159+2914	2.59*	QSO	0.729	vs05b	V	2.6	0.03	1.07 – 380
J1205−2634	1.1	QSO	0.786	vs11c†	1			–
J1209−2406	1.1	QSO	1.299*	vs11b†	1			–
J1215−1731	1.95†	G		vs05a	III	2.1	0.04	0.39 – 540
J1218−4600	2.02†	QSO	0.529*	vs04h	V			–
J1219+4829	1.0	QSO	1.076	vs11a†	1			–
J1224+0330	1.00†	QSO	0.960	vs09e	V	0.5	0.04	0.16 – 380
J1224+2122	1.73*	QSO	0.435	vs06o	V	0.1	0.16	0.23 – 260
J1229+0203	0.65†	QSO	0.158	vs01b	III	0.5	0.36	0.21 – 540
J1230+1223	61.2	G	0.004*	vs01a	III	>0.2	0	0.12 – 540
J1246−0730	1.1	QSO	1.286	vs10z†	1			–
J1246−2547	1.15†	QSO	0.638	vs04r	III	0.7	0.04	0.27 – 500
J1256−0547	5.07†	QSO	0.538	vs01g	III	2.0	0.21	0.71 – 540
J1257−3155	1.79†	QSO	1.924	vs06u	V	1.3	0	0.19 – 380
J1305−1033	0.80*	QSO	0.286	vs11q	V	>0.6	0	0.44 – 420
J1309+1154	1.3	QSO		vs09d†	1			–
J1310+3220	2.79*	QSO	0.997	vs02e	III	1.2	0.04	0.58 – 460
J1316−3338	1.37†	QSO	1.210	vs05q	V	0.7	0.06	0.31 – 500
J1337−1257	3.74†	QSO	0.539	vs01y	III	1.7	0.1	1.42 – 500
J1351−1449	0.73†	VisS		vs10y	V	0.0	1	0.11 – 140
J1357+1919	2.7	QSO	0.719	vs03x	V	0.0	0.49	0.18 – 220
J1357−1744	1.16†	QSO	3.147	vs08j	III	0.3	0.09	0.15 – 500
J1405+0415	1.0	QSO	3.211	vs10x	V	>0.2	0	0.21 – 500
J1407+2827	2.45*	G	0.077*	vs03o	III	>0.1	0	0.19 – 500
J1408−0752	1.0	QSO	1.493	vs11p†	1			–
J1415+1320	1.22*	QSO	0.247*	vs09v	V	1.5	0.04	0.16 – 420
J1419−1928	1.0	G	0.120*	vs11o†	1			–
J1424−4913	4.96†	G	1.840*	vs01v	V			–
J1427−4206	3.02†	QSO	1.522	vs02i	V	1.1	0.09	0.50 – 420
J1430+1043	1.2	QSO	1.710	vs09c	III	0.2	0.22	0.39 – 460
J1435−4821	1.1	RadioS		vs10o†				–
J1436+6336	1.1	QSO	2.066	vs08i	V	>0.2	0	0.25 – 500
J1454−3747	2.4	QSO	0.314	vs03n†	1			–
J1504+1029	1.8	QSO	1.839	vs04z	V	>0.7	0	0.42 – 300
J1506+3730	1.0	G	0.671*	vs10w†	1,4			–
J1507−1652	2.70†	QSO	0.876	vs03m	III	1.0	0.05	0.70 – 460
J1510−0543	1.7	QSO	1.191	vs06t	III	0.5	0.04	0.30 – 460
J1512−0905	2.49†	QSO	0.360*	vs02x	III	2.0	0.04	0.30 – 460
J1513−1012	1.2	QSO	1.513	vs09u†	1,4			–
J1516+0015	0.92†	G	0.052*	vs07h	V	>0.7	0	0.48 – 460
J1517−2422	2.92†	G	0.049*	vs03u	III	1.1	0.09	0.47 – 540
J1522−2730	1.79†	QSO	1.294*	vs04q	V	2.9	0.03	0.18 – 500
J1540+1447	1.2	QSO	0.605	vs09t†	1,4			–

Table 1—*Continued*

(1) IAU Name	(2) S_5 [Jy]	(3) ID	(4) z	(5) Exp	(6) Paper	(7) T_b [10^{12} K]	(8) area [mas^2]	(9) Jy – Mλ
J1546+0026	1.3	G	0.550*	vs09b†	1			–
J1549+0237	2.49†	QSO	0.412	vs06e	III	1.6	0.08	0.48 – 460
J1550+0527	2.87†	QSO	1.422	vs02r	V	>3.1	0	0.98 – 300
J1556−7914	4.7	G	0.150*	vs02d†				–
J1557−0001	2.3	QSO	1.772	vs04p	V	0.4	0.04	0.19 – 500
J1602+3326	1.81*	G	1.100*	vs04y	V	>0.2	0	0.17 – 500
J1608+1029	1.53*	QSO	1.226	vs06s	V	0.1	0.2	0.04 – 420
J1613+3412	4.11*	QSO	1.401	vs02b	III	>0.9	0	0.66 – 540
J1617−7717	2.85†	QSO	1.710	vs02u	III	>0.0	0	0.47 – 340
J1624−6809	2.1	QSO	1.354	vs05g†				–
J1625−2527	1.07†	QSO	0.786	vs02h	V	1.4	0.05	0.51 – 260
J1626−2951	2.41†	QSO	0.815	vs03l	III	0.3	0.12	0.20 – 460
J1635+3808	2.47*	QSO	1.807	vs03d	III	>0.3	0	0.45 – 500
J1637+4717	1.3	QSO	0.740	vs09a†	1			–
J1638+5720	0.92*	QSO	0.751	vs06n	III	>0.0	0	0.25 – 460
J1640+3946	1.3	QSO	1.666	vs08y	III	0.5	0.12	0.30 – 420
J1640+1220	1.3	G	1.152*	vs08z†	1			–
J1642+3948	8.28*	QSO	0.594	vs01k	III	1.0	0.08	0.43 – 500
J1642+6856	1.26*	QSO	0.751*	vs07w	III	>0.0	0	0.51 – 540
J1647−6437	1.3	VisS		vs08t	V	0.1	0.27	0.25 – 180
J1653+3945	1.71*	G	0.034*	vs08h	III	0.6	0.04	0.26 – 460
J1658+4737	1.4	QSO	1.622	vs08g	V	0.5	0.09	0.33 – 380
J1658+0741	1.93†	QSO	0.621	vs07g	III	0.3	0.04	0.47 – 460
J1658+0515	1.28†	QSO	0.879	vs05i	III	0.2	0.09	0.30 – 500
J1723−6500	4.71†	G	0.014*	vs02f	III	-		0.12 – 420
J1726−6427	1.27†	RadioS		vs08s	V	>0.0	0	0.06 – 140
J1727+4530	1.3	QSO	0.714	vs07f†	1,5			–
J1733−1304	8.26†	QSO	0.902	vs01m	III	1.7	0.15	0.94 – 340
J1734+3857	1.3	QSO	0.976	vs07e†	1			–
J1740+5211	2.16*	QSO	1.379	vs10v	III	1.2	0.12	0.34 – 500
J1743−0350	4.60*	QSO	1.057	vs03k	V	>2.9	0	1.34 – 460
J1744−5144	3.87†	G	0.630*	vs02p	V	>0.0	0	0.09 – 140
J1751+0939	2.80†	QSO	0.320	vs04o	III	6.7	0.01	1.27 – 500
J1753+4409	1.0	QSO	0.871	vs11n	V	>0.4	0	0.22 – 380
J1800+7828	2.25*	QSO	0.680	vs02w	III	2.7	0.04	0.81 – 540
J1801+4404	1.1	QSO	0.663	vs10u†	1,2			–
J1806+6949	1.68*	G	0.051*	vs04x	III	0.8	0.04	0.48 – 500
J1809−4552	0.88†	G	0.070*	vs10n	V	0.5	0.05	0.26 – 460
J1819−5521	1.1	QSO		vs10m†				–
J1824+1044	1.1	QSO	1.364	vs10t	V	0.4	0.04	0.17 – 420
J1824+5651	1.61*	QSO	0.663	vs06d	III	1.0	0.06	0.67 – 420
J1832+2833	1.1	QSO	0.594	vs10s†	1			–
J1837−7108	2.26†	QSO	1.356	vs04m	V	0.5	0.18	0.58 – 380
J1842+7946	4.45*	G	0.056*	vs11m	V	0.1	0.09	0.11 – 140
J1902+3159	1.17*	QSO	0.635	vs06c	III	0.4	0.08	0.26 – 340
J1911−2006	3.39†	QSO	1.119	vs04n	V	>0.4	0	0.53 – 500
J1912−8010	0.98†	QSO	1.756	vs08r	V	0.1	0.36	0.33 – 180
J1924−2914	3.26†	QSO	0.352	vs01e	III	>0.8	0	2.04 – 420

TABLE 1—*Continued*

(1) IAU Name	(2) S_5 [Jy]	(3) ID	(4) z	(5) Exp	(6) Paper	(7) T_b [10^{12} K]	(8) area [mas^2]	(9) Jy – Mλ
J1925+2106	1.5	VisS		vs07v	V	0.4	0.2	0.42 – 420
J1927+7358	3.66*	QSO	0.303	vs02m	V	0.1	0.16	0.13 – 540
J1932−4536	0.74†	QSO	0.652*	vs11k	V	0.1	1.2	0.10 – 140
J1937−3958	0.99†	QSO	0.965	vs08f	V	0.6	0.06	0.41 – 460
J1939−6342	5.76†	G	0.183*	vs01u	V	0.1	2.25	0.11 – 140
J1939−1525	1.4	QSO	1.657	vs06m	III	1.4	0.01	0.37 – 540
J1940−6907	0.89†	QSO	3.170	vs11j	V	0.1	0.81	0.21 – 180
J1949−1957	1.3	RadioS		vs13c†	1			–
J1955+5131	1.17*	QSO	1.223	vs13d	V	0.2	0.09	0.20 – 340
J1957−3845	4.4	QSO	0.630	vs01x†	1,6			–
J2000−1748	2.31†	QSO	0.652	vs04w	III	2.5	0.06	1.16 – 460
J2003−3251	1.2	QSO	3.783	vs08x†	1			–
J2005+7752	1.35*	QSO	0.342*	vs06r	III	0.8	0.06	0.50 – 460
J2009−4849	1.19†	QSO	0.071*	vs09n	V	0.0	1.17	0.09 – 140
J2011−1546	1.4	QSO	1.180	vs07d	V	0.4	0.09	0.30 – 420
J2022+6136	2.81*	G	0.227*	vs02q	III	0.0	0.16	0.20 – 500
J2031+1219	1.2	QSO	1.215	vs08w†	1			–
J2040−2507	1.2	QSO	1.574	vs09s†	1,6			–
J2101+0341	0.64†	QSO	1.015	vs08v	III	>0.6	0	0.96 – 340
J2109−4110	2.3	QSO	1.055	vs03w†	1			–
J2110−1020	1.2	QSO		vs09r†	1			–
J2115+2933	1.2	QSO	1.514	vs09q†	1,2			–
J2123+0535	0.88†	QSO	1.941	vs03c	V	0.5	0.06	0.37 – 380
J2129−1538	1.19†	QSO	3.280	vs08e	III	>0.2	0	0.16 – 380
J2131−1207	3.0	QSO	0.501	vs13e†	1,4			–
J2134−0153	2.0	QSO	1.284	vs05p†	1,2			–
J2136+0041	9.19†	QSO	1.932	vs01h	III	2.5	0.05	0.73 – 380
J2139+1423	1.65*	QSO	2.427	vs04c	V	>0.2	0	0.29 – 220
J2147+0929	1.1	QSO	1.113	vs10r†	1,2			–
J2148+0657	6.21†	QSO	0.999	vs01l	V	1.0	0.27	1.79 – 300
J2151+0552	0.85*	G	0.740	vs10q	V	>0.1	0	0.17 – 420
J2152−7807	1.16†	QSO		vs10l	V	0.2	0.27	0.36 – 140
J2158−1501	1.94†	QSO	0.672	vs03g	III	>0.2	0	0.52 – 380
J2202+4216	4.52*	QSO	0.069*	vs01q	III	3.1	0.01	0.27 – 540
J2207−5346	1.31†	QSO	1.206	vs08d	V	>0.7	0	0.36 – 460
J2212+2355	1.30*	QSO	1.125	vs06l	III	1.4	0.03	0.84 – 220
J2218−0335	2.11†	QSO	0.901	vs03j	V	0.1	0.39	1.02 – 460
J2225−0457	5.51†	QSO	1.404	vs01s	III	2.3	0.08	1.54 – 340
J2229−0832	0.85†	QSO	1.562	vs04i	III	0.4	0.04	0.20 – 500
J2232+1143	4.76*	QSO	1.037	vs01w	V	0.6	0.16	0.86 – 260
J2235−4835	1.1	QSO	0.510	vs10k†				–
J2236+2828	1.6	QSO	0.795	vs07c	V	0.6	0.15	0.30 – 460
J2239−5701	0.70†	VisS		vs10p	V	0.1	0.36	0.41 – 140
J2246−1206	2.06†	QSO	0.630	vs03v	V	>0.4	0	0.21 – 300
J2253+1608	12.23*	QSO	0.859	vs01d	III	2.3	0.16	0.71 – 420
J2258−2758	3.48†	QSO	0.927	vs03f	V	4.1	0.04	1.50 – 500
J2320+0513	1.41†	QSO	0.623	vs09p	III	0.2	0.06	0.22 – 500
J2329−4730	1.65†	QSO	1.306	vs04t	III	>0.3	0	0.41 – 460

TABLE 1—*Continued*

(1) IAU Name	(2) S_5 [Jy]	(3) ID	(4) z	(5) Exp	(6) Paper	(7) T_b [10^{12} K]	(8) area [mas^2]	(9) Jy – Mλ
J2331−1556	1.25†	QSO	1.153	vs06b	III	>0.2	0	0.49 – 380
J2336−5236	1.60†	QSO		vs07b	V	0.1	1.44	0.13 – 140
J2341−5816	1.1	G	0.640*	vs10j†				–
J2348−1631	2.6	QSO	0.576	vs03b	III	>0.2	0	0.91 – 300
J2357−5311	1.42†	QSO	1.006	vs06j	V	0.6	0.09	0.25 – 500
J2358−1020	0.60†	QSO	1.622	vs06k	V			0.15 – 500

NOTE.—Column (2): Total flux density, from Tingay et al. (2003) where marked with a †, where marked with a * from UMRAO, otherwise as given by NED. Column (3): ID class listed in NED, where QSO – quasar, G – galaxy, RadioS – radio source, and VisS – visual source. Column (4): Redshift measurement from Véron-Cetty & Véron (2006), except where marked with a *, in which case it is from NED. Column (5): VSOP experiment code (if not observed marked with †), Column (6): Paper in which the results are to be found (III or V), or, if not observed, other images to be found in: 1=Fomalont et al. (2000b), 2=Kellermann et al. (1998), 3=Fey & Charlot (2000), 4=Zensus et al. (2002), 5=Ojha et al. (2004), 6=Lister & Homan (2005) Column (7): Observer frame brightness temperature, or lower limit, Column (8): Detected core area in mas^2 (point sources being 0). Column (9): Flux density (in Jy) remaining at the longest baselines, and the length of that baseline (in Mλ).

Table 2

Survey Experiment Details

(1)	(2)	(3)	(4)	(5)	(6)	(7)	(8)	(9)	(10)	(11)
Source Names		Obs. Code	Obs. Date (yyyy-mmm-dd)	GRTs	TSs	Time On Src. (hh:mm)	HALCA Time On Src. (hh:mm)	Corr.	ID	z
J2000	B1950									
J0013+4051	0010+405	vs13a	2002 Jul 23	KRN	U	04:40	04:00	P	g	0.256
J0105+4819	0102+480	vs08q	2002 Jan 17	URP	T	03:10	03:10	S	e	
J0108+0135	0106+013	vs02t	2002 Jul 13	NHR	U	03:00	02:30	M	q	2.107
J0116−1136	0113−118	vs06h	2001 Jul 15	SHC	U	03:50	00:00	P	q	0.672
J0121+0422	0119+041	vs05y	1998 Aug 01	GH	R	03:15	02:00	P	q	0.637
J0125−0005	0122−003	vs05x	2002 Jul 16	NR	U	02:20	02:20	M	q	1.070
J0141−0928	0138−097	vs10i	2002 Jan 11	CKMS	T	05:45	04:20	P	b	0.733*
J0149+0555	0146+056	vs06z	2001 Jul 27	CRMS	UR	09:00	05:00	P	q	2.345
J0152+2207	0149+218	vs08n	2002 Jan 19	CHKRMS	T	04:20	04:10	P	q	1.320
J0204+1514	0202+149	vs03i	2002 Jul 28	HR	U	04:15	03:30	M	q	0.405*
J0204−1701	0202−172	vs08b	2002 Jan 15	CHKRMS	U	06:00	02:30	P	q	1.740
J0217+0144	0215+015	vs07r	1998 Aug 03 + 2002 Jul 20	H+HRN	R+0	03:40	03:00	PM	b	1.715
J0224+0659	0221+067	vs12b	2002 Jan 21	MHCS	T	05:00	04:30	P	q	0.511*
J0231+1322	0229+131	vs04l	2002 Feb 02	SMTC	T	04:30	02:00	P	q	2.065
J0237+2848	0234+285	vs02s	1999 Aug 14	mskb	RN	09:30	06:30	S	q	1.207
J0239+0416	0237+040	vs11i	2002 Jul 31	NHR	U	03:50	03:20	M	q	0.978
J0242+1101	0239+108	vs05w	2002 Jan 29	CRMSU	U	04:00	04:00	P	q	2.694*
J0253−5441	0252−549	vs09o	2002 Dec 23	THM	U	03:10	01:10	P	q*	0.537
J0259+0747	0256+075	vs12a*	2001 Feb 07	mpos	T	05:20	03:00	S	b	0.893
J0303−6211	0302−623	vs04v	2001 Jun 08	MH	U	01:50	01:40	P	q*	
J0309−6058	0308−611	vs08u	2001 Jun 04	HM	R	04:30	02:45	P	q*	
J0312+0133	0310+013	vs11z	2002 Jan 31	CMKRS	U	08:00	05:00	P	q	0.664
J0321+1221	0319+121	vs07p	2001 Feb 14	MKS	T	04:00	02:00	P	q	2.670
J0336+3218	0333+321 NRAO140	vs05f	2002 Aug 25	SK	U	02:40	00:30	M	q	1.259
J0339−0146	0336−019 CTA26	vs03q	2002 Feb 17	TMK	U	05:00	03:00	P	q	0.852
J0359+5057	0355+508 NRAO150	vs01i	2000 Aug 31	bhkm	GR	09:00	00:30	M	q*	
J0402−3147	0400−319	vs11y	2002 Feb 12	CKM	U	04:30	02:00	P	q	1.288
J0403+2600	0400+258	vs11x*	2001 Aug 23	CMS	U	04:15	04:00	P	q	2.109
J0406−3826	0405−385	vs07o*	1999 Sep 15	fpsm	R	04:50	02:50	S	q	1.285
J0414+0534	0411+341	vs13b	2002 Aug 27	KS		03:40	00:00	P	q	2.639
J0416−1851	0414−189	vs08a	1999 Sep 13	KMH		04:00	00:00	M	q*	1.536
J0424+0036	0422+004	vs07z	2001 Feb 17	KMS	T	02:50	01:50	M	b	0.310*
J0424−3756	0422−380	vs06y	1999 Feb 20	HKMS	T	05:00	02:00	P	q	0.782
J0428−3756	0426−380	vs05e	2002 Feb 14	KMT	U	04:20	03:10	P	b	1.112
J0433+0521	0430+052 3C120	vs02n	1999 Feb 11	sOGN	R	03:00	02:30	S	g	0.033*
J0437−1844	0434−188	vs09m	2002 Feb 22	MK	U	01:30	01:30	P	q	2.702
J0442−0017	0440−003 NRAO190	vs03h	2002 Mar 01	HMT		05:00	00:00	P	Q	0.844
J0449+1121	0446+112	vs10h	1999 Dec 10	TMSHK		11:00	00:00	PM	g	1.207*
J0450−8101	0454−810	vs08l	2001 May 07	MCH	U	11:00	05:00	P	q*	0.444*
J0508+8432	0454+844	vs11h	2002 Sep 22	SU	U	04:30	04:30	M	b	
J0509+0541	0506+056	vs11w	2002 Sep 11	KMST		02:45	00:00	P	b	
J0513−2159	0511−220	vs09l	2002 Feb 24	USMH		04:00	00:00	P	q*	1.296

TABLE 2—*Continued*

(1)	(2)	(3)	(4)	(5)	(6)	(7)	(8)	(9)	(10)	(11)
Source Names		Obs. Code	Obs. Date (yyyy-mmm-dd)	GRTs	TSs	Time On Src. (hh:mm)	HALCA Time On Src. (hh:mm)	Corr.	ID	z
J2000	B1950									
J0522−3627	0521−365	vs01j	2001 Sep 11	CfkmM	TN	07:10	03:00	P	g*	0.055*
J0530+1331	0528+134	vs01o	1999 Dec 17	bflmp	RN	08:50	03:20	S	q	2.070
J0541−0541	0539−057	vs07y	2002 Mar 10	SMT	U	05:00	00:00	P	q	0.839
J0607+6720	0602+673	vs11v	2002 Sep 25	KS	U	01:40	01:20	M	q*	1.970
J0614+6046	0609+607	vs10f	2002 Sep 19	KS	U	04:50	02:00	M	q	2.702
J0626+8202	0615+820	vs11u	1999 Sep 18	EOSI	RN	08:30	06:30	S	q	0.710
J0646+4451	0642+449	vs05l	1999 Mar 26	Ebkh	GR	08:50	06:00	S	q	3.408
J0648−3044	0636−306	vs11t*	2001 Oct 06	fmpn	N	04:45	02:00	S	q	1.153
J0713+4349	0710+439	vs06p	2000 Oct 02 + 2002 Apr 10	U+HR	U+0	05:00	01:00	MP	q	0.518*
J0739+0137	0736+017	vs05c	1999 Apr 03	MS	T	05:50	04:20	P	q	0.191
J0743−6726	0743−673	vs04u	1999 Jul 21	THM		04:00	00:00	P	q*	1.510
J0745+1011	0742+103	vs02j	1999 Apr 26	HGX	NT	05:30	04:10	P	q*	2.624*
J0750+1231	0748+126	vs04k	2002 Apr 14	KTM	U	04:50	03:30	M	q	0.889
J0808+4950	0804+499	vs09j*	2000 Oct 12	snhb	TR	08:40	02:40	S	q	1.432
J0820−1258	0818−128	vs11s	2002 Apr 27	KTM	U	03:40	01:15	P	b	
J0825+0309	0823+033	vs05v	1999 Apr 28	HTUM	R	04:30	03:30	PM	b	0.506*
J0831+0429	0829+046	vs05k	2002 Apr 29	TM	U	04:40	03:20	M	b	0.174*
J0842+1835	0839+187	vs10a	2002 May 04	TMK	U	01:00	01:00	P	q	1.272
J0854+5757	0850+581	vs09z*	2000 Oct 26	bhmn	R	04:00	01:45	S	q	1.322
J0909+4253	0906+432 3C216	vs07m*	1999 Feb 15	EGPJ	GT	04:30	02:25	S	q*	0.670*
J0921−2618	0919−260	vs04s	2002 Dec 02	KST	U	04:00	00:00	P	q	2.300
J0948+4039	0945+408	vs05u*	2000 Oct 30	bhns	R	04:00	01:50	S	q	1.252
J0956+2515	0953+254 OK290	vs07l	1999 Apr 29	HNG	R	04:30	02:45	P	q	0.712
J0958+4725	0955+476	vs07k	2002 Nov 07	KU	U	03:30	03:30	P	q	1.873
J0958+6533	0954+658	vs08k	2000 Oct 20	sEnshf	R	10:50	02:30	S	b	0.368*
J1014+2301	1012+232	vs11g	1999 May 19	MTKS		06:00	00:00	M	q	0.565
J1035−2011	1032−199	vs11f	1998 Feb 21	HMTU	G	04:00	02:00	P	q	2.198
J1041+0610	1038+064	vs05j	2002 Jun 06	UT	U	05:00	04:45	M	q	1.265
J1048−1909	1045−188	vs11d	2001 Dec 14	HMS	RTN	07:00	01:50		q	0.595
J1051+2119	1049+215	vs07j	2001 Dec 01	MKSR	T	05:15	00:40	P	q	1.300
J1051−3138	1048−313	vs09y*	1999 May 20	smhp	G	03:45	02:00	S	e	1.429
J1058+1951	1055+201	vs06x	2001 Dec 03	MR		03:10	00:00	P	q	1.110
J1058−8003	1057−797	vs05h*	2001 Mar 20	MH	U	03:50	02:30	P	q*	
J1118−4634	1116−462	vs05z	1999 Jul 22 + 2002 Jul 03	HT+HTSM		03:15	00:00	P	q*	0.713
J1125+2610	1123+264	vs09f	2001 Dec 05	SMR	T	04:30	00:30	P	q	2.341
J1127−1857	1124−186	vs07i	2001 Dec 20	CMS	TR	05:50	01:50		q	1.048
J1130−1449	1127−145	vs01z	2002 Jun 12	TM	U	03:30	02:20	P	q*	1.187
J1150−0023	1148−001	vs05r	2002 Jun 14	MTK		03:30	00:00	M	q	1.980
J1153+4931	1150+497	vs09w	2001 Dec 08	SRK		01:00	00:00	P	q	0.334
J1153+8058	1150+812	vs06v	2002 Oct 12	SK	U	04:30	00:15	P	q	1.250
J1159+2914	1156+295	vs05b*	2001 Dec 12	mlsn	T	03:15	01:30	S	q	0.729
J1218−4600	1215−457	vs04h	1999 Jul 04+1998 Feb 01			00:00	00:00	P	q*	0.529*

Table 2—*Continued*

(1) Source Names J2000	(2) B1950	(3) Obs. Code	(4) Obs. Date (yyyy-mmm-dd)	(5) GRTs	(6) TSs	(7) Time On Src. (hh:mm)	(8) HALCA Time On Src. (hh:mm)	(9) Corr.	(10) ID	(11) z
J1224+0330	1222+037	vs09e	2002 Jun 27	UTM	U	03:00	03:00	P	q	0.960
J1224+2122	1222+216	vs06o	2001 Dec 18	CKMS	T	02:50	00:50	P	q	0.435
J1257−3155	1255−316	vs06u	1999 May 25	TSH	R	04:30	03:00	M	q	1.924
J1305−1033	1302−102	vs11q	1998 Jan 07	HM	TG	05:30	03:45	P	q	0.286
J1316−3338	1313−333	vs05q	1998 Jan 20	MKSHU	G	05:30	01:15	P	q	1.210
J1351−1449	1349−145	vs10y	1999 Jun 04	STM		07:30	00:00	P	e	
J1357+1919	1354+195	vs03x	1999 Jul 19	XN	N	02:20	00:40	P	q	0.719
J1405+0415	1402+044	vs10x	2001 Jan 20	snhY	R	06:30	03:00	S	q	3.211
J1415+1320	1413+135	vs09v	1998 Jul 29	pkmf	RN	8:00	2:00	S	b	0.247*
J1424−4913	1421−490	vs01v	2002 Aug 15			00:00	00:00	P	e*	1.840*
J1427−4206	1424−418	vs02i*	1999 Aug 01	mkpls	G	04:30	02:45	S	q	1.522
J1436+6336	1435+638	vs08i	2001 Jun 21	KUS	N	04:10	02:10	M	q	2.066
J1504+1029	1502+106	vs04z	2000 Jul 27	HTRMS	RT	11:00	02:40	P	q	1.839
J1516+0015	1514+004	vs07h	1998 Apr 28	TK	N	00:00	01:10	P	g	0.052*
J1522−2730	1519−273	vs04q	1999 Feb 05	Afop	R	03:30	01:40	S	b	1.294*
J1550+0527	1548+056	vs02r	2003 Aug 21	MT	U	03:45	03:30	M	q	1.422
J1557−0001	1555+001	vs04p	1998 Jun 13	NSH	G	03:40	00:50	P	q	1.772
J1602+3326	1600+335	vs04y	1998 Aug 01	XGH	R	05:10	02:10	P	g	1.100*
J1608+1029	1606+106	vs06s	1998 Aug 02	XGH	R	02:00	02:00	P	q	1.226
J1625−2527	1622−253	vs02h	2000 May 22	SCM	U	06:00	00:50	P	g	0.786
J1647−6437	1642−645	vs08t	1999 Apr 02 + 2002 Mar 25	HM+CHT	T+0	07:00	00:20	P	g*	
J1658+4737	1656+477	vs08g	1999 Aug 28	N	N	04:00	04:00	M	q	1.622
J1726−6427	1722−644	vs08s	2003 Sep 27	HT		03:40	00:00	M	e*	
J1743−0350	1741−038	vs03k	1998 Apr 06	STM	UG	05:30	04:30	P	q	1.057
J1744−5144	1740−517	vs02p	2003 Sep 18	HT		01:20	00:00	M	g*	0.630*
J1753+4409	1751+441	vs11n	2002 Oct 03	U	U	00:00	03:20	M	q	0.871
J1809−4552	1806−458	vs10n	2003 Oct 02	TH	U	04:45	04:30	M	g*	0.070*
J1824+1044	1821+107	vs10t	1998 Jul 08	XG	N	03:00	02:30	P	q	1.364
J1837−7108	1831−711	vs04m	1999 May 14	HTM	U	05:00	00:20	P	q*	1.356
J1842+7946	1845+797 3C390.3	vs11m*	1998 Aug 06	spnm		05:00	00:00	S	G	0.056*
J1911−2006	1908−201	vs04n	2000 Jul 01	HC	U R	04:00	03:10	P	Q	1.119
J1912−8010	1903−802	vs08r	2002 Mar 30	HT		03:40	00:00	P	q*	1.756
J1925+2106	1923+210	vs07v	2002 Oct 19	MTUS	U	01:45	01:30	P	e*	
J1927+7358	1928+738 4C+73.18	vs02m	1997 Dec 16	Epm	T	04:00	04:00	S	q	0.303
J1932−4546	1929−457	vs11k	2003 Oct 06	TH		04:00	00:00	M	q*	0.652*
J1937−3958	1933−400	vs08f	1998 Jun 12	HS	T G	06:30	05:30	P	q	0.965
J1939−6342	1934−638	vs01u	1999 Apr 22	HT		01:50	00:00	P	g*	0.183*
J1940−6907	1935−692	vs11j*	1999 Mar 30	THM		08:30	00:00	P	q*	3.170
J1955+5131	1954+513	vs13d	2002 Oct 23	US	U	03:00	03:20	P	q	1.223
J2009−4849	2005−489	vs09n	2003 Oct 11	HTM		02:30	00:00	M	q*	0.071*
J2011−1546	2008−159	vs07d	1997 Oct 25	HUT	R	04:00	01:45	M	q	1.180
J2123+0535	2121+053	vs03c	1997 Nov 25	MAU	T	05:30	02:00	M	q	1.941

Table 2—*Continued*

(1) Source Names J2000	(2) B1950	(3) Obs. Code	(4) Obs. Date (yyyy-mmm-dd)	(5) GRTs	(6) TSs	(7) Time On Src. (hh:mm)	(8) HALCA Time On Src. (hh:mm)	(9) Corr.	(10) ID	(11) z
J2139+1423	2136+141	vs04c	1998 May 28	XHG	R	05:00	02:50	P	q	2.427
J2148+0657	2145+067	vs01l*	1998 May 15	NHTS	GNTU	09:00	07:00	M	q	0.999
J2151+0552	2149+056	vs10q	2000 Nov 21	bmsl	T	04:00	01:30	S	g	0.740
J2152−7807	2146−783	vs10l	2002 Apr 01	THM	U	03:20	00:00	P	q*	
J2207−5346	2204−540	vs08d	2002 May 14	TMH	U	04:20	02:15	P	q*	1.206
J2218−0335	2216−038	vs03j	1997 Dec 03	CMU	RNTU	03:30	02:00	P	q	0.901
J2232+1143	2230+114 CTA102	vs01w*	1998 May 25	lnms	N	04:30	04:00	S	Q	1.037
J2236+2828	2234+282	vs07c	1999 Jul 24	HN	T	03:45	02:20	P	q	0.795
J2239−5701	2236−572	vs10p	2002 May 17	TH		01:00	00:00	P	q*	
J2246−1206	2243−123	vs03v	1998 Jun 03	MS	NU	06:40	05:00	P	q	0.630
J2258−2758	2255−282	vs03f	1999 May 18	spmbMT	R	03:20	02:30	S	q	0.927
J2336−5236	2333−528	vs07b	2002 May 25	HTM	U	03:00	00:00	P	q*	
J2357−5311	2355−534	vs06j	2002 May 29	THM	U	02:50	01:45	P	q*	1.006
J2358−1020	2355−106	vs06k	2000 Dec 10	AHTMN	R	04:30	03:30	P	q*	1.622

Note.—Col. (1): J2000 name,
Col. (2): Other names,
Col. (3): Experiment code, if appended by an asterisk (*) also a GOT experiment.
Col. (4): Starting date of the observation. If experiments from different epochs were merged both dates are provided.
Col. (5): Ground radio telescopes to which fringes were successfully obtained. Lower case letters indicate VLBA GRTs: b=Brewster, f=Fort Davis, h=Hancock, k=Kitt Peak, l=Los Alamos, m=Mauna Kea, n=North Liberty, o=Owens Valley, p=Pie Town, s=St. Croix. Upper Case letters indicate other GRTs: X=Arecibo, A=ATCA, C=Ceduna, E=Effelsburg, I=Medicina, G=Green Bank 140′, H=Hartebeesthoek, T=Hobart, J=Jodrell Bank MkII, R=Kalyazin, K=Kashima, N=Noto, M=Mopra, O=Onsala, S=Sheshan, P=Torun, U=Usuda, Y=VLA
Col. (6): Tracking Stations to which fringes were successfully obtained: G=Goldstone, N=Green Bank, R=Robledo, T=Tidbinbilla, U=Usuda
Col. (7): Approximate time on source over which fringes were found
Col. (8): Approximate time on source over which fringes were found on space baselines
Col. (9): Correlator: M=Mitaka, P=Penticton, S=Socorro
Col. (10):Optical classification: q – quasar, b – BL Lac object, g – AGN other than b and q (e.g. Seyfert galaxy), e – empty field or unidentified optical counterpart; from Véron-Cetty & Véron (2006) unless appended by an asterisk (*) in which case it is from NED
Col. (11): Redshift from Véron-Cetty & Véron (2006) unless appended by an asterisk (*) in which case it is from NED.

Table 3

Source Component Parameters

Source	S (Jy)	Rad (mas)	ϕ ($^\circ$)	$\theta_{\rm maj}$ (mas)	$\theta_{\rm min}$ (mas)	P.A. ($^\circ$)	$T_b/10^{12}$ (K)	$T_b/10^{12}$ (K)
J0013+4051	0.19	0.1	143	0.1	0.1	...	1.29	0.32
	0.11	0.4	-34	0.2	0.2	...		
J0105+4819	0.29	0.0	...	0.2	0.2	...	0.32	0.18*
J0108+0135	1.35	0.1	-5	0.2	0.2	...	1.71	4.03
	0.73	0.6	-108	0.4	0.4	...		
J0116−1136	0.65	0.0	...	0.8	0.2	-35	0.21	0.25
	0.05	1.0	-41	0.6	0.6	...		
J0121+0422	0.76	0.0	...	0.4	0.1	-55	0.79	0.86
	0.07	0.7	96	0.0	0.0	...		
J0125−0005	0.50	0.1	0	0.3	0.3	...	0.29	0.34
	0.36	0.8	-85	0.9	0.4	90		
J0141−0928	0.93	0.0	...	0.4	0.3	54	0.48	0.64
J0149+0555	1.00	0.0	...	0.3	0.1	-51	1.87	4.70
	0.59	0.9	113	0.7	0.4	-47		
J0152+2207	0.49	0.0	...	0.4	0.1	13	0.44	0.66
	0.03	0.3	-24	0.0	0.0	...		
J0204+1514	1.39	0.1	-20	0.2	0.2	...	2.60	2.35
	0.27	0.4	156	0.2	0.2	...		
J0204−1701	0.61	0.0	...	0.6	0.3	16	0.16	0.34
	0.11	1.0	-3	0.0	0.0	...		
J0217+0144	0.34	0.1	49	0.0	0.0	...	>	3.26
	0.21	0.1	38	0.8	0.8	...		
J0224+0659	0.37	0.0	...	0.3	0.3	...	0.25	0.18
	0.07	0.9	-68	0.5	0.5	...		
J0231+1322	1.23	0.0	...	0.4	0.4	...	0.37	0.91
	0.17	1.4	24	0.3	0.3	...		
J0237+2848	0.54	0.2	150	0.0	0.0	...	>	1.59
	0.63	0.1	-41	0.2	0.2	...		
	0.42	3.8	-13	3.8	1.7	-11		
J0239+0416	0.22	0.1	164	0.2	0.2	...	0.47	0.37
	0.12	1.1	-49	0.4	0.4	...		
J0242+1101	0.36	0.2	41	0.2	0.2	...	0.65	1.46
	0.05	0.4	118	0.3	0.3	...		
J0253−5441	0.92	0.1	-54	0.3	0.3	...	0.53	0.69
J0442−0017	2.21	0.0	...	1.1	1.1	...	0.10	0.16
J0449+1121	1.14	0.2	-93	0.0	0.0	...	>	3.16
	1.06	0.3	84	0.2	0.2	...		
J0450−8101	0.68	0.0	...	0.1	0.1	...	2.24	1.01
	0.32	0.3	47	0.2	0.2	...		
	0.15	0.5	-148	0.0	0.0	...		
J0508+8432	0.23	0.0	...	0.4	0.2	-18	0.19	0.09*
J0509+0541	0.33	0.2	-92	0.0	0.0	...	>	0.07*
	0.14	3.3	104	1.1	1.1	...		
	0.10	0.9	-174	0.0	0.0	...		
J0259+0747	0.44	0.1	170	0.8	0.2	-28	0.14	0.18
J0303−6211	1.68	0.0	...	0.6	0.4	76	0.38	0.32*
	0.15	1.1	82	0.0	0.0	...		
J0309−6058	0.33	0.3	35	0.1	0.1	...	0.92	0.25*
	0.63	0.2	-143	0.2	0.2	...		
J0312+0133	0.23	0.0	...	0.1	0.1	...	1.14	0.50
	0.05	1.1	91	1.1	0.3	90		
J0321+1221	0.20	0.9	-167	0.0	0.0	...	>	1.68
	1.46	0.0	...	0.9	0.5	-33		
J0336+3218	0.50	0.1	-1	0.4	0.4	...	0.14	0.21
J0339−0146	1.13	0.2	-131	0.2	0.2	...	1.52	1.24
	1.05	0.7	51	1.1	0.7	39		
J0359+5057	1.51	0.1	158	1.1	0.5	-86	0.16	0.14*
	0.27	2.7	44	2.5	1.1	50		
J0402−3147	0.49	0.0	...	0.3	0.3	...	0.27	0.23
	0.09	1.2	-38	1.4	1.4	...		
J0403+2600	0.58	0.1	28	0.3	0.3	...	0.27	0.49
	0.12	2.0	93	1.0	1.0	...		
J0406−3826	0.62	0.2	146	0.2	0.2	...	1.34	1.14
	0.15	0.6	-87	0.3	0.3	...		
J0414+0534	0.09	0.0	...	1.6	1.6	...	0.00	0.00
J0416−1851	0.20	0.0	...	0.5	0.5	...	0.03	0.05
J0424+0036	0.57	0.0	...	0.2	0.2	...	0.99	0.53
	0.07	0.8	-14	0.0	0.0	...		
J0424−3756	1.32	0.0	...	0.5	0.1	57	1.84	2.34
	0.33	3.7	83	1.6	1.6	...		
J0428−3756	0.68	0.0	...	0.4	0.4	...	0.24	0.25
	0.14	1.1	108	1.2	1.2	...		
J0433+0521	0.36	0.0	...	0.0	0.0	...	>	0.20
	1.12	0.6	-129	0.3	0.3	...		
	1.89	1.4	-122	0.4	0.4	...		
	0.92	4.1	-114	0.7	0.7	...		
J0437−1844	0.62	0.1	138	0.7	0.7	...	0.08	0.19
	0.35	1.1	-41	0.6	0.6	...		
	0.62	29.2	92	5.4	0.9	72		
J0745+1011	0.81	0.0	...	0.4	0.2	-23	0.51	1.48
	0.44	1.3	-177	0.6	0.6	...		
	0.86	1.5	-14	2.0	2.0	...		
J0750+1231	1.06	0.0	...	0.6	0.3	76	0.34	0.37
	0.40	1.8	116	0.9	0.9	...		
J0808+4950	0.57	0.1	-35	0.2	0.2	...	0.95	1.38
	0.15	1.1	134	1.2	1.2	...		
	0.06	0.4	25	0.0	0.0	...		
J0820−1258	0.27	0.1	-112	0.0	0.0	...	>	0.16*

TABLE 3—*Continued*

Source	S (Jy)	Rad (mas)	ϕ (°)	$\theta_{\rm maj}$ (mas)	$\theta_{\rm min}$ (mas)	P.A. (°)	$T_b/10^{12}$ (K)	$T_b/10^{12}$ (K)
J0513−2159	0.51	0.1	138	1.1	0.3	-37	0.08	0.15
J0522−3627	0.80	0.0	...	0.4	0.2	-33	0.42	0.30
	0.28	1.1	-47	0.6	0.6	...		
	0.11	0.7	142	0.0	0.0	...	>	0.16
J0530+1331	0.23	0.4	-116	0.2	0.2	...	0.48	0.41
	1.77	0.0	...	1.1	0.3	22		
	0.60	1.7	28	1.3	1.3	...		
J0541−0541	0.85	0.0	...	1.2	1.2	...	0.03	0.05
J0607+6720	0.43	0.1	-19	0.0	0.0	...	>	1.69
	0.24	0.3	153	0.0	0.0	...		
J0614+6046	0.33	0.1	167	0.3	0.3	...	0.27	0.39
J0626+8202	0.35	0.1	26	0.3	0.1	-59	0.49	0.49
	0.19	0.5	-158	0.8	0.8	...		
	0.07	0.5	-161	0.0	0.0	...		
J0646+4451	0.32	0.2	-75	0.0	0.0	...	>	3.30
	1.66	0.0	...	0.4	0.2	-81		
J0648−3044	0.52	0.1	-108	0.4	0.4	...	0.22	0.20
	0.18	1.5	121	4.0	3.4	63		
	0.11	0.8	92	0.5	0.5	...		
J0713+4349	0.20	0.0	...	0.0	0.0	...	>	0.41
J0739+0137	0.60	0.1	131	0.2	0.2	...	0.82	0.42
	0.26	0.4	-49	0.4	0.4	...		
	0.12	2.1	-64	0.9	0.9	...		
J0743−6726	0.61	0.2	54	0.7	0.7	...	0.06	0.13
J1014+2301	0.99	0.2	74	0.8	0.8	...	0.08	0.10
J1035−2011	0.35	0.0	...	0.0	0.0	...	>	2.45
J1041+0610	0.51	0.0	...	0.5	0.2	-17	0.28	0.38
	0.39	1.6	157	0.5	0.3	7		
J1048−1909	0.63	0.0	...	0.0	0.0	...	>	5.30
	0.36	0.7	165	1.2	0.2	-7		
	0.24	2.5	166	1.4	0.8	-27		
J1051+2119	0.23	0.1	-55	0.2	0.2	...	0.39	0.31
	0.59	0.9	115	1.0	0.6	-80		
J1051−3138	0.12	0.0	...	0.0	0.0	...	>	0.38
	0.20	0.2	-163	0.8	0.8	...		
	0.10	1.2	-141	0.5	0.5	...		
J1058+1951	0.07	0.0	...	0.0	0.0	...	>	0.03
J1058−8003	2.43	0.0	...	0.4	0.2	-75	2.35	1.90*
J1118−4634	0.27	0.0	...	0.7	0.7	...	0.03	0.04
J1125+2610	0.33	0.0	...	0.8	0.1	-55	0.18	0.34
J1127−1857	0.61	0.1	-26	0.1	0.1	...	3.88	1.66
	0.28	0.6	-165	0.2	0.2	...		
J1130−1449	1.89	0.0	...	0.4	0.4	...	0.78	1.32
	1.68	1.0	87	1.2	0.6	73		
	0.08	1.0	80	0.4	0.4	...		
J0825+0309	0.90	0.0	...	0.0	0.0	...	>	6.78
J0831+0429	0.71	0.1	-42	0.5	0.5	...	0.13	0.09
	0.39	1.7	66	3.1	3.1	...		
J0842+1835	0.12	0.0	...	0.0	0.0	...	>	0.17
	0.40	0.6	-3	0.3	0.3	...		
J0854+5757	0.66	0.1	-18	0.3	0.2	-28	0.46	0.83
	0.23	1.7	155	2.1	0.7	-36		
	0.07	7.2	152	2.1	0.9	-12		
	0.08	0.7	-28	0.0	0.0	...		
J0909+4253	0.35	0.1	-30	0.0	0.0	...	>	1.29
	0.28	0.2	154	0.2	0.2	...		
	0.06	0.7	128	0.0	0.0	...		
J0921−2618	1.71	0.0	...	0.9	0.0	-69	2.07	6.13
J0948+4039	0.70	0.1	-18	0.0	0.0	...	>	3.69
	0.99	0.4	90	0.8	0.3	-39		
	0.16	1.3	91	1.0	0.2	-31		
J0956+2515	0.37	0.1	51	0.0	0.0	...	>	0.79
	1.00	0.1	-150	1.1	0.5	43		
	0.45	1.0	-101	0.9	0.9	...		
J0958+4725	1.94	0.0	...	0.3	0.3	...	1.15	2.57
J0958+6533	0.27	0.1	131	0.1	0.1	...	1.69	0.46
	0.13	0.4	-39	0.1	0.1	...		
	0.03	1.8	-41	0.9	0.9	...		
J1305−1033	0.49	0.0	...	0.0	0.0	...	>	0.79
J1316−3338	0.65	0.0	...	0.3	0.2	82	0.72	0.90
	1.00	0.6	-106	1.4	0.7	71		
J1351−1449	0.49	0.1	73	1.0	1.0	...	0.02	0.02*
J1357+1919	0.19	0.0	...	0.7	0.7	...	0.02	0.02
	0.81	2.4	151	0.8	0.5	-43		
	0.17	5.0	147	1.4	1.4	...		
J1405+0415	0.17	0.0	...	0.0	0.0	...	>	0.93
	0.71	0.0	...	0.8	0.4	-47		
	0.01	3.2	-63	0.5	0.5	...		
	0.05	8.8	-45	0.6	0.6	...		
J1415+1320	0.92	0.0	...	0.4	0.1	58	1.52	1.51
	0.12	1.9	-112	2.7	2.7	...		
J1427−4206	1.37	0.0	...	0.3	0.3	...	1.12	1.98
	0.53	0.9	61	1.7	0.5	65		
	0.48	1.1	31	0.4	0.4	...		
J1436+6336	0.12	0.0	...	0.0	0.0	...	>	0.47
	0.83	1.0	17	0.8	0.4	72		
	0.14	3.0	-114	0.5	0.5	...		
J1504+1029	0.56	0.1	-69	0.0	0.0	...	>	2.12

Table 3—*Continued*

Source	S (Jy)	Rad (mas)	ϕ (°)	$\theta_{\rm maj}$ (mas)	$\theta_{\rm min}$ (mas)	P.A. (°)	$T_b/10^{12}$ (K)	$T_b/10^{12}$ (K)
	0.50	16.6	45	2.3	0.7	0		
J1150−0023	0.13	0.7	91	0.0	0.0	...	>	0.08
J1153+4931	0.96	0.0	...	2.8	1.5	26	0.01	0.01
J1153+8058	0.81	0.1	-168	0.3	0.3	...	0.58	0.70
	0.15	3.8	166	0.0	0.0	...		
J1159+2914	2.24	0.0	...	0.3	0.1	30	2.62	2.50
	0.21	0.8	15	0.4	0.4	...		
J1224+0330	0.25	0.1	-108	0.2	0.2	...	0.53	0.39
	0.19	0.4	-85	0.2	0.2	...		
	0.33	2.9	-76	0.6	0.6	...		
J1224+2122	0.35	0.0	...	0.4	0.4	...	0.14	0.16
	0.32	2.6	-8	1.0	1.0	...		
	0.16	5.8	7	1.2	1.2	...		
J1257−3155	0.40	0.0	...	0.3	0.0	50	1.26	3.38
J1647−6437	0.47	0.0	...	0.9	0.3	38	0.09	0.07*
J1658+4737	0.90	0.0	...	0.3	0.3	...	0.49	0.73
J1726−6427	0.04	0.0	...	0.0	0.0	...	>	0.01*
J1743−0350	1.22	0.1	5	0.0	0.0	...	>	5.90
	4.74	0.1	164	0.5	0.3	-69		
J1744−5144	0.07	0.0	...	0.0	0.0	...	>	0.06
J1753+4409	0.19	0.1	29	0.0	0.0	...	>	0.84
J1809−4552	0.26	0.0	...	0.5	0.1	-64	0.52	0.29
J1824+1044	0.19	0.0	...	0.2	0.2	...	0.40	0.54
	0.12	1.8	-15	0.4	0.4	...		
J1837−7108	1.65	0.1	130	0.6	0.3	-15	0.46	0.76
	0.61	0.7	-1	0.4	0.4	...		
J1842+7946	0.12	0.0	...	0.3	0.3	...	0.08	0.03
	0.09	0.8	-28	0.7	0.0	-56		
	0.16	6.4	-37	2.5	0.8	-36		
J1911−2006	0.32	0.4	-42	0.0	0.0	...	>	0.85
	3.60	0.1	-1	0.5	0.4	-4		
J1912−8010	0.58	0.2	-72	0.6	0.6	...	0.09	0.10
J1925+2106	1.51	0.0	...	0.5	0.4	64	0.39	0.27*
	0.33	5.3	-111	1.4	1.4	...		
J1927+7358	0.45	0.0	...	0.4	0.4	...	0.12	0.08
	0.25	0.5	146	0.1	0.1	...		
	1.03	0.8	150	0.3	0.3	...		
J1932−4546	1.79	0.0	...	1.3	1.3	...	0.06	0.09
J1937−3958	0.56	0.0	...	0.3	0.2	-4	0.63	0.60
J1939−6342	5.36	0.0	...	1.5	1.5	...	0.12	0.14
J1940−6907	0.97	0.0	...	0.9	0.9	...	0.06	0.17
J1955+5131	0.46	0.0	...	0.3	0.3	...	0.22	0.29
	0.17	1.3	-67	0.5	0.5	...		
J2009−4849	0.64	0.0	...	1.3	0.9	-33	0.03	0.03
	0.30	0.5	109	0.6	0.6	...		
	0.22	1.5	116	0.8	0.8	...		
J1516+0015	0.50	0.0	...	0.0	0.0	...	>	0.70
J1522−2730	1.60	0.0	...	0.3	0.1	61	2.86	4.56
	0.25	1.0	-118	0.9	0.5	55		
J1550+0527	0.58	0.0	...	0.0	0.0	...	>	7.49
	2.82	0.8	-19	0.6	0.2	-27		
J1557−0001	0.37	0.0	...	0.2	0.2	...	0.39	0.51
J1602+3326	0.12	0.0	...	0.0	0.0	...	>	0.33
	1.46	0.6	147	0.7	0.7	...		
J1608+1029	0.42	0.1	-168	0.5	0.4	-40	0.10	0.16
	0.09	0.5	-81	0.3	0.3	...		
	0.21	2.5	-45	1.0	1.0	...		
J1625−2527	1.16	0.2	89	0.5	0.1	-1	1.37	1.69
	0.29	1.8	11	1.6	0.3	22		
J2123+0535	0.58	0.0	...	0.3	0.2	-4	0.47	0.79
	0.19	1.6	-48	1.2	1.2	...		
J2139+1423	0.36	0.1	-46	0.0	0.0	...	>	0.69
	0.59	0.4	112	0.5	0.5	...		
	0.12	0.6	-130	0.3	0.3	...		
J2148+0657	5.25	0.0	...	0.9	0.3	-52	1.02	1.81
	0.72	4.3	148	0.6	0.6	...		
J2151+0552	0.13	0.0	...	0.0	0.0	...	>	0.13
	0.56	0.1	33	0.7	0.2	81		
	0.08	1.7	-55	0.7	0.7	...		
J2152−7807	0.84	0.2	-85	0.9	0.3	33	0.19	0.11*
J2207−5346	0.30	0.1	-124	0.0	0.0	...	>	1.58
	0.95	0.2	99	1.5	0.3	21		
J2218−0335	1.04	0.0	...	1.3	0.3	8	0.13	0.21
J2232+1143	1.44	0.1	137	0.4	0.4	...	0.61	0.76
	0.87	1.8	140	0.5	0.5	...		
	1.14	7.6	159	2.1	2.1	...		
	0.82	5.8	145	1.9	1.9	...		
	0.91	25.5	143	3.7	3.7	...		
J2236+2828	1.87	0.0	...	0.5	0.3	-54	0.57	0.84
J2239−5701	0.72	0.0	...	0.6	0.6	...	0.09	0.07*
J2246−1206	0.33	0.1	156	0.0	0.0	...	>	0.72
	0.27	0.4	-13	0.2	0.2	...		
	0.23	1.4	-2	0.0	0.0	...		
J2258−2758	2.58	0.1	19	0.2	0.2	...	4.07	4.84
	0.81	0.3	-159	0.2	0.2	...		
	0.12	1.4	-115	0.5	0.5	...		
J2336−5236	1.63	0.0	...	1.2	1.2	...	0.06	0.05*
J2357−5311	0.83	0.1	43	0.3	0.3	...	0.56	0.81

Table 3—*Continued*

Source	S (Jy)	Rad (mas)	ϕ (°)	$\theta_{\rm maj}$ (mas)	$\theta_{\rm min}$ (mas)	P.A. (°)	$T_b/10^{12}$ (K)	$T_b/10^{12}$ (K)	Source	S (Jy)	Rad (mas)	ϕ (°)	$\theta_{\rm maj}$ (mas)	$\theta_{\rm min}$ (mas)	P.A. (°)	$T_b/10^{12}$ (K)	$T_b/10^{12}$ (K)
J2011−1546	0.61	0.2	7	0.3	0.3	...	0.39	0.61		0.31	4.2	-143	1.1	1.1	...		
	0.38	0.4	-170	0.3	0.3	...				0.20	1.0	-129	0.7	0.7	...		

Note.—Col. (2): The integrated flux density of the component,
Col. (3): The radial distance of the component center from the center of the map
Col. (4): The position angle of the center of the component, measured counterclockwise from an imaginary vertical line from the map center towards the north
Col. (5): The FWHM of the major axis of the component
Col. (6): The FWHM of the minor axis of the component
Col. (7): The position angle of the major axis of the component, measured from the north towards the east
Col. (8): The measured observer frame brightness temperature of the component, where resolved, in units of 10^{12}K. This can be converted to source frame temperature by multiplying by 1+z, where z is to be found in Table 2.
Col. (9): The lower limit to the brightness temperature of the component, in units of 10^{12}K, in the source frame, unless appended by an asterisk (*), in which case it is in the observer frame.

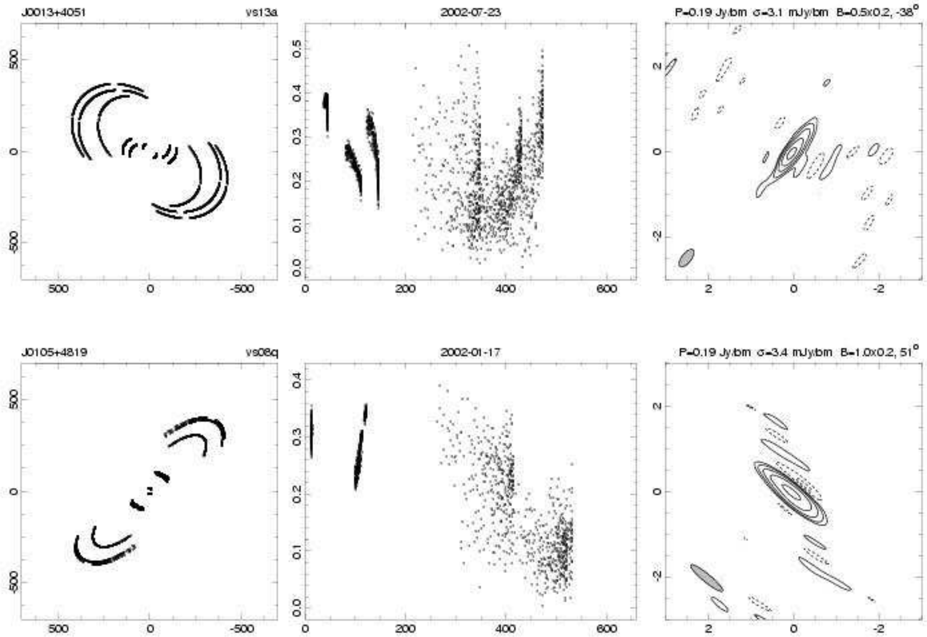

Fig. 1. – Images of the Survey sources: For each source three separate panels are presented horizontally across the page. The first panel shows a plot of the (u,v) coverage, with u on the horizontal axis and v on the vertical axis. Both axes are measured in units of Mλ. The second panel shows a plot of the amplitude of the visibilities (in Janskys) vs. (u,v) radius, with the latter again measured in Mλ (time-averaged to 150 seconds). For both of these plots only data that were actually used to make the final image are shown. Finally, a contour plot of the cleaned image is shown on the right. The contour levels double with each level and start at three times the image RMS, listed above the image, along with an additional negative contour, equal in magnitude to the minimum positive contour level. The peak flux, minimum contour level, and synthesized HPBW in milliarcsecond are shown on the top border.

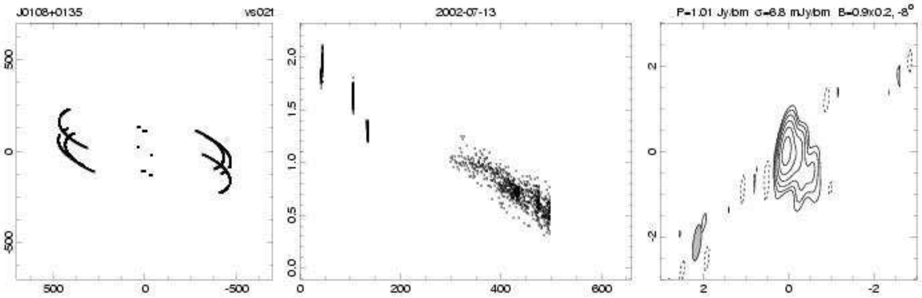
J0108+0135
vs02l
2002-07-13
P=1.01 Jy/bm σ=6.8 mJy/bm B=0.9x0.2, -8°
500
0
-500
0.0
0.5
1.0
1.5
2.0
200
400
600
2
-2

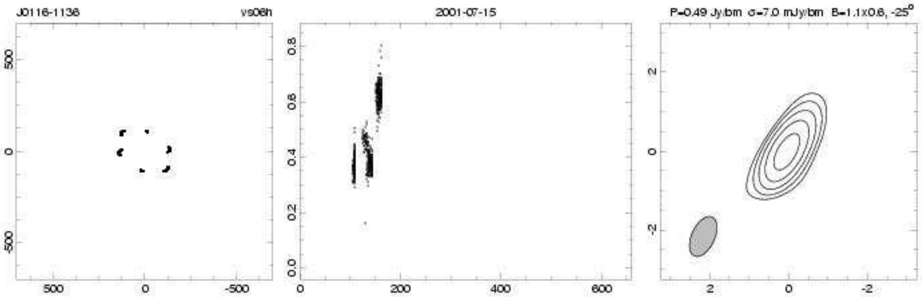
J0116-1136
vs06h
2001-07-15
P=0.49 Jy/bm σ=7.0 mJy/bm B=1.1x0.6, -25°
500
0
-500
0.0
0.2
0.4
0.6
0.8
200
400
600
2
-2

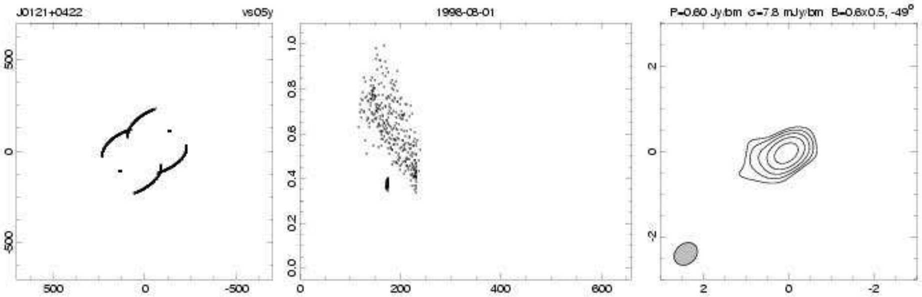
J0121+0422
vs05y
1998-08-01
P=0.60 Jy/bm σ=7.8 mJy/bm B=0.6x0.5, -49°
500
0
-500
0.0
0.2
0.4
0.6
0.8
1.0
200
400
600
2
-2

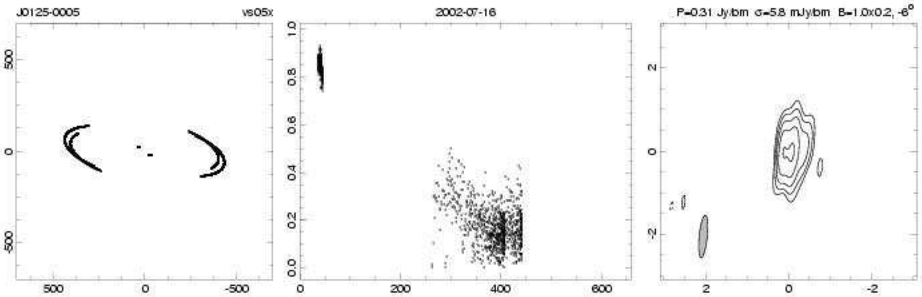
J0125-0005
vs05x
2002-07-16
P=0.31 Jy/bm σ=5.8 mJy/bm B=1.0x0.2, -6°
500
0
-500
0.0
0.2
0.4
0.6
0.8
1.0
200
400
600
2
-2

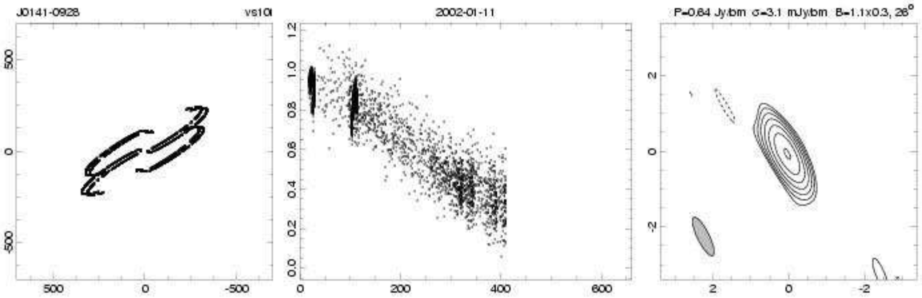
J0141-0928
vs10l
2002-01-11
P=0.64 Jy/bm σ=3.1 mJy/bm B=1.1x0.3, 26°
500
0
-500
0.0
0.2
0.4
0.6
0.8
1.0
1.2
200
400
600
2
-2

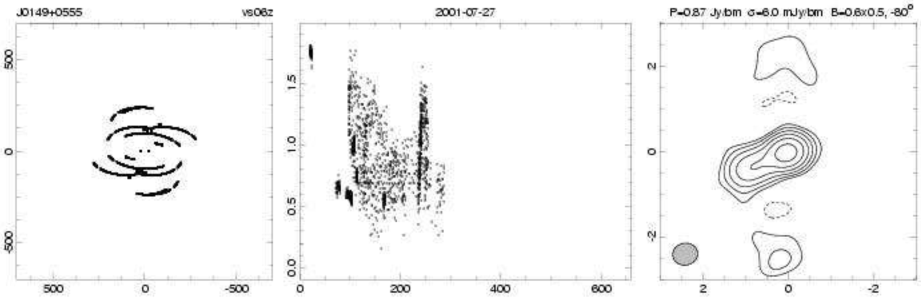
J0149+0555
vs06z
2001-07-27
P=0.87 Jy/bm σ=6.0 mJy/bm B=0.6x0.5, -80°
500
0
-500
0.0
0.5
1.0
1.5
200
400
600
2
-2

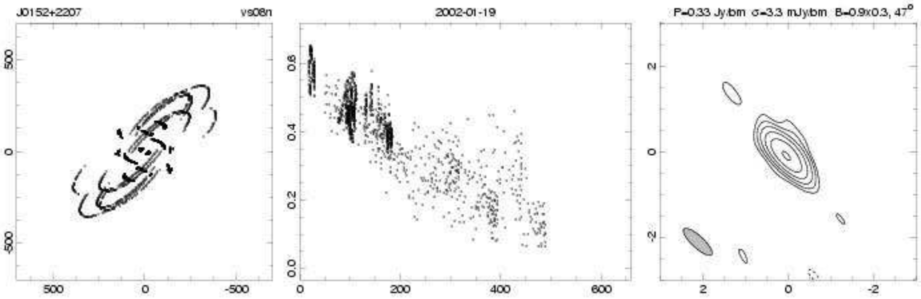
J0152+2207
vs08n
2002-01-19
P=0.33 Jy/bm σ=3.3 mJy/bm B=0.9x0.3, 47°
500
0
-500
0.0
0.2
0.4
0.6
200
400
600
2
-2

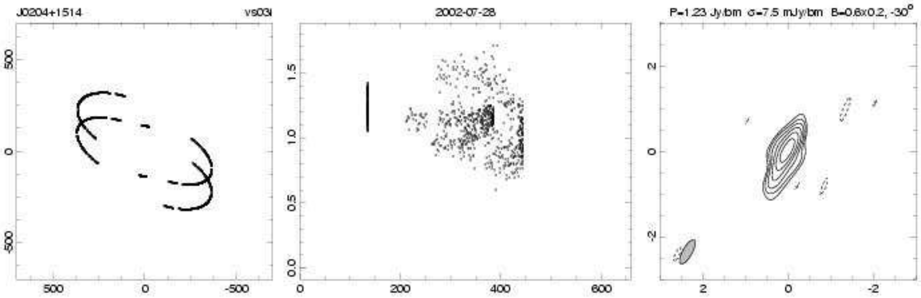
J0204+1514
vs03i
2002-07-28
P=1.23 Jy/bm σ=7.5 mJy/bm B=0.6x0.2, -30°
500
0
-500
0.0
0.5
1.0
1.5
200
400
600
2
-2

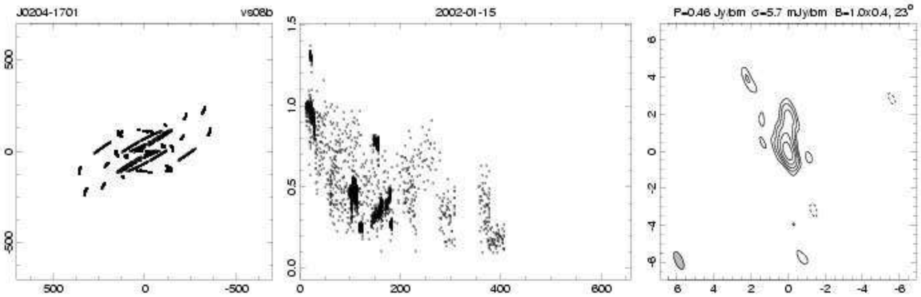
J0204-1701
vs08b
2002-01-15
P=0.46 Jy/bm σ=5.7 mJy/bm B=1.0x0.4, 23°
500
0
-500
0.0
0.5
1.0
1.5
200
400
600
6
4
2
-2
-4
-6

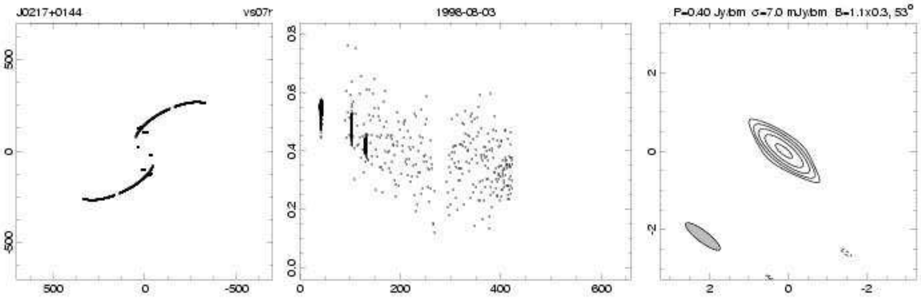
J0217+0144
vs07r
1998-08-03
P=0.40 Jy/bm σ=7.0 mJy/bm B=1.1x0.3, 53°
500
0
-500
0.0
0.2
0.4
0.6
0.8
200
400
600
2
-2

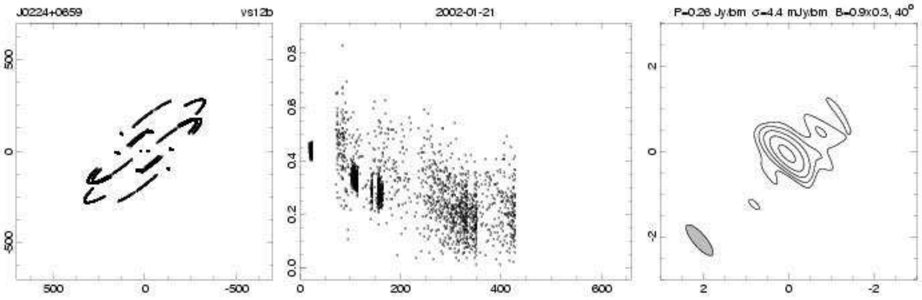
J0224+0659
vs12b
500
0
-500
500
0
-500
2002-01-21
0.0
0.2
0.4
0.6
0.8
0
200
400
600
P=0.28 Jy/bm σ=4.4 mJy/bm B=0.9x0.3, 40°
2
0
-2
2
0
-2

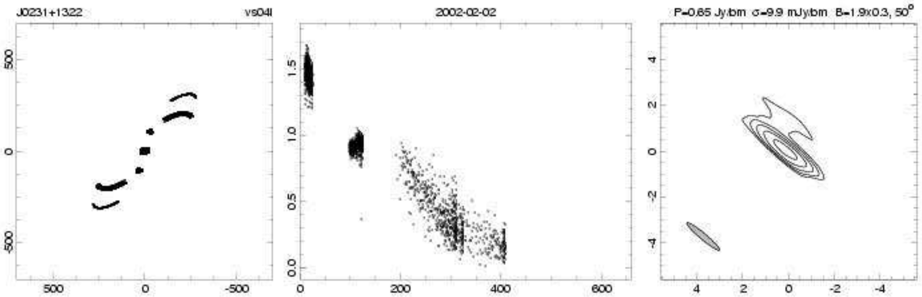
J0231+1322
vs04l
500
0
-500
500
0
-500
2002-02-02
0.0
0.5
1.0
1.5
0
200
400
600
P=0.65 Jy/bm σ=9.9 mJy/bm B=1.9x0.3, 50°
4
2
0
-2
-4
4
2
0
-2
-4

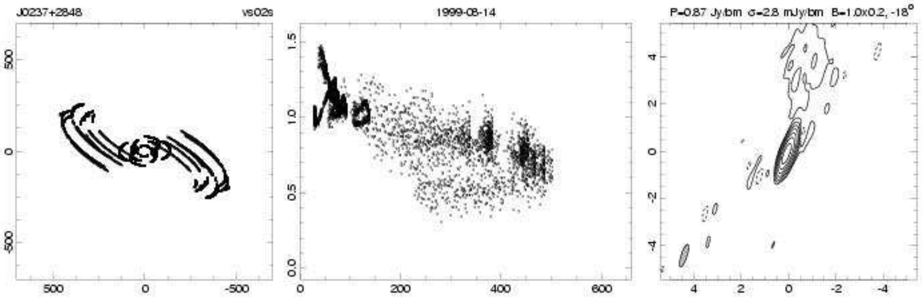
J0237+2848
vs02s
500
0
-500
500
0
-500
1999-08-14
0.0
0.5
1.0
1.5
0
200
400
600
P=0.87 Jy/bm σ=2.8 mJy/bm B=1.0x0.2, -18°
4
2
0
-2
-4
4
2
0
-2
-4

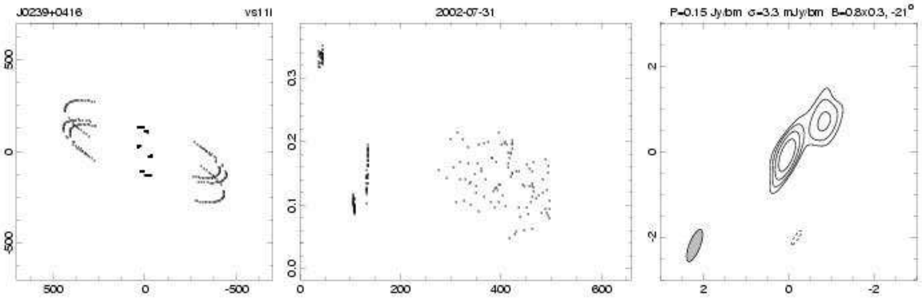
J0239+0416
vs11l
500
0
-500
500
0
-500
2002-07-31
0.0
0.1
0.2
0.3
0
200
400
600
P=0.15 Jy/bm σ=3.3 mJy/bm B=0.8x0.3, -21°
2
0
-2
2
0
-2

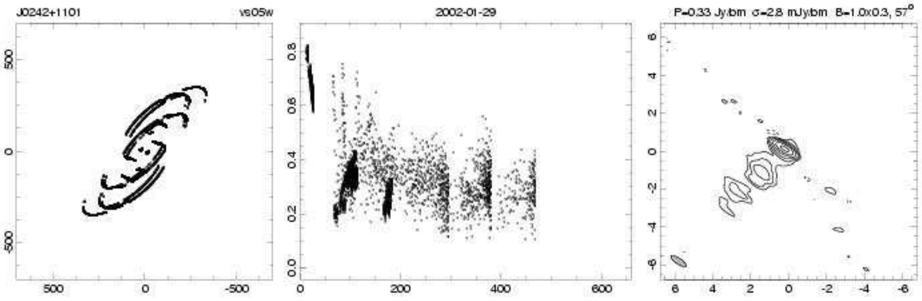
J0242+1101
vs05w
500
0
-500
500
0
-500
2002-01-29
0.0
0.2
0.4
0.6
0.8
0
200
400
600
P=0.33 Jy/bm σ=2.8 mJy/bm B=1.0x0.3, 57°
6
4
2
0
-2
-4
-6
6
4
2
0
-2
-4
-6

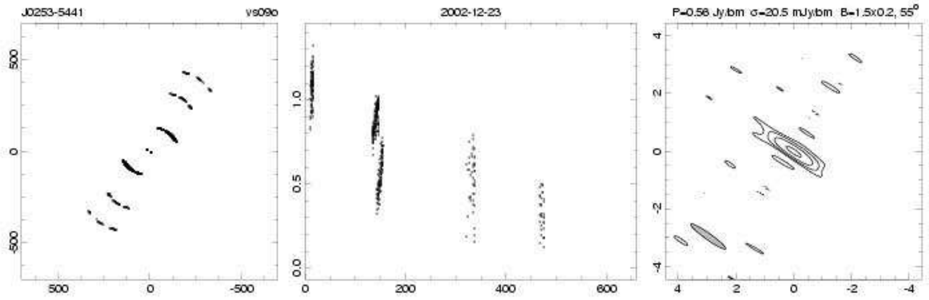
J0253-5441
vs09o
2002-12-23
P=0.56 Jy/bm σ=20.5 mJy/bm B=1.5x0.2, 55°
500
0
-500
0.0
0.5
1.0
200
400
600
4
2
0
-2
-4

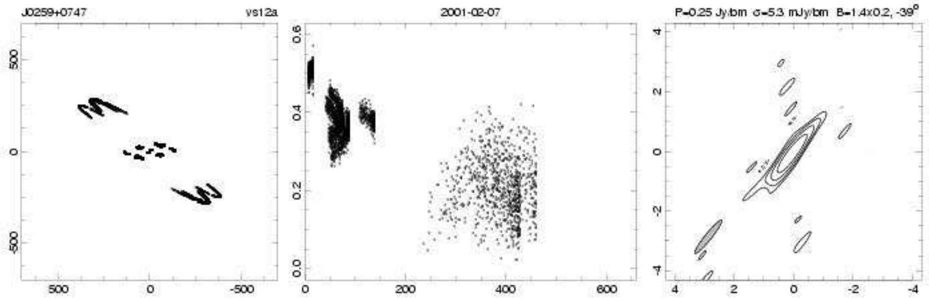
J0259+0747
vs12a
2001-02-07
P=0.25 Jy/bm σ=5.3 mJy/bm B=1.4x0.2, -39°
500
0
-500
0.0
0.2
0.4
0.6
200
400
600
4
2
0
-2
-4

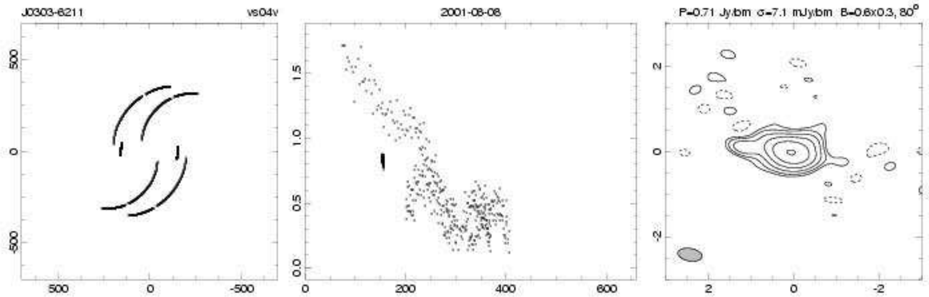
J0303-6211
vs04v
2001-08-08
P=0.71 Jy/bm σ=7.1 mJy/bm B=0.6x0.3, 80°
500
0
-500
0.0
0.5
1.0
1.5
200
400
600
2
0
-2

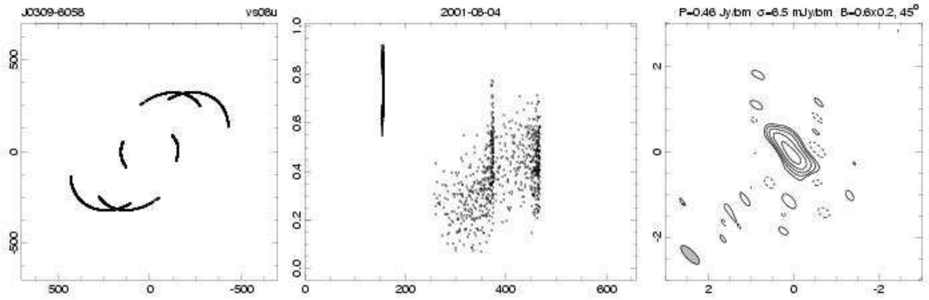
J0309-6058
vs08u
2001-08-04
P=0.46 Jy/bm σ=6.5 mJy/bm B=0.6x0.2, 45°
500
0
-500
0.0
0.2
0.4
0.6
0.8
1.0
200
400
600
2
0
-2

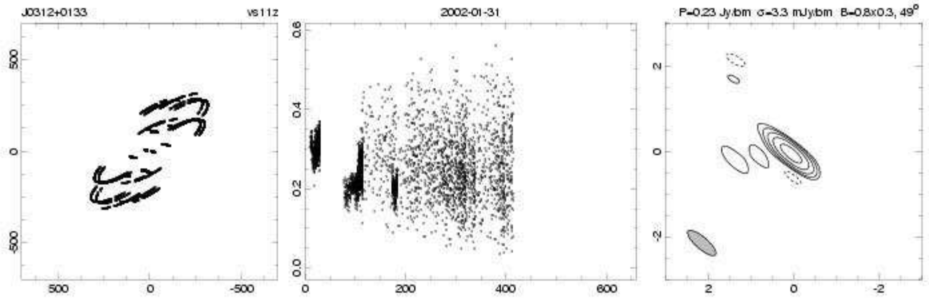
J0312+0133
vs11z
2002-01-31
P=0.23 Jy/bm σ=3.3 mJy/bm B=0.8x0.3, 49°
500
0
-500
0.0
0.2
0.4
0.6
200
400
600
2
0
-2

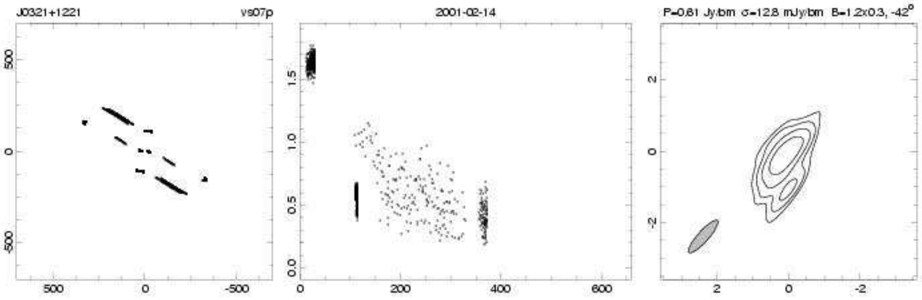
J0321+1221
vs07p
2001-02-14
P=0.61 Jy/bm σ=12.8 mJy/bm B=1.2x0.3, -42°
500
0
-500
0.0
0.5
1.0
1.5
0
200
400
600
2
0
-2

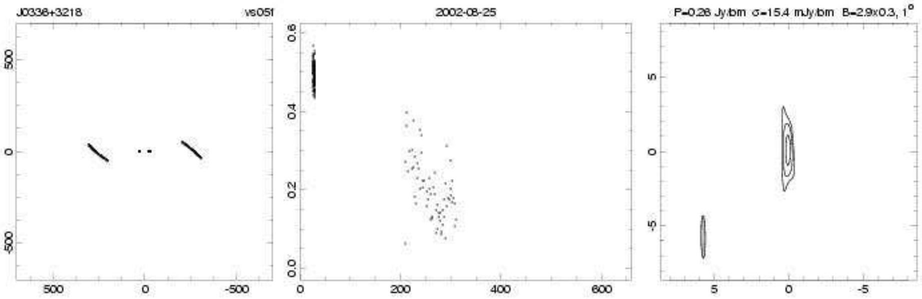
J0336+3218
vs05f
2002-08-25
P=0.26 Jy/bm σ=15.4 mJy/bm B=2.9x0.3, 1°
500
0
-500
0.0
0.2
0.4
0.6
0
200
400
600
5
0
-5

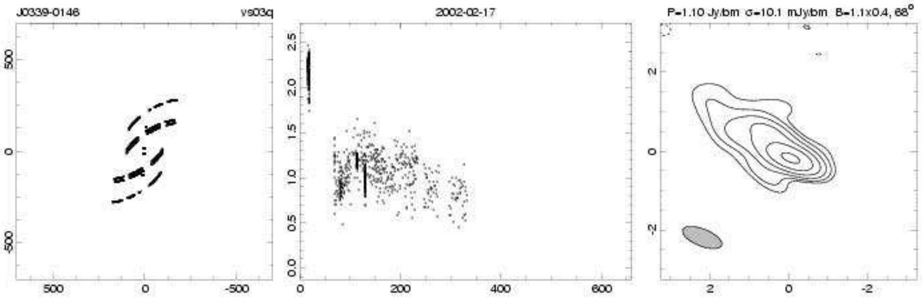
J0339-0146
vs03q
2002-02-17
P=1.10 Jy/bm σ=10.1 mJy/bm B=1.1x0.4, 68°
500
0
-500
0.0
0.5
1.0
1.5
2.0
2.5
0
200
400
600
2
0
-2

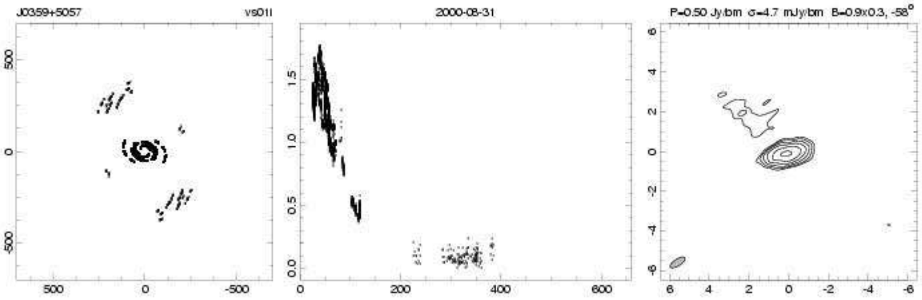
J0359+5057
vs01l
2000-08-31
P=0.50 Jy/bm σ=4.7 mJy/bm B=0.9x0.3, -58°
500
0
-500
0.0
0.5
1.0
1.5
0
200
400
600
6
4
2
0
-2
-4
-6

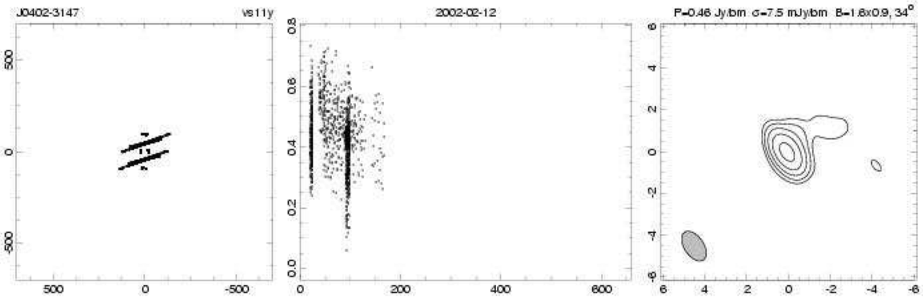
J0402-3147
vs11y
2002-02-12
P=0.46 Jy/bm σ=7.5 mJy/bm B=1.6x0.9, 34°
500
0
-500
0.0
0.2
0.4
0.6
0.8
0
200
400
600
6
4
2
0
-2
-4
-6

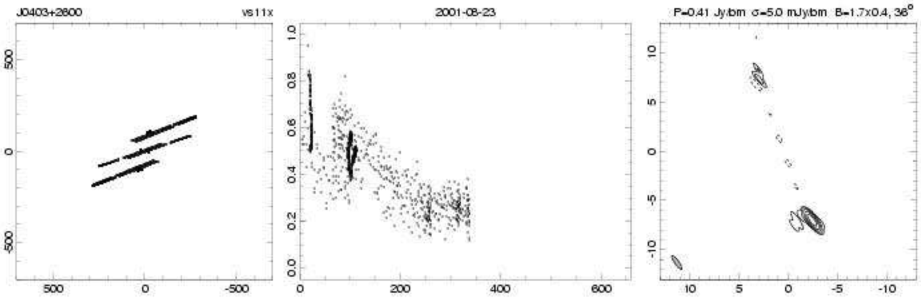
J0403+2600
vs11x
2001-08-23
P=0.41 Jy/bm σ=5.0 mJy/bm B=1.7x0.4, 36°
500
0
-500
0
200
400
600
0.0
0.2
0.4
0.6
0.8
1.0
10
5
0
-5
-10

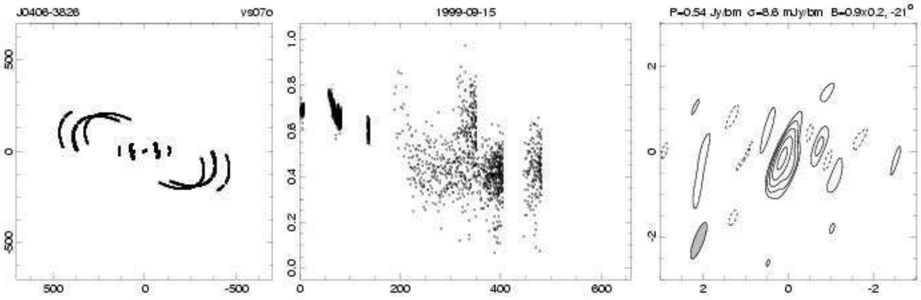
J0406-3826
vs07o
1999-09-15
P=0.54 Jy/bm σ=8.6 mJy/bm B=0.9x0.2, -21°
500
0
-500
0
200
400
600
0.0
0.2
0.4
0.6
0.8
1.0
2
0
-2

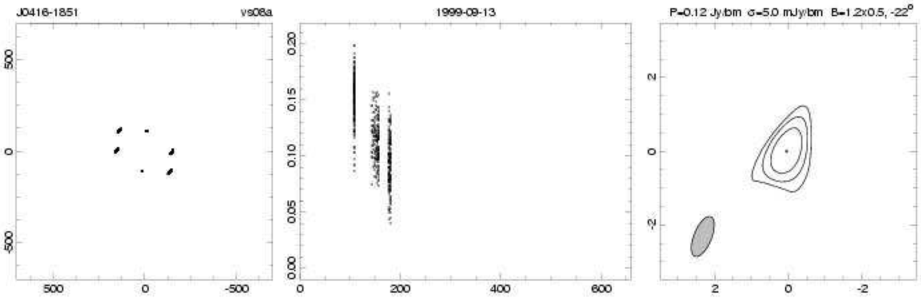
J0416-1851
vs08a
1999-09-13
P=0.12 Jy/bm σ=5.0 mJy/bm B=1.2x0.5, -22°
500
0
-500
0
200
400
600
0.00
0.05
0.10
0.15
0.20
2
0
-2

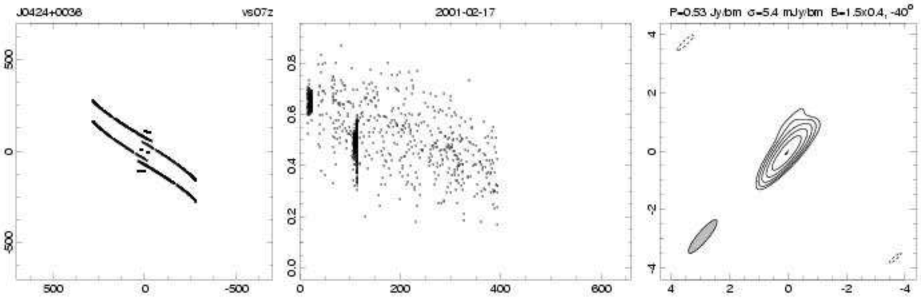
J0424+0036
vs07z
2001-02-17
P=0.53 Jy/bm σ=5.4 mJy/bm B=1.5x0.4, -40°
500
0
-500
0
200
400
600
0.0
0.2
0.4
0.6
0.8
4
2
0
-2
-4

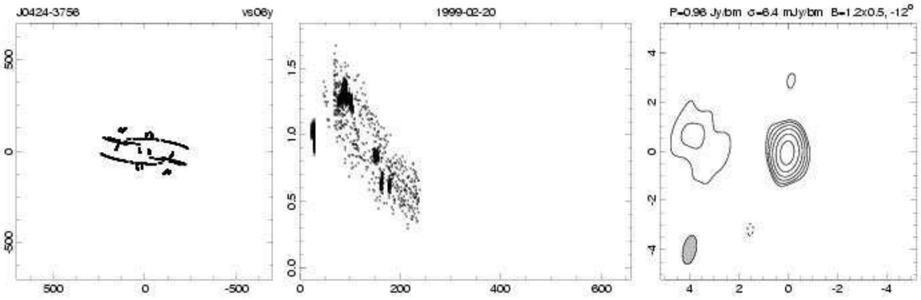
J0424-3756
vs08y
1999-02-20
P=0.96 Jy/bm σ=6.4 mJy/bm B=1.2x0.5, -12°
500
0
-500
0
200
400
600
0.0
0.5
1.0
1.5
4
2
0
-2
-4

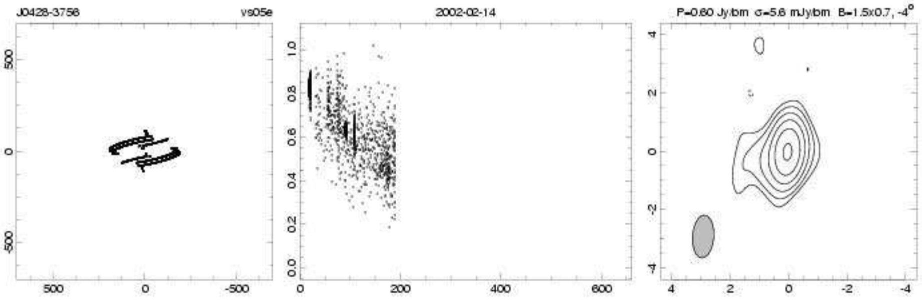
J0428-3756
vs05e
2002-02-14
P=0.60 Jy/bm σ=5.6 mJy/bm B=1.5x0.7, -4°
500
0
-500
0.0
0.2
0.4
0.6
0.8
1.0
200
400
600
4
2
0
-2
-4

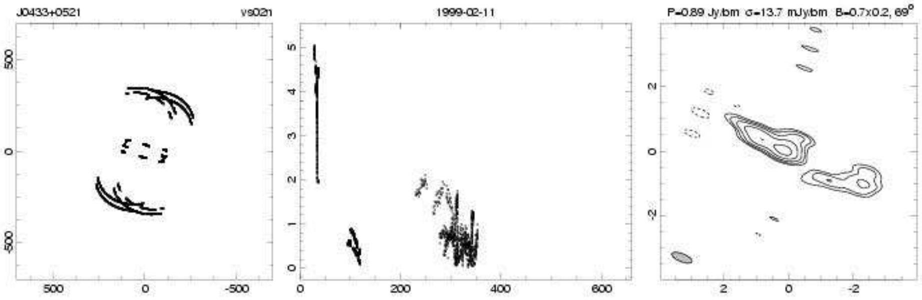
J0433+0521
vs02n
1999-02-11
P=0.89 Jy/bm σ=13.7 mJy/bm B=0.7x0.2, 69°
500
0
-500
0
1
2
3
4
5
200
400
600
2
0
-2

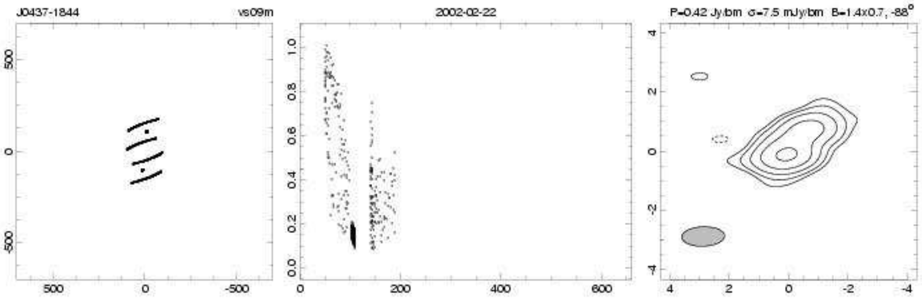
J0437-1844
vs09m
2002-02-22
P=0.42 Jy/bm σ=7.5 mJy/bm B=1.4x0.7, -88°
500
0
-500
0.0
0.2
0.4
0.6
0.8
1.0
200
400
600
4
2
0
-2
-4

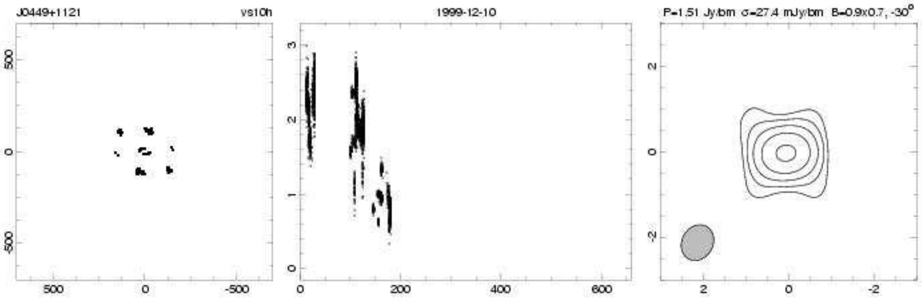
J0449+1121
vs10h
1999-12-10
P=1.51 Jy/bm σ=27.4 mJy/bm B=0.9x0.7, -30°
500
0
-500
0
1
2
3
200
400
600
2
0
-2

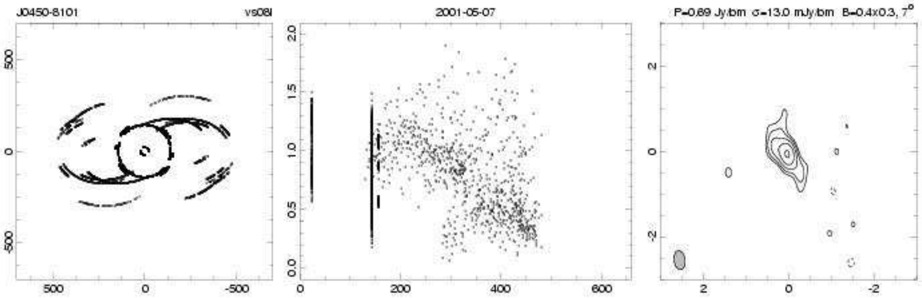
J0450-8101
vs08l
2001-05-07
P=0.69 Jy/bm σ=13.0 mJy/bm B=0.4x0.3, 7°
500
0
-500
0.0
0.5
1.0
1.5
2.0
200
400
600
2
0
-2

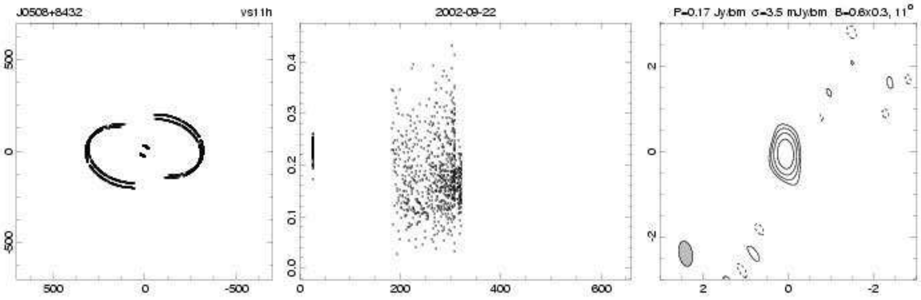
J0508+8432
vs11h
2002-09-22
P=0.17 Jy/bm σ=3.5 mJy/bm B=0.6x0.3, 11°
500
0
-500
0.4
0.3
0.2
0.1
0.0
200
400
600
2
0
-2

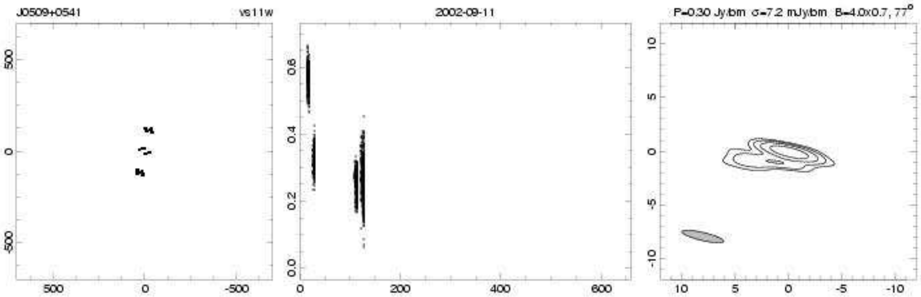
J0509+0541
vs11w
2002-09-11
P=0.30 Jy/bm σ=7.2 mJy/bm B=4.0x0.7, 77°
500
0
-500
0.6
0.4
0.2
0.0
200
400
600
10
5
0
-5
-10

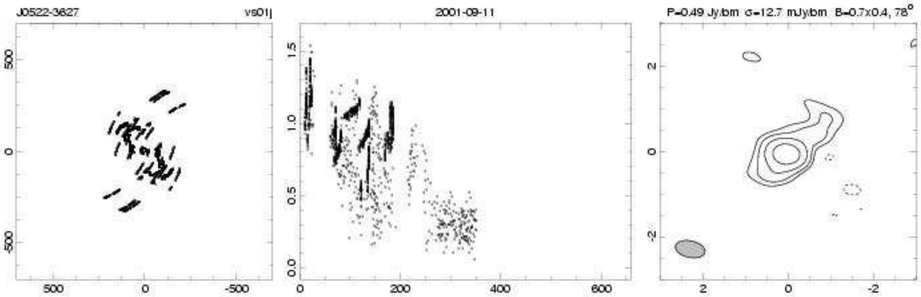
J0522-3627
vs01j
2001-09-11
P=0.49 Jy/bm σ=12.7 mJy/bm B=0.7x0.4, 78°
500
0
-500
1.5
1.0
0.5
0.0
200
400
600
2
0
-2

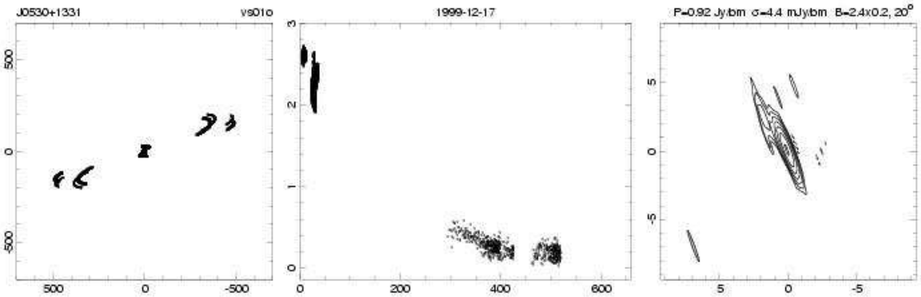
J0530+1331
vs01o
1999-12-17
P=0.92 Jy/bm σ=4.4 mJy/bm B=2.4x0.2, 20°
500
0
-500
3
2
1
0
200
400
600
5
0
-5

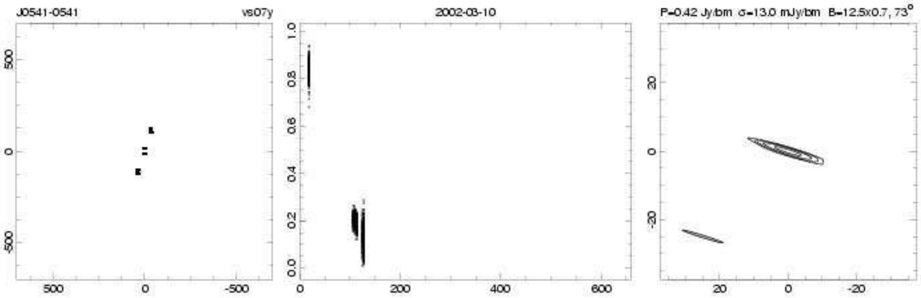
J0541-0541
vs07y
2002-03-10
P=0.42 Jy/bm σ=13.0 mJy/bm B=12.5x0.7, 73°
500
0
-500
1.0
0.8
0.6
0.4
0.2
0.0
200
400
600
20
0
-20

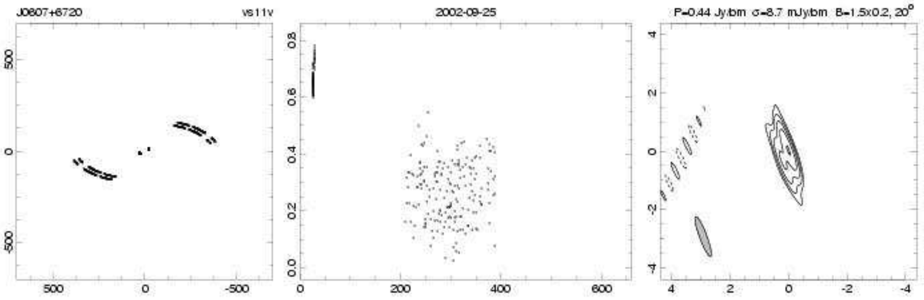
J0807+6720
vs11v
500
0
-500
500
0
-500
2002-09-25
0.0
0.2
0.4
0.6
0.8
0
200
400
600
P=0.44 Jy/bm σ=8.7 mJy/bm B=1.5x0.2, 20°
4
2
0
-2
-4
4
2
0
-2
-4

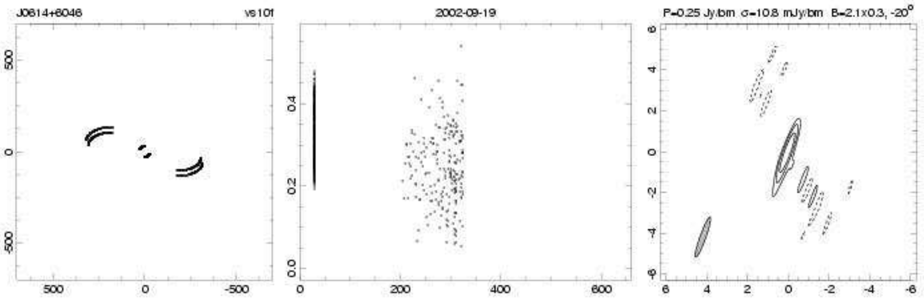
J0814+6046
vs10f
500
0
-500
500
0
-500
2002-09-19
0.0
0.2
0.4
0
200
400
600
P=0.25 Jy/bm σ=10.8 mJy/bm B=2.1x0.3, -20°
6
4
2
0
-2
-4
-6
6
4
2
0
-2
-4
-6

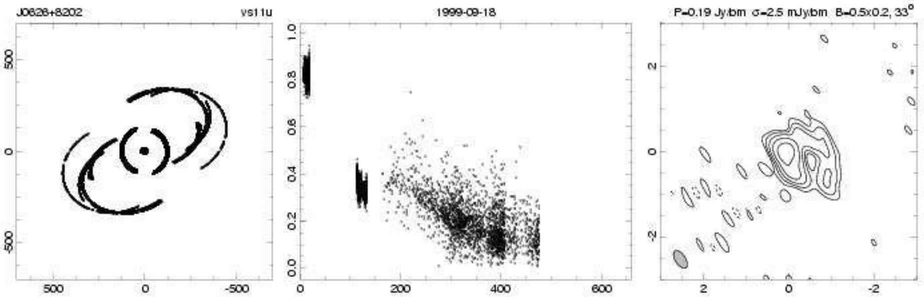
J0628+8202
vs11u
500
0
-500
500
0
-500
1999-09-18
0.0
0.2
0.4
0.6
0.8
1.0
0
200
400
600
P=0.19 Jy/bm σ=2.5 mJy/bm B=0.5x0.2, 33°
2
0
-2
2
0
-2

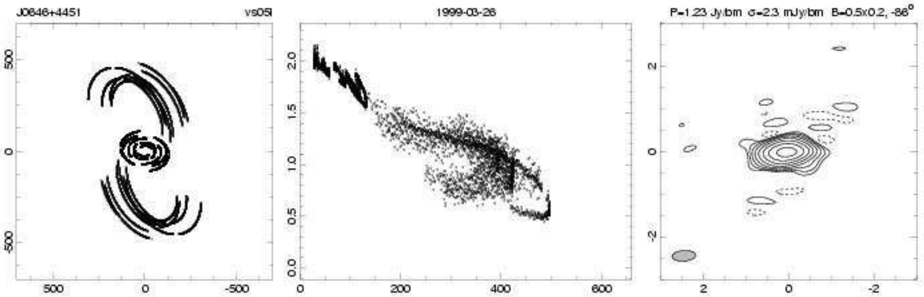
J0646+4451
vs05l
500
0
-500
500
0
-500
1999-03-26
0.0
0.5
1.0
1.5
2.0
0
200
400
600
P=1.23 Jy/bm σ=2.3 mJy/bm B=0.5x0.2, -86°
2
0
-2
2
0
-2

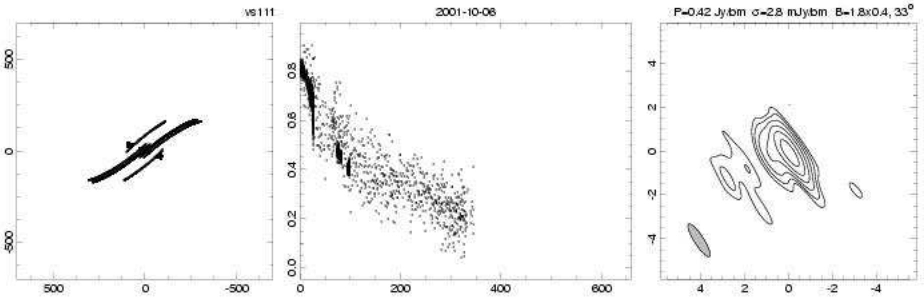
vs111
500
0
-500
500
0
-500
2001-10-06
0.0
0.2
0.4
0.6
0.8
0
200
400
600
P=0.42 Jy/bm σ=2.8 mJy/bm B=1.8x0.4, 33°
4
2
0
-2
-4
4
2
0
-2
-4

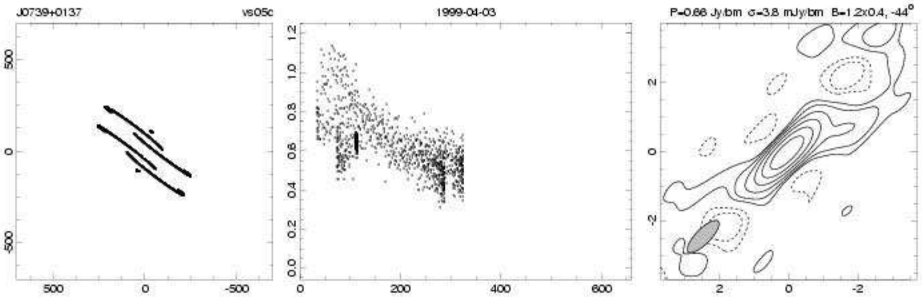

J0739+0137
vs05c
500
0
-500
500
0
-500
1999-04-03
0.0
0.2
0.4
0.6
0.8
1.0
1.2
0
200
400
600
P=0.66 Jy/bm σ=3.8 mJy/bm B=1.2x0.4, -44°
2
0
-2
2
0
-2

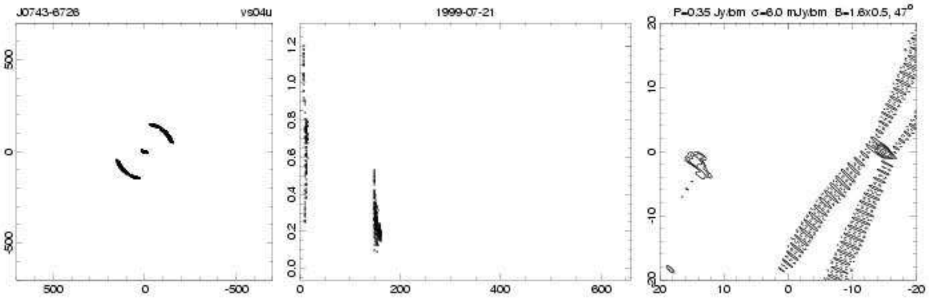

J0743-6726
vs04u
500
0
-500
500
0
-500
1999-07-21
0.0
0.2
0.4
0.6
0.8
1.0
1.2
0
200
400
600
P=0.35 Jy/bm σ=6.0 mJy/bm B=1.6x0.5, 47°
20
10
0
-10
-20
20
10
0
-10
-20

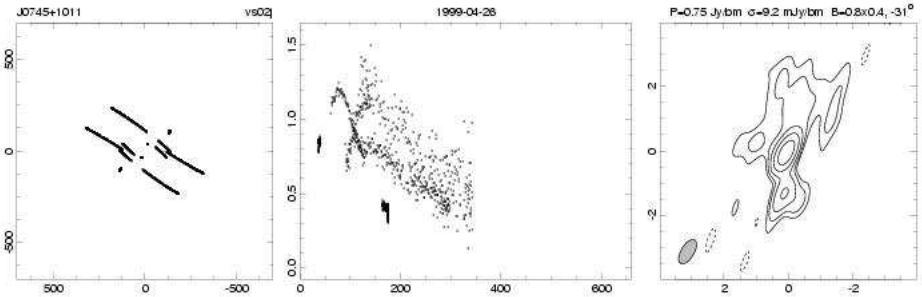

J0745+1011
vs02j
500
0
-500
500
0
-500
1999-04-26
0.0
0.5
1.0
1.5
0
200
400
600
P=0.75 Jy/bm σ=9.2 mJy/bm B=0.8x0.4, -31°
2
0
-2
2
0
-2

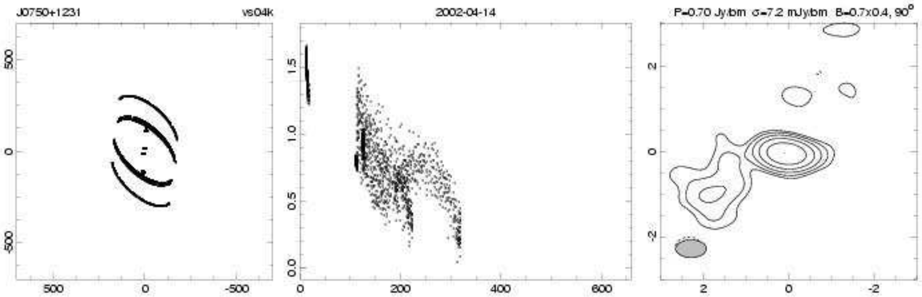

J0750+1231
vs04k
500
0
-500
500
0
-500
2002-04-14
0.0
0.5
1.0
1.5
0
200
400
600
P=0.70 Jy/bm σ=7.2 mJy/bm B=0.7x0.4, 90°
2
0
-2
2
0
-2

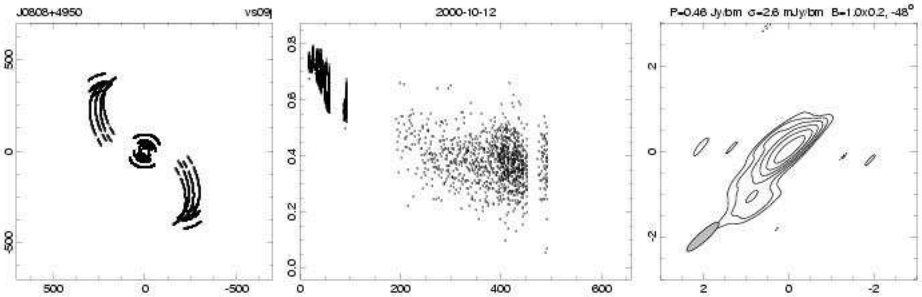

J0808+4950
vs09j
500
0
-500
500
0
-500
2000-10-12
0.0
0.2
0.4
0.6
0.8
0
200
400
600
P=0.46 Jy/bm σ=2.6 mJy/bm B=1.0x0.2, -48°
2
0
-2
2
0
-2

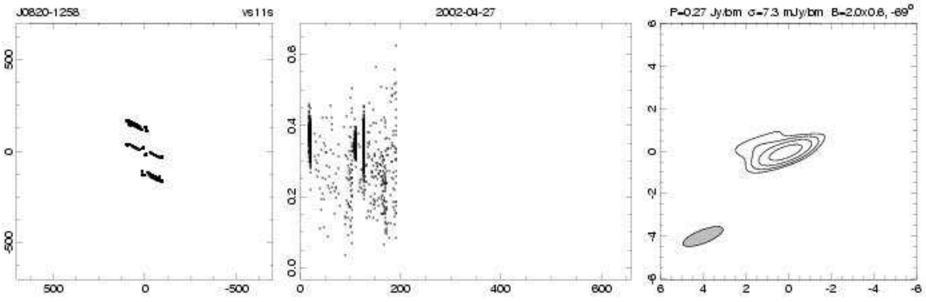
J0820-1258
vs11s
500
0
-500
2002-04-27
0.0
0.2
0.4
0.6
200
400
600
P=0.27 Jy/bm σ=7.3 mJy/bm B=2.0x0.6, -69°
6
4
2
0
-2
-4
-6

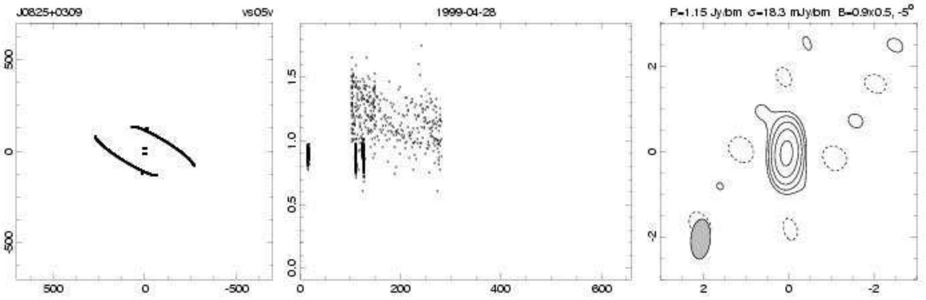
J0825+0309
vs05v
500
0
-500
1999-04-28
0.0
0.5
1.0
1.5
200
400
600
P=1.15 Jy/bm σ=18.3 mJy/bm B=0.9x0.5, -5°
2
0
-2

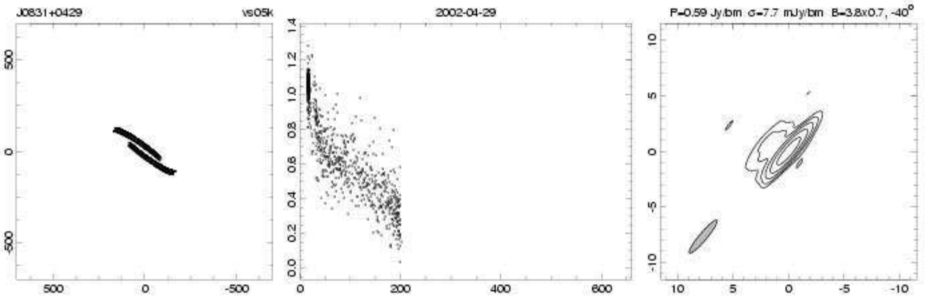
J0831+0429
vs05k
500
0
-500
2002-04-29
0.0
0.2
0.4
0.6
0.8
1.0
1.2
1.4
200
400
600
P=0.59 Jy/bm σ=7.7 mJy/bm B=3.8x0.7, -40°
10
5
0
-5
-10

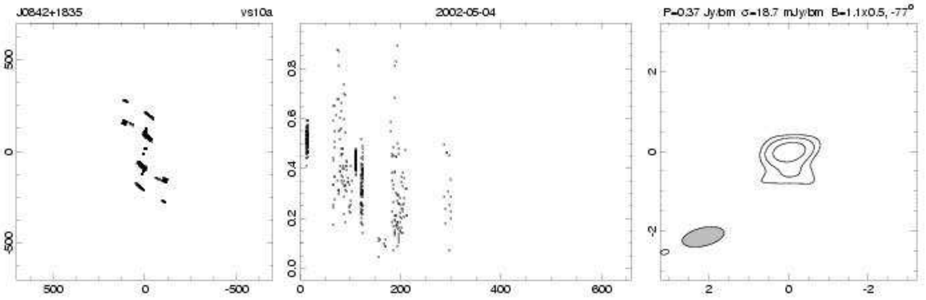
J0842+1835
vs10a
500
0
-500
2002-05-04
0.0
0.2
0.4
0.6
0.8
200
400
600
P=0.37 Jy/bm σ=18.7 mJy/bm B=1.1x0.5, -77°
2
0
-2

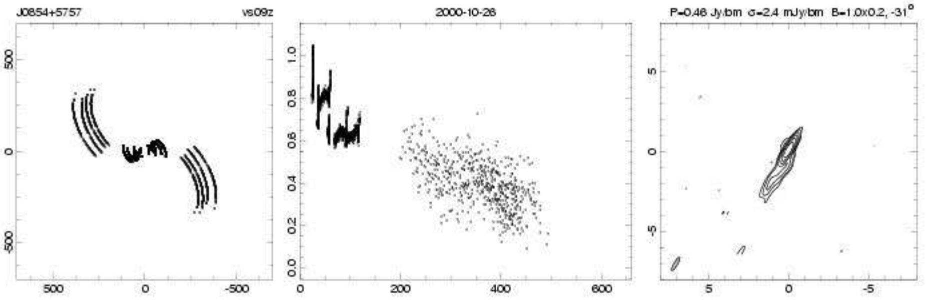
J0854+5757
vs09z
500
0
-500
2000-10-26
0.0
0.2
0.4
0.6
0.8
1.0
200
400
600
P=0.46 Jy/bm σ=2.4 mJy/bm B=1.0x0.2, -31°
5
0
-5

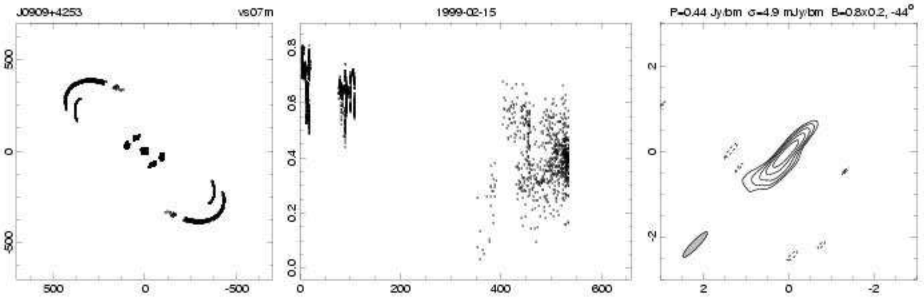

J0909+4253
vs07m
1999-02-15
P=0.44 Jy/bm σ=4.9 mJy/bm B=0.8x0.2, -44°
500
0
-500
0.0
0.2
0.4
0.6
0.8
200
400
600
2
-2

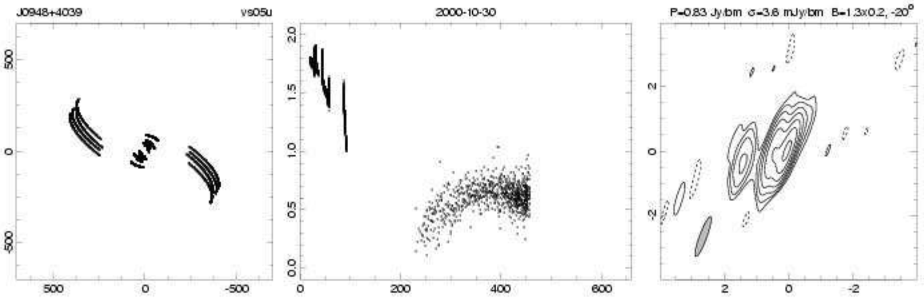

J0948+4039
vs05u
2000-10-30
P=0.83 Jy/bm σ=3.6 mJy/bm B=1.3x0.2, -20°
500
0
-500
0.0
0.5
1.0
1.5
2.0
200
400
600
2
-2

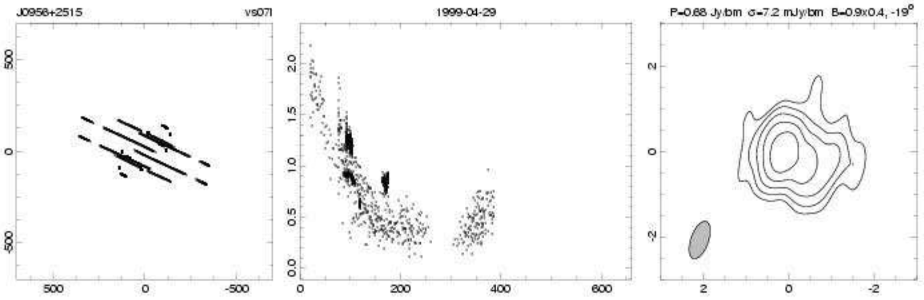

J0956+2515
vs07l
1999-04-29
P=0.68 Jy/bm σ=7.2 mJy/bm B=0.9x0.4, -19°
500
0
-500
0.0
0.5
1.0
1.5
2.0
200
400
600
2
-2

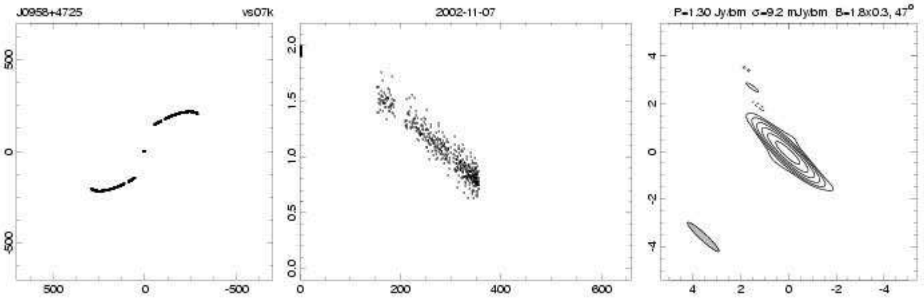

J0958+4725
vs07k
2002-11-07
P=1.30 Jy/bm σ=9.2 mJy/bm B=1.8x0.3, 47°
500
0
-500
0.0
0.5
1.0
1.5
2.0
200
400
600
4
2
-2
-4

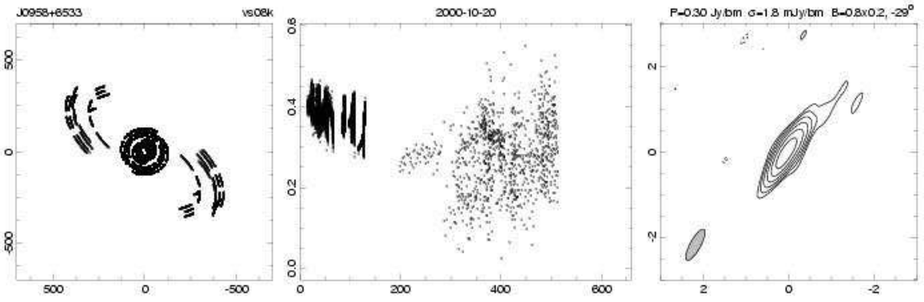

J0958+6533
vs08k
2000-10-20
P=0.30 Jy/bm σ=1.8 mJy/bm B=0.8x0.2, -29°
500
0
-500
0.0
0.2
0.4
0.6
200
400
600
2
-2

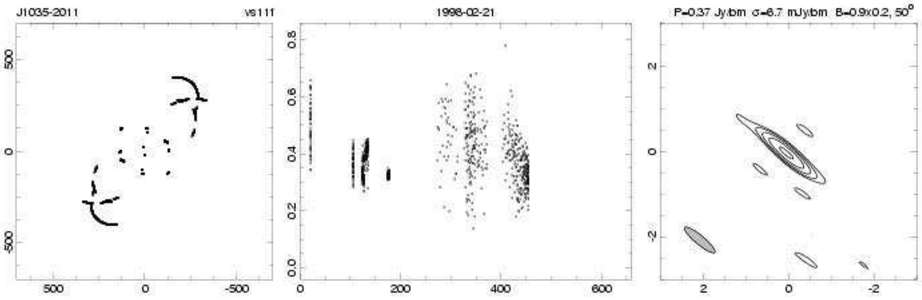
J1035-2011
vs11l
1998-02-21
P=0.37 Jy/bm σ=6.7 mJy/bm B=0.9x0.2, 50°
500
0
-500
0.0
0.2
0.4
0.6
0.8
200
400
600
2
-2

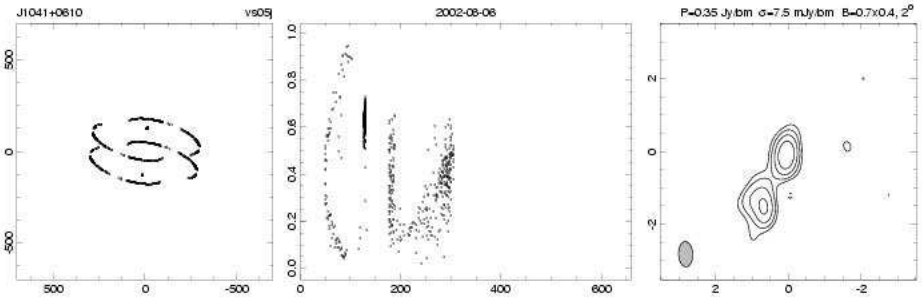
J1041+0610
vs05j
2002-08-06
P=0.35 Jy/bm σ=7.5 mJy/bm B=0.7x0.4, 2°
500
0
-500
0.0
0.2
0.4
0.6
0.8
1.0
200
400
600
2
-2

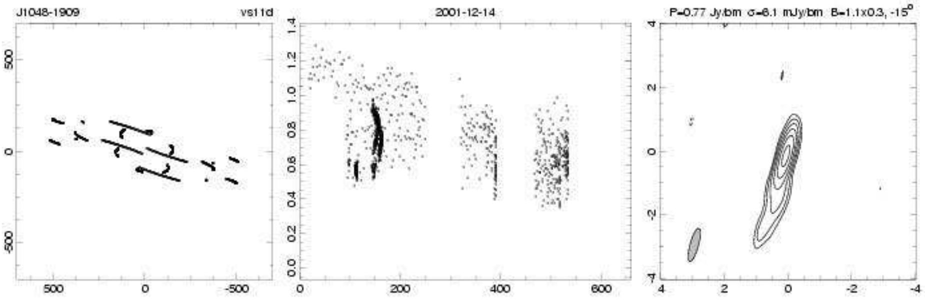
J1048-1909
vs11d
2001-12-14
P=0.77 Jy/bm σ=6.1 mJy/bm B=1.1x0.3, -15°
500
0
-500
0.0
0.2
0.4
0.6
0.8
1.0
1.2
1.4
200
400
600
4
2
-2
-4

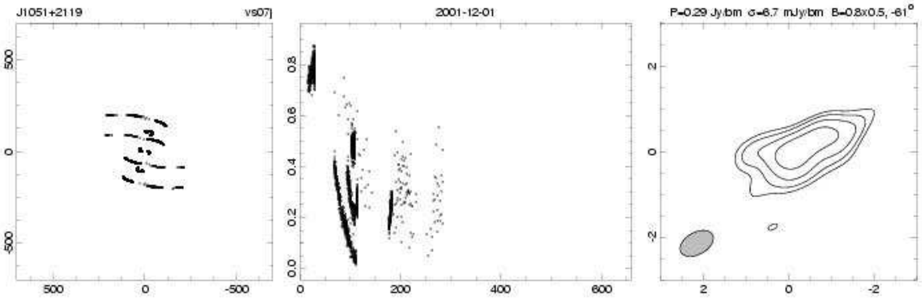
J1051+2119
vs07j
2001-12-01
P=0.29 Jy/bm σ=6.7 mJy/bm B=0.8x0.5, -61°
500
0
-500
0.0
0.2
0.4
0.6
0.8
200
400
600
2
-2

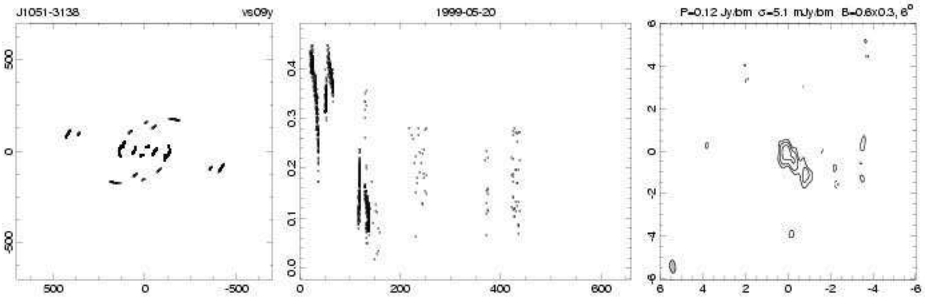
J1051-3138
vs09y
1999-05-20
P=0.12 Jy/bm σ=5.1 mJy/bm B=0.6x0.3, 6°
500
0
-500
0.0
0.1
0.2
0.3
0.4
200
400
600
6
4
2
-2
-4
-6

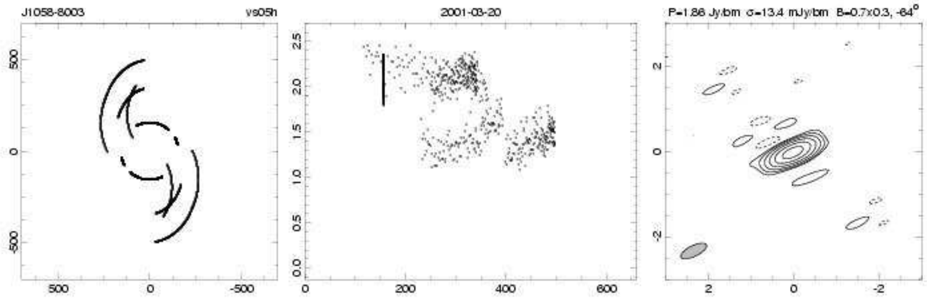
J1058-8003
vs05h
2001-03-20
P=1.86 Jy/bm σ=13.4 mJy/bm B=0.7x0.3, -64°
500
0
-500
0.0
0.5
1.0
1.5
2.0
2.5
200
400
600
2
-2

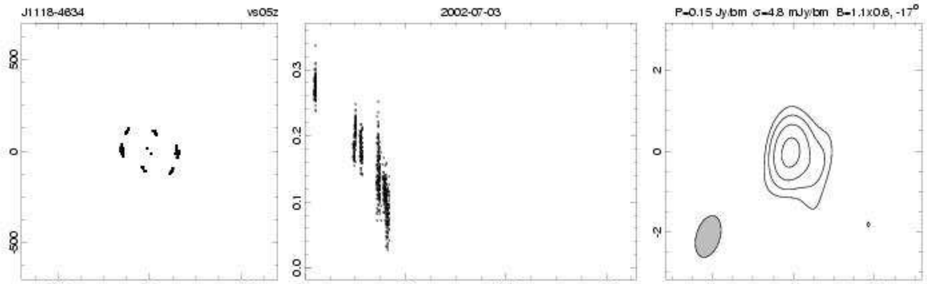
J1118-4634
vs05z
2002-07-03
P=0.15 Jy/bm σ=4.8 mJy/bm B=1.1x0.6, -17°
500
0
-500
0.0
0.1
0.2
0.3
200
400
600
2
-2

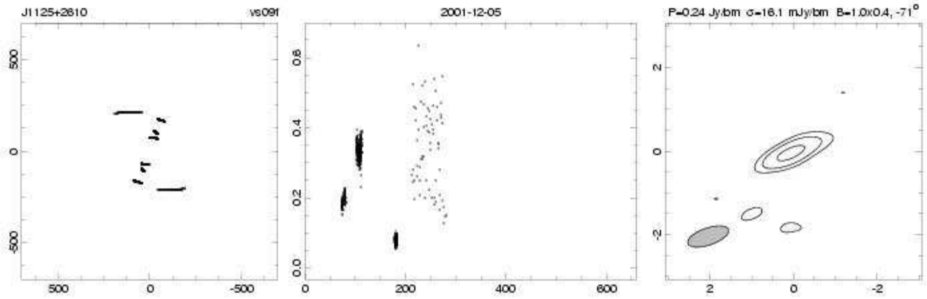
J1125+2610
vs09f
2001-12-05
P=0.24 Jy/bm σ=16.1 mJy/bm B=1.0x0.4, -71°
500
0
-500
0.0
0.2
0.4
0.6
200
400
600
2
-2

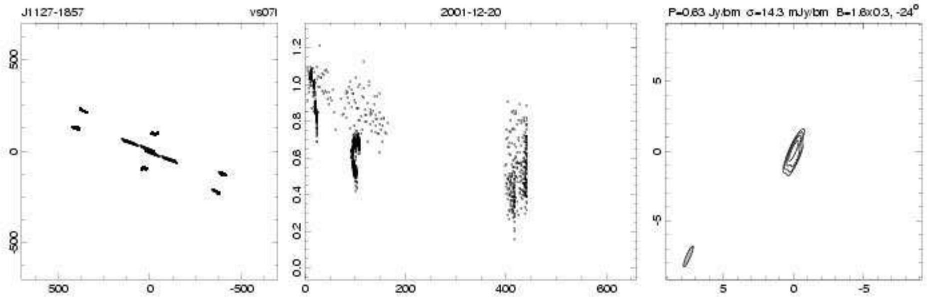
J1127-1857
vs07i
2001-12-20
P=0.63 Jy/bm σ=14.3 mJy/bm B=1.6x0.3, -24°
500
0
-500
0.0
0.2
0.4
0.6
0.8
1.0
1.2
200
400
600
5
-5

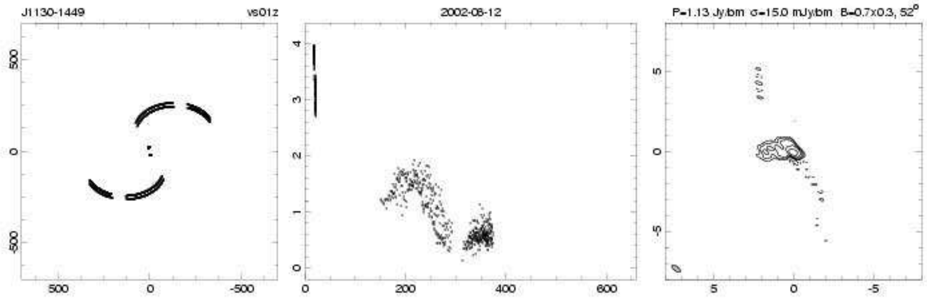
J1130-1449
vs01z
2002-08-12
P=1.13 Jy/bm σ=15.0 mJy/bm B=0.7x0.3, 52°
500
0
-500
1
2
3
4
200
400
600
5
-5

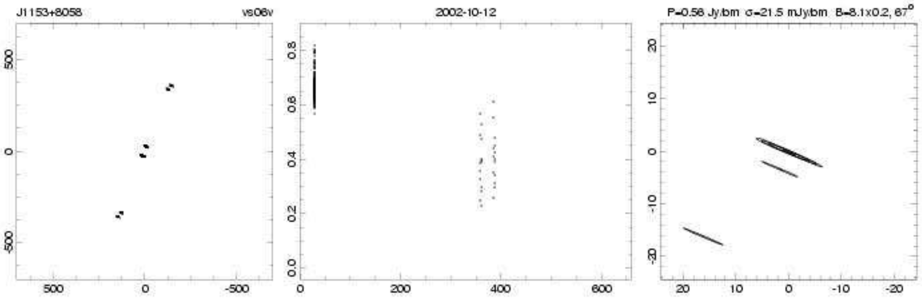
J1153+8058
vs06v
2002-10-12
P=0.56 Jy/bm σ=21.5 mJy/bm B=8.1x0.2, 67°
500
0
-500
0.0
0.2
0.4
0.6
0.8
200
400
600
20
10
-10
-20

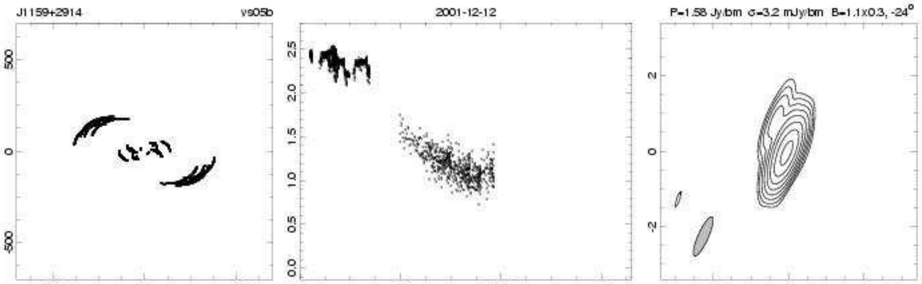
J1159+2914
vs05b
2001-12-12
P=1.58 Jy/bm σ=3.2 mJy/bm B=1.1x0.3, -24°
500
0
-500
0.0
0.5
1.0
1.5
2.0
2.5
200
400
600
2
-2

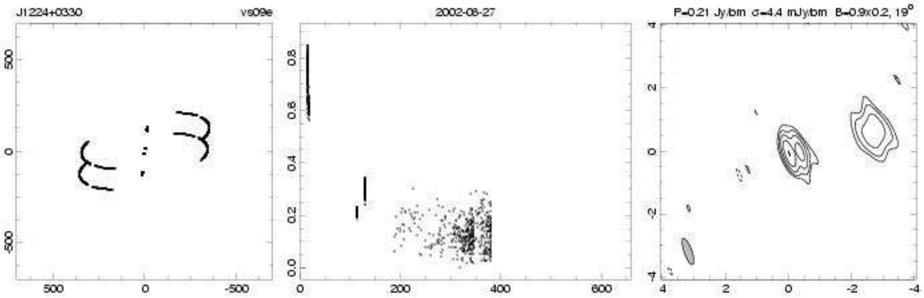
J1224+0330
vs09e
2002-08-27
P=0.21 Jy/bm σ=4.4 mJy/bm B=0.9x0.2, 19°
500
0
-500
0.0
0.2
0.4
0.6
0.8
200
400
600
4
2
-2
-4

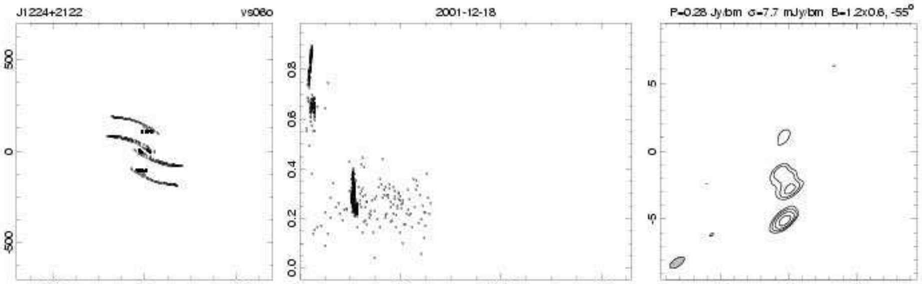
J1224+2122
vs06o
2001-12-18
P=0.28 Jy/bm σ=7.7 mJy/bm B=1.2x0.6, -55°
500
0
-500
0.0
0.2
0.4
0.6
0.8
200
400
600
5
-5

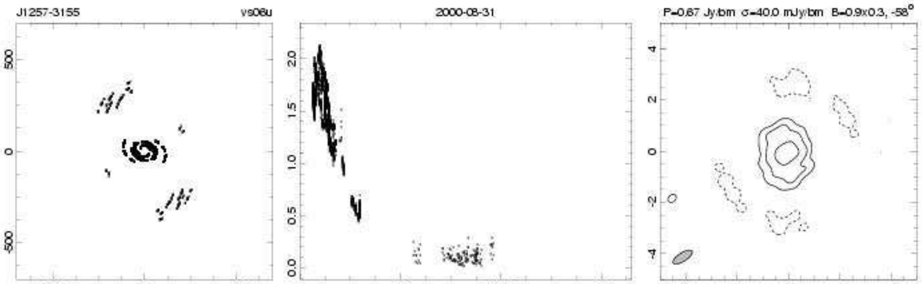
J1257-3155
vs06u
2000-08-31
P=0.67 Jy/bm σ=40.0 mJy/bm B=0.9x0.3, -58°
500
0
-500
0.0
0.5
1.0
1.5
2.0
200
400
600
4
2
-2
-4

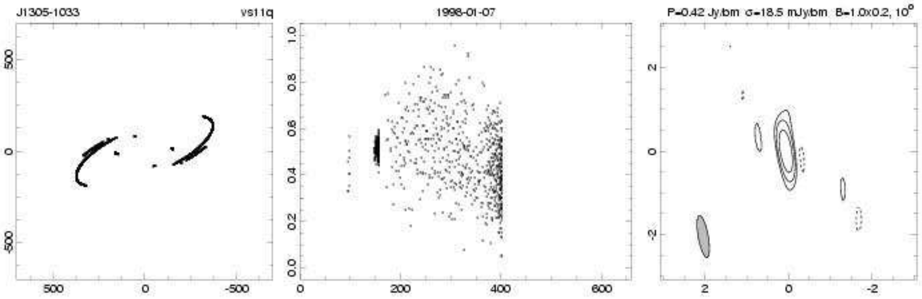
J1305-1033
vs11q
1998-01-07
P=0.42 Jy/bm σ=18.5 mJy/bm B=1.0x0.2, 10°
500
0
-500
0.0
0.2
0.4
0.6
0.8
1.0
200
400
600
2
-2

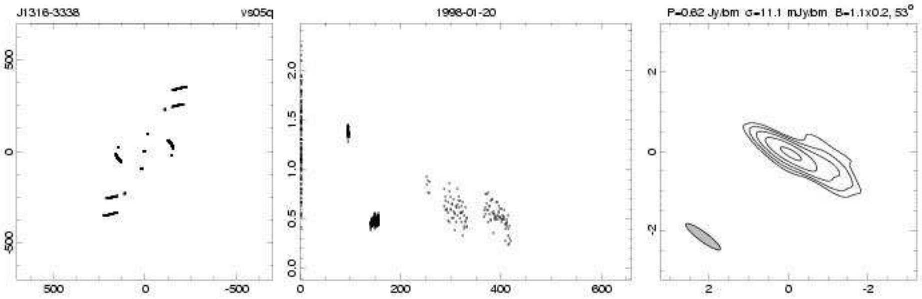
J1316-3338
vs05q
1998-01-20
P=0.62 Jy/bm σ=11.1 mJy/bm B=1.1x0.2, 53°
500
0
-500
0.0
0.5
1.0
1.5
2.0
200
400
600
2
-2

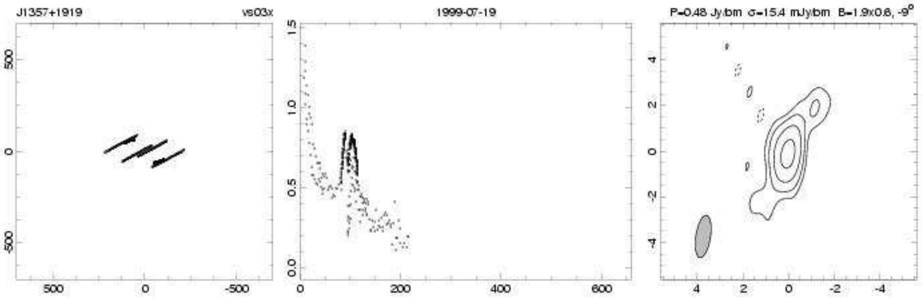
J1357+1919
vs03x
1999-07-19
P=0.48 Jy/bm σ=15.4 mJy/bm B=1.9x0.6, -9°
500
0
-500
0.0
0.5
1.0
1.5
200
400
600
4
2
-2
-4

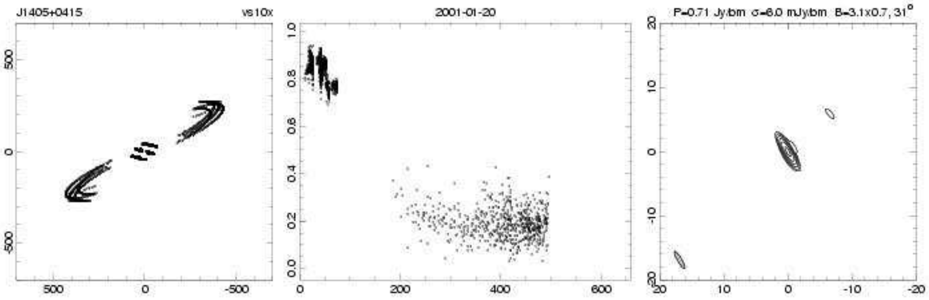
J1405+0415
vs10x
2001-01-20
P=0.71 Jy/bm σ=6.0 mJy/bm B=3.1x0.7, 31°
500
0
-500
0.0
0.2
0.4
0.6
0.8
1.0
200
400
600
20
10
-10
-20

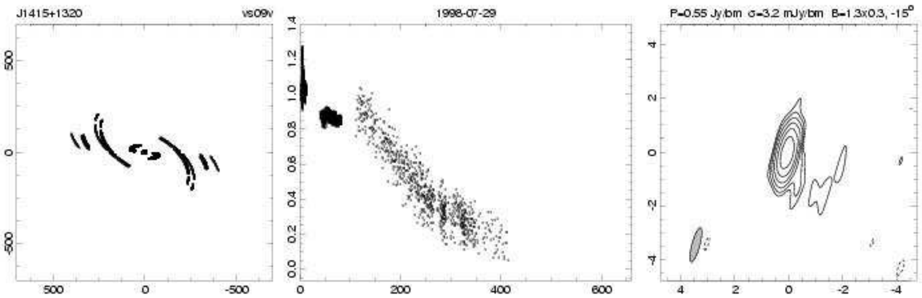
J1415+1320
vs09v
1998-07-29
P=0.55 Jy/bm σ=3.2 mJy/bm B=1.3x0.3, -15°
500
0
-500
0.0
0.2
0.4
0.6
0.8
1.0
1.2
1.4
200
400
600
4
2
-2
-4

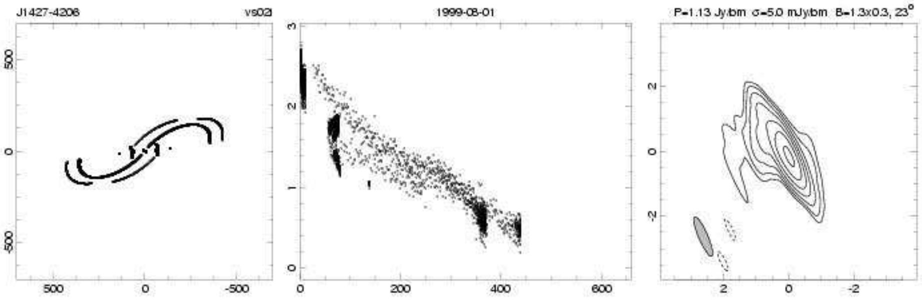
J1427-4206
vs02l
500
0
-500
500
0
-500
1999-08-01
3
2
1
0
0
200
400
600
P=1.13 Jy/bm σ=5.0 mJy/bm B=1.3x0.3, 23°
2
0
-2
2
0
-2

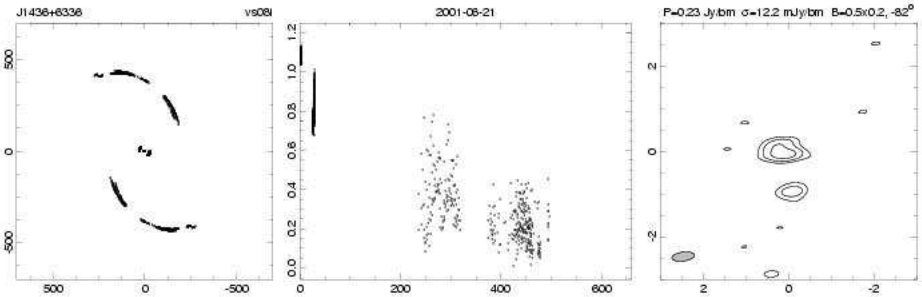
J1436+6336
vs08l
500
0
-500
500
0
-500
2001-08-21
1.2
1.0
0.8
0.6
0.4
0.2
0.0
0
200
400
600
P=0.23 Jy/bm σ=12.2 mJy/bm B=0.5x0.2, -82°
2
0
-2
2
0
-2

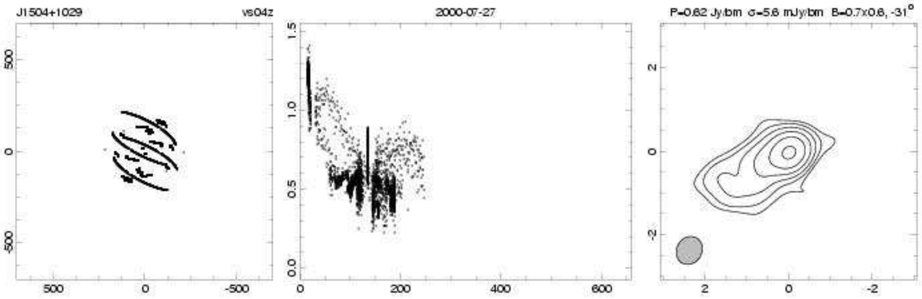
J1504+1029
vs04z
500
0
-500
500
0
-500
2000-07-27
1.5
1.0
0.5
0.0
0
200
400
600
P=0.82 Jy/bm σ=5.8 mJy/bm B=0.7x0.8, -31°
2
0
-2
2
0
-2

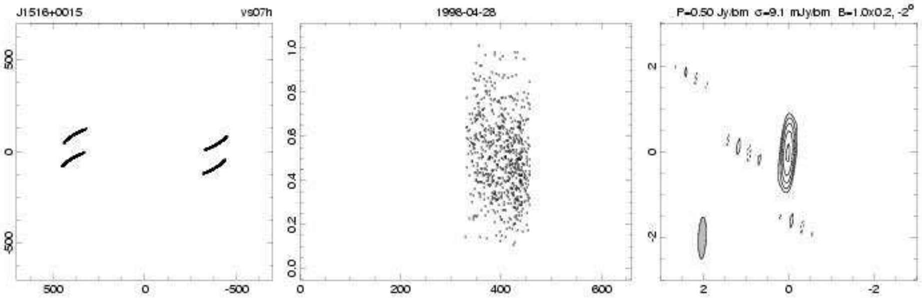
J1516+0015
vs07h
500
0
-500
500
0
-500
1998-04-28
1.0
0.8
0.6
0.4
0.2
0.0
0
200
400
600
P=0.50 Jy/bm σ=9.1 mJy/bm B=1.0x0.2, -2°
2
0
-2
2
0
-2

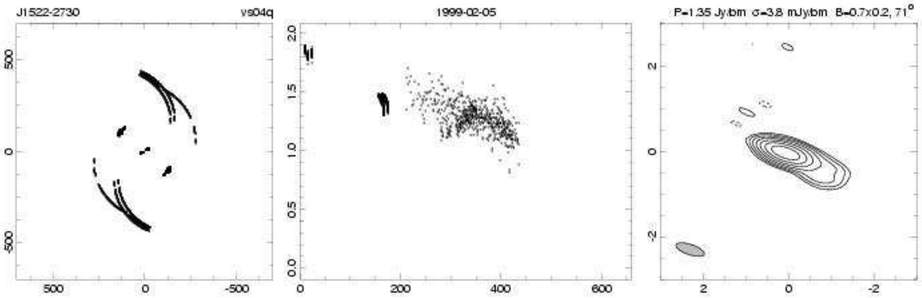
J1522-2730
vs04q
500
0
-500
500
0
-500
1999-02-05
2.0
1.5
1.0
0.5
0.0
0
200
400
600
P=1.35 Jy/bm σ=3.8 mJy/bm B=0.7x0.2, 71°
2
0
-2
2
0
-2

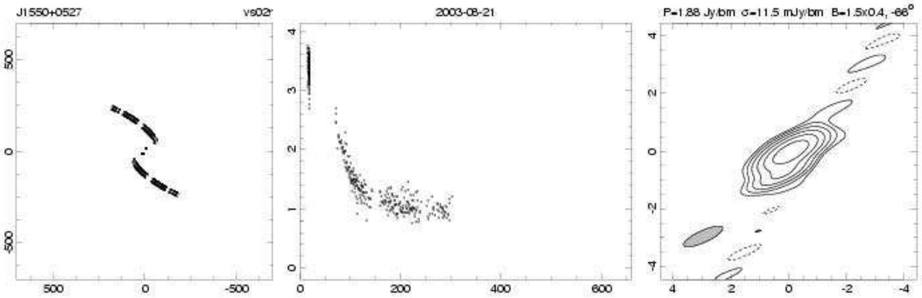
J1550+0527
vs02r
500
0
-500
500
0
-500
2003-08-21
0
1
2
3
4
0
200
400
600
P=1.88 Jy/bm σ=11.5 mJy/bm B=1.5x0.4, -66°
4
2
0
-2
-4
4
2
0
-2
-4

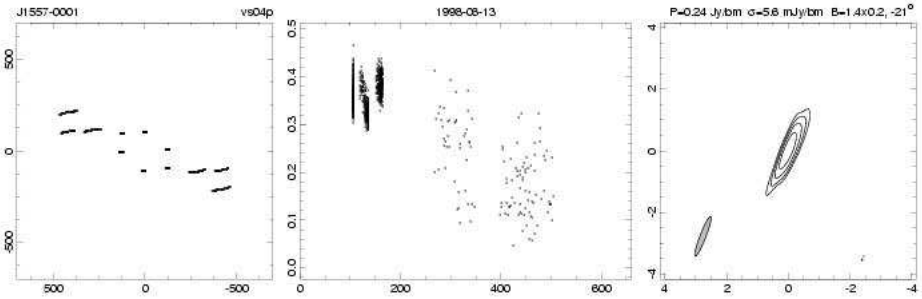
J1557-0001
vs04p
500
0
-500
500
0
-500
1998-08-13
0.0
0.1
0.2
0.3
0.4
0.5
0
200
400
600
P=0.24 Jy/bm σ=5.8 mJy/bm B=1.4x0.2, -21°
4
2
0
-2
-4
4
2
0
-2
-4

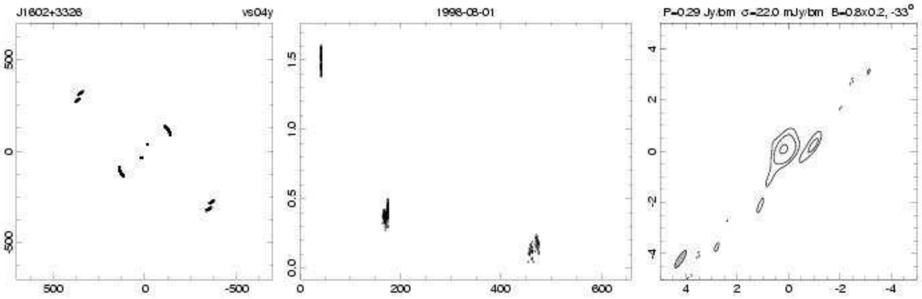
J1602+3326
vs04y
500
0
-500
500
0
-500
1998-08-01
0.0
0.5
1.0
1.5
0
200
400
600
P=0.29 Jy/bm σ=22.0 mJy/bm B=0.8x0.2, -33°
4
2
0
-2
-4
4
2
0
-2
-4

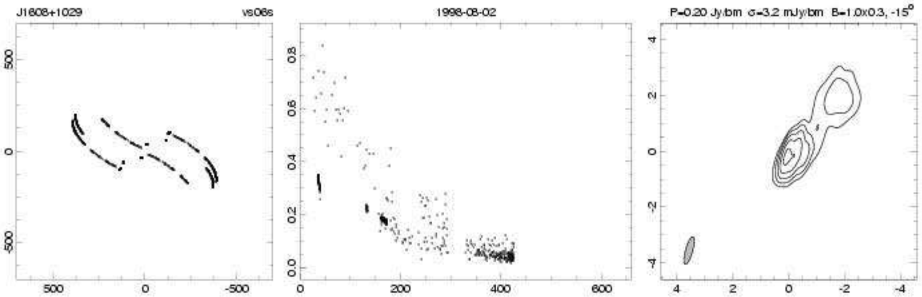
J1608+1029
vs06s
500
0
-500
500
0
-500
1998-08-02
0.0
0.2
0.4
0.6
0.8
0
200
400
600
P=0.20 Jy/bm σ=3.2 mJy/bm B=1.0x0.3, -15°
4
2
0
-2
-4
4
2
0
-2
-4

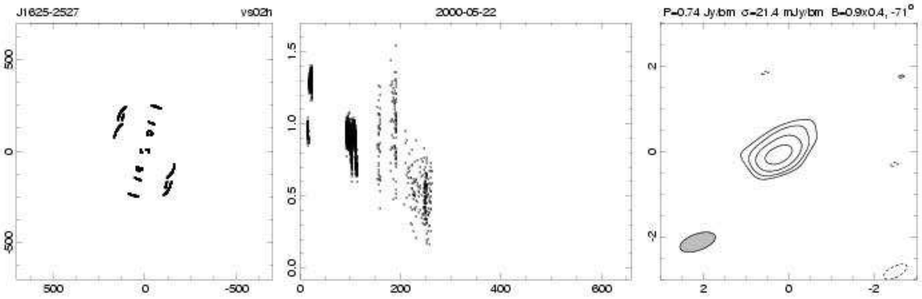
J1625-2527
vs02h
500
0
-500
500
0
-500
2000-05-22
0.0
0.5
1.0
1.5
0
200
400
600
P=0.74 Jy/bm σ=21.4 mJy/bm B=0.9x0.4, -71°
2
0
-2
2
0
-2

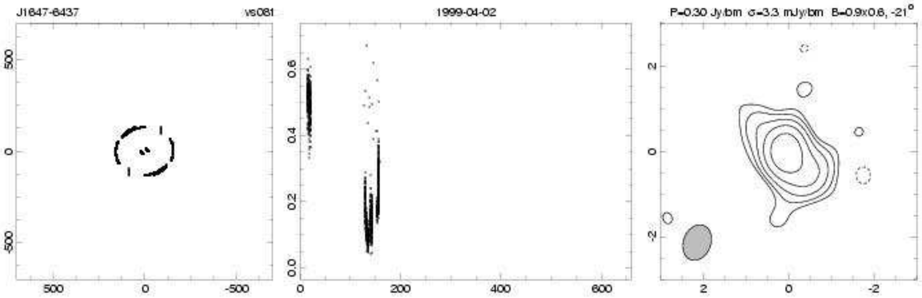
J1647-6437
vs081
1999-04-02
P=0.30 Jy/bm σ=3.3 mJy/bm B=0.9x0.6, -21°
500
0
-500
0.0
0.2
0.4
0.6
200
400
600
2
-2

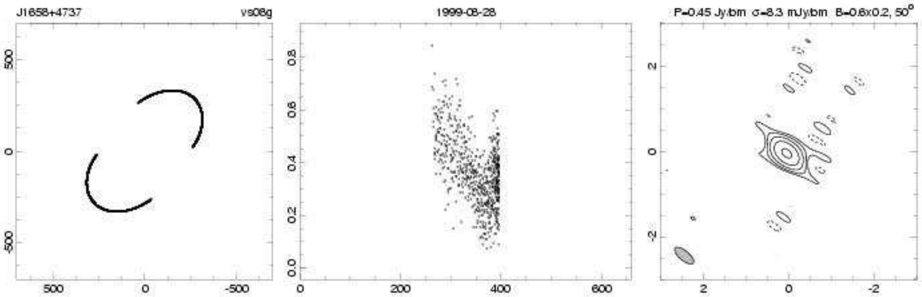
J1658+4737
vs08g
1999-08-28
P=0.45 Jy/bm σ=8.3 mJy/bm B=0.6x0.2, 50°
500
0
-500
0.0
0.2
0.4
0.6
0.8
200
400
600
2
-2

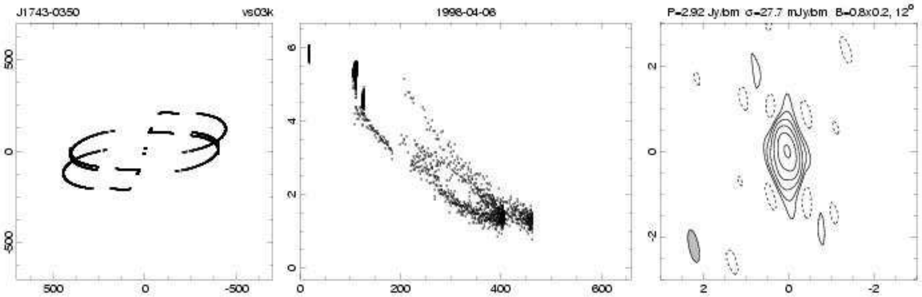
J1743-0350
vs03k
1998-04-06
P=2.92 Jy/bm σ=27.7 mJy/bm B=0.8x0.2, 12°
500
0
-500
2
4
6
200
400
600
-2

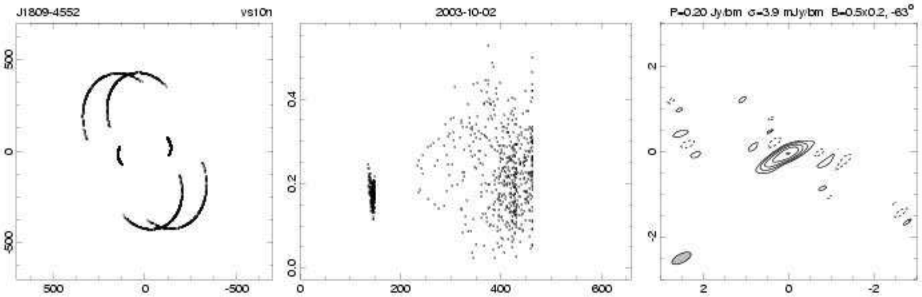
J1809-4552
vs10n
2003-10-02
P=0.20 Jy/bm σ=3.9 mJy/bm B=0.5x0.2, -63°
500
0
-500
0.0
0.2
0.4
200
400
600
2
-2

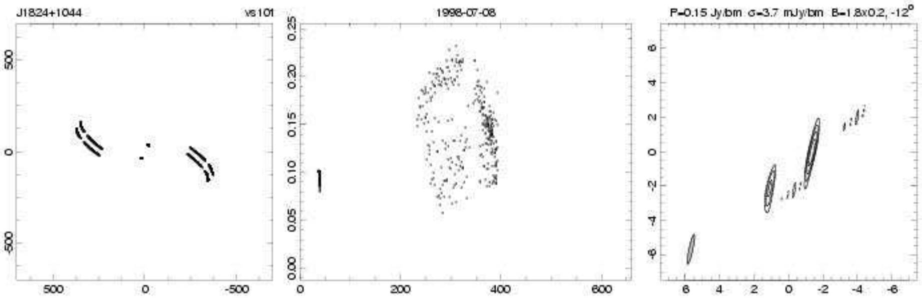
J1824+1044
vs101
1998-07-08
P=0.15 Jy/bm σ=3.7 mJy/bm B=1.8x0.2, -12°
500
0
-500
0.00
0.05
0.10
0.15
0.20
0.25
200
400
600
6
4
2
-2
-4
-6

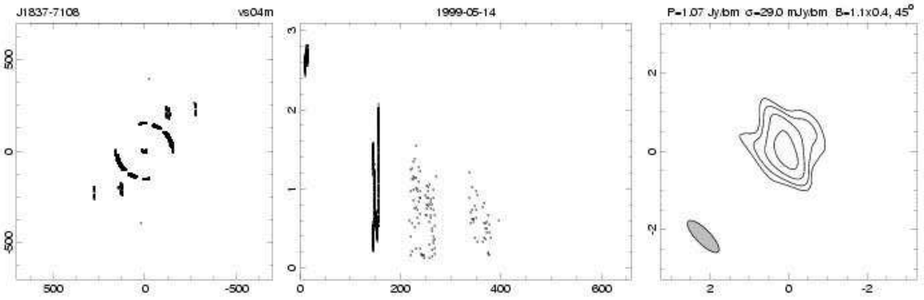
J1837-7108
vs04m
1999-05-14
P=1.07 Jy/bm σ=29.0 mJy/bm B=1.1x0.4, 45°
500
0
-500
500
0
-500
0
1
2
3
0
200
400
600
2
0
-2
2
0
-2

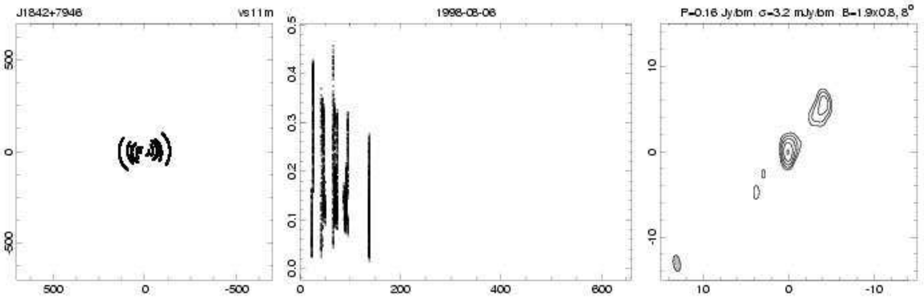
J1842+7946
vs11m
1998-08-06
P=0.16 Jy/bm σ=3.2 mJy/bm B=1.9x0.8, 8°
500
0
-500
500
0
-500
0.0
0.1
0.2
0.3
0.4
0.5
0
200
400
600
10
0
-10
10
0
-10

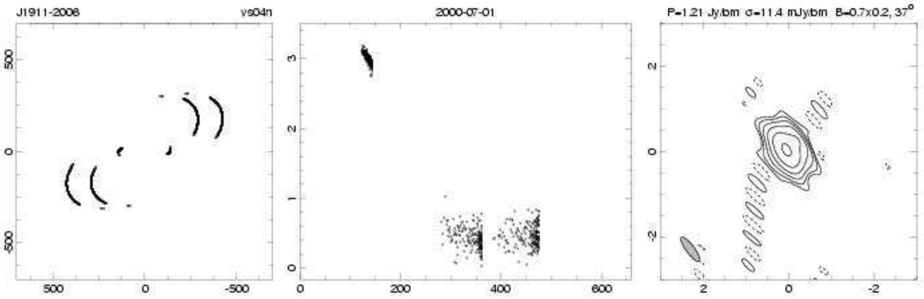
J1911-2006
vs04n
2000-07-01
P=1.21 Jy/bm σ=11.4 mJy/bm B=0.7x0.2, 37°
500
0
-500
500
0
-500
0
1
2
3
0
200
400
600
2
0
-2
2
0
-2

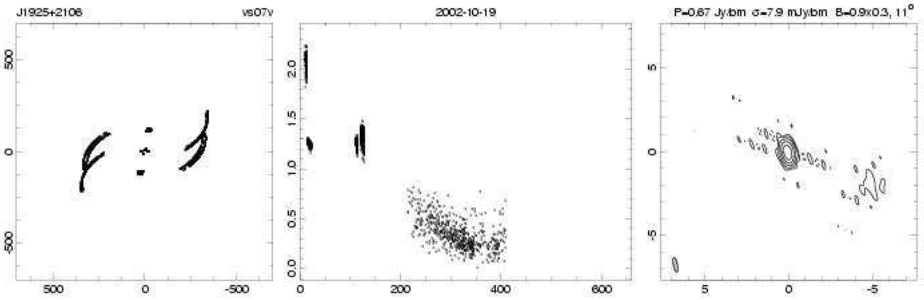
J1925+2106
vs07v
2002-10-19
P=0.67 Jy/bm σ=7.9 mJy/bm B=0.9x0.3, 11°
500
0
-500
500
0
-500
0.0
0.5
1.0
1.5
2.0
0
200
400
600
5
0
-5
5
0
-5

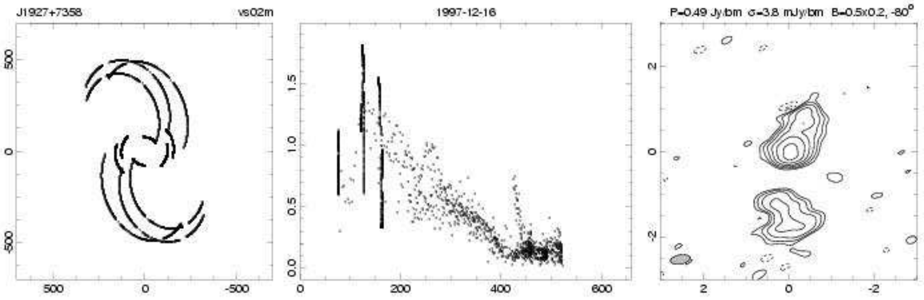
J1927+7358
vs02m
1997-12-16
P=0.49 Jy/bm σ=3.8 mJy/bm B=0.5x0.2, -80°
500
0
-500
500
0
-500
0.0
0.5
1.0
1.5
0
200
400
600
2
0
-2
2
0
-2

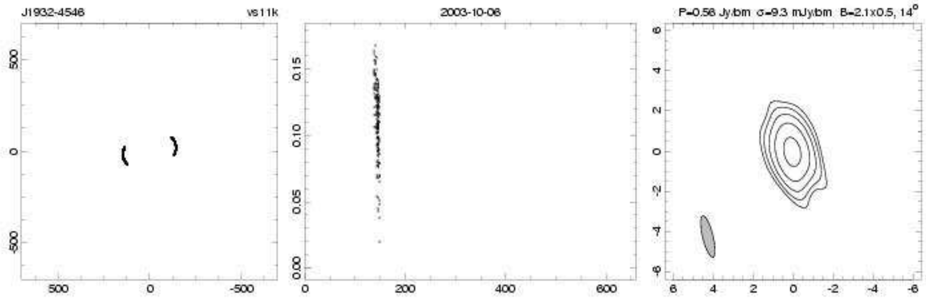
J1932-4546
vs11k
2003-10-06
P=0.56 Jy/bm σ=9.3 mJy/bm B=2.1x0.5, 14°
500
0
-500
0.15
0.10
0.05
0.00
0
200
400
600
6
4
2
0
-2
-4
-6

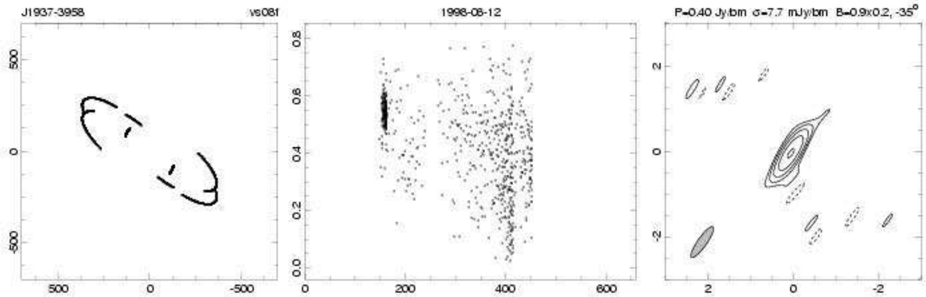
J1937-3958
vs08f
1998-08-12
P=0.40 Jy/bm σ=7.7 mJy/bm B=0.9x0.2, -35°
500
0
-500
0.8
0.6
0.4
0.2
0.0
0
200
400
600
2
0
-2

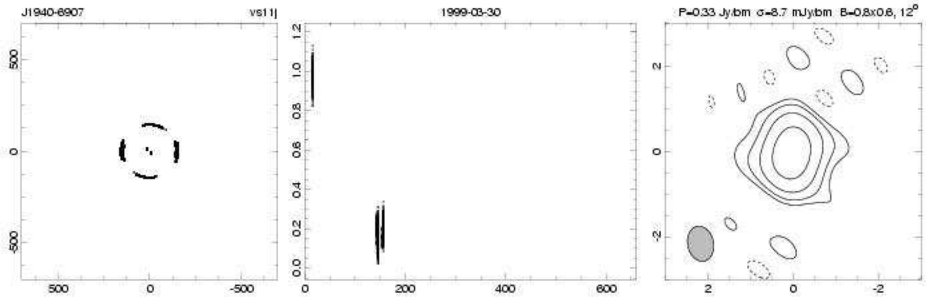
J1940-6907
vs11j
1999-03-30
P=0.33 Jy/bm σ=8.7 mJy/bm B=0.8x0.6, 12°
500
0
-500
1.2
1.0
0.8
0.6
0.4
0.2
0.0
0
200
400
600
2
0
-2

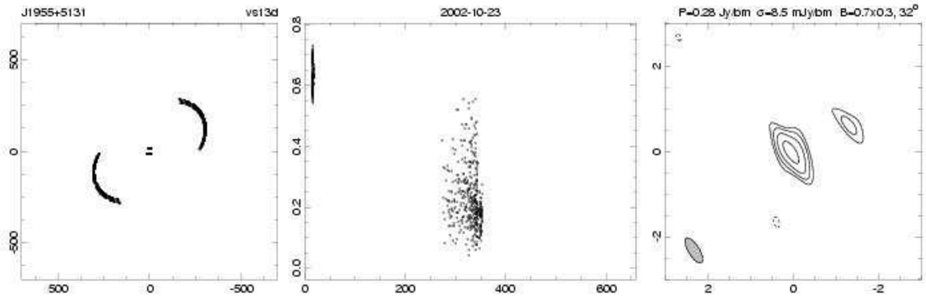
J1955+5131
vs13d
2002-10-23
P=0.28 Jy/bm σ=8.5 mJy/bm B=0.7x0.3, 32°
500
0
-500
0.8
0.6
0.4
0.2
0.0
0
200
400
600
2
0
-2

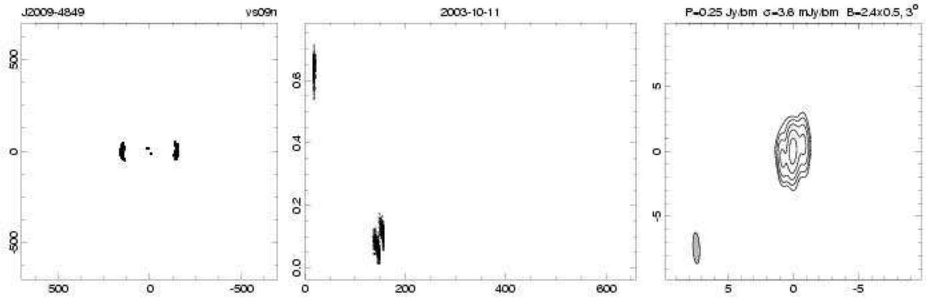
J2009-4849
vs09n
2003-10-11
P=0.25 Jy/bm σ=3.6 mJy/bm B=2.4x0.5, 3°
500
0
-500
0.6
0.4
0.2
0.0
0
200
400
600
5
0
-5

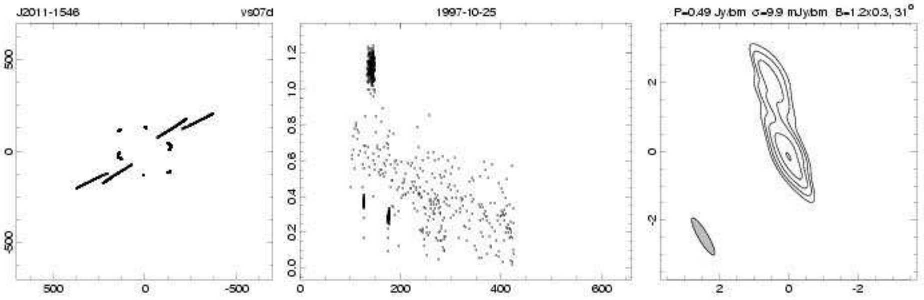
J2011-1546
vs07d
500
0
-500
500
0
-500
1997-10-25
0.0
0.2
0.4
0.6
0.8
1.0
1.2
0
200
400
600
P=0.49 Jy/bm σ=9.9 mJy/bm B=1.2x0.3, 31°
2
0
-2
2
0
-2

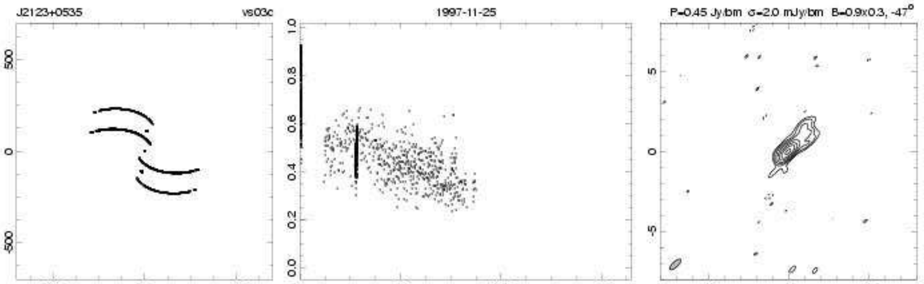
J2123+0535
vs03c
500
0
-500
500
0
-500
1997-11-25
0.0
0.2
0.4
0.6
0.8
1.0
0
200
400
600
P=0.45 Jy/bm σ=2.0 mJy/bm B=0.9x0.3, -47°
5
0
-5
5
0
-5

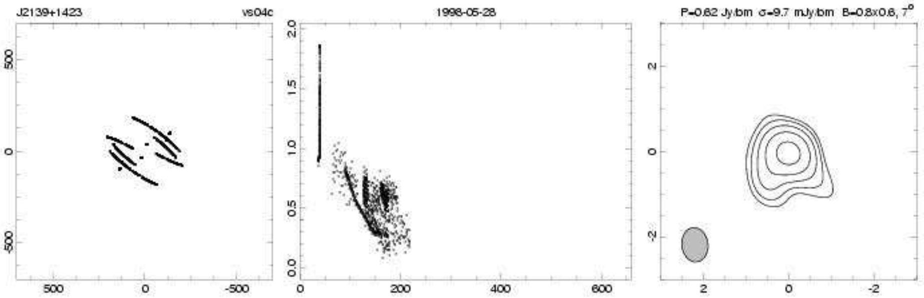
J2139+1423
vs04c
500
0
-500
500
0
-500
1998-05-28
0.0
0.5
1.0
1.5
2.0
0
200
400
600
P=0.62 Jy/bm σ=9.7 mJy/bm B=0.8x0.6, 7°
2
0
-2
2
0
-2

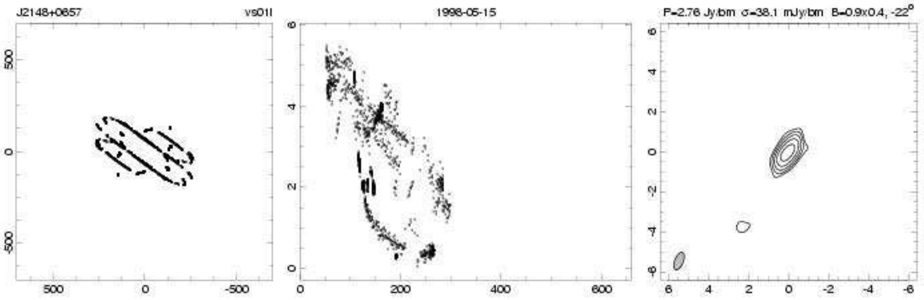
J2148+0657
vs01l
500
0
-500
500
0
-500
1998-05-15
0
2
4
6
0
200
400
600
P=2.76 Jy/bm σ=38.1 mJy/bm B=0.9x0.4, -22°
6
4
2
0
-2
-4
-6
6
4
2
0
-2
-4
-6

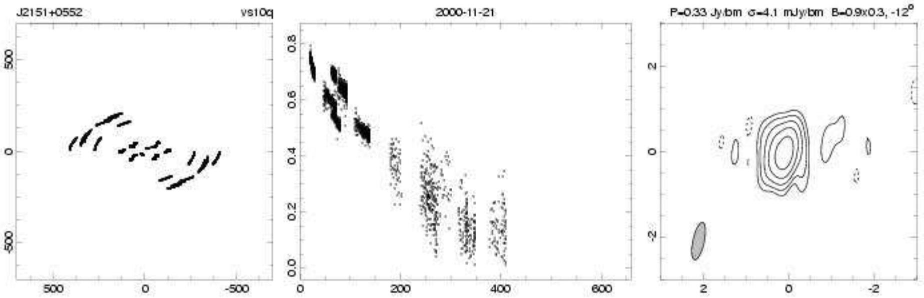
J2151+0552
vs10q
500
0
-500
500
0
-500
2000-11-21
0.0
0.2
0.4
0.6
0.8
0
200
400
600
P=0.33 Jy/bm σ=4.1 mJy/bm B=0.9x0.3, -12°
2
0
-2
2
0
-2

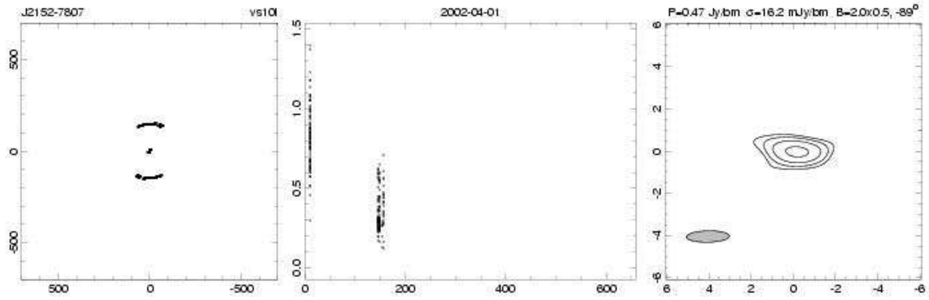
J2152-7807
vs10l
500
0
-500
2002-04-01
0.0
0.5
1.0
1.5
0
200
400
600
P=0.47 Jy/bm σ=16.2 mJy/bm B=2.0x0.5, -89°
6
4
2
0
-2
-4
-6

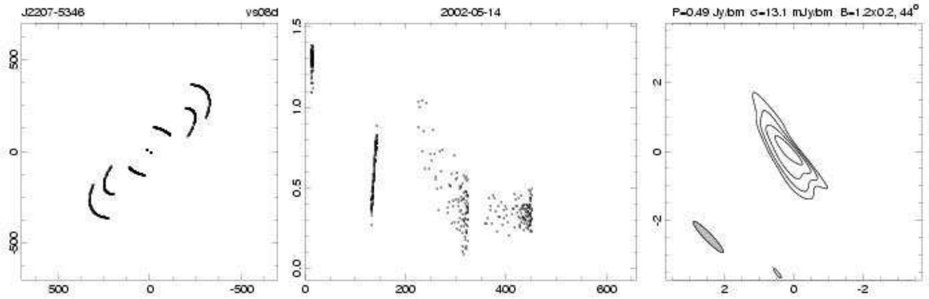
J2207-5346
vs08d
500
0
-500
2002-05-14
0.0
0.5
1.0
1.5
0
200
400
600
P=0.49 Jy/bm σ=13.1 mJy/bm B=1.2x0.2, 44°
2
0
-2

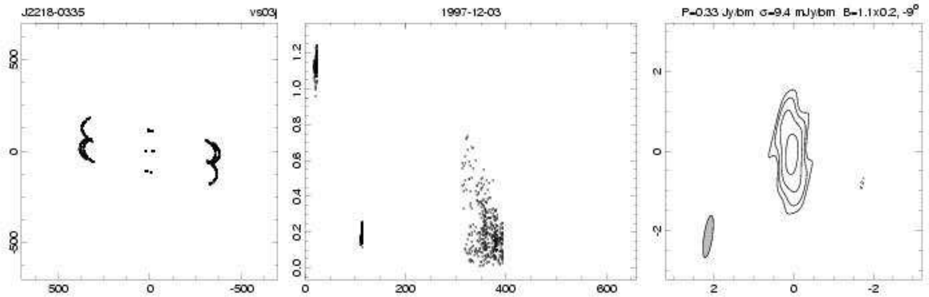
J2218-0335
vs03j
500
0
-500
1997-12-03
0.0
0.2
0.4
0.6
0.8
1.0
1.2
0
200
400
600
P=0.33 Jy/bm σ=9.4 mJy/bm B=1.1x0.2, -9°
2
0
-2

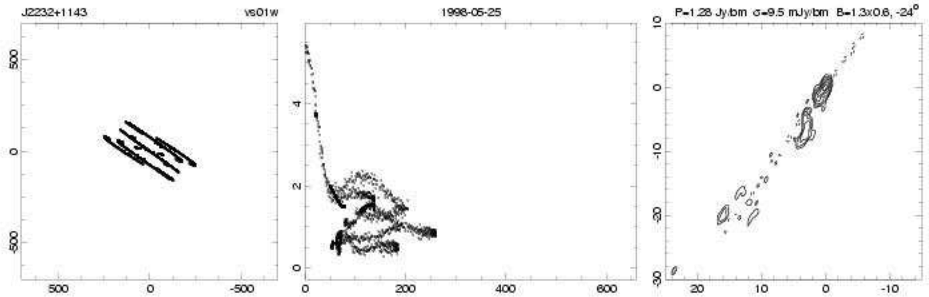
J2232+1143
vs01w
500
0
-500
1998-05-25
0
2
4
0
200
400
600
P=1.28 Jy/bm σ=9.5 mJy/bm B=1.3x0.6, -24°
10
0
-10
-20
-30
20
10
0
-10

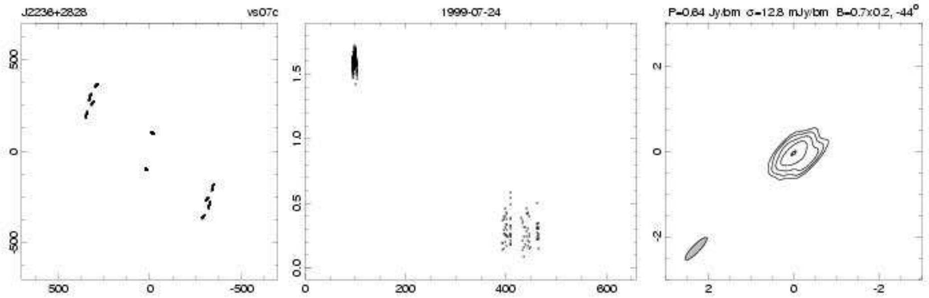
J2236+2828
vs07c
500
0
-500
1999-07-24
0.0
0.5
1.0
1.5
0
200
400
600
P=0.64 Jy/bm σ=12.8 mJy/bm B=0.7x0.2, -44°
2
0
-2

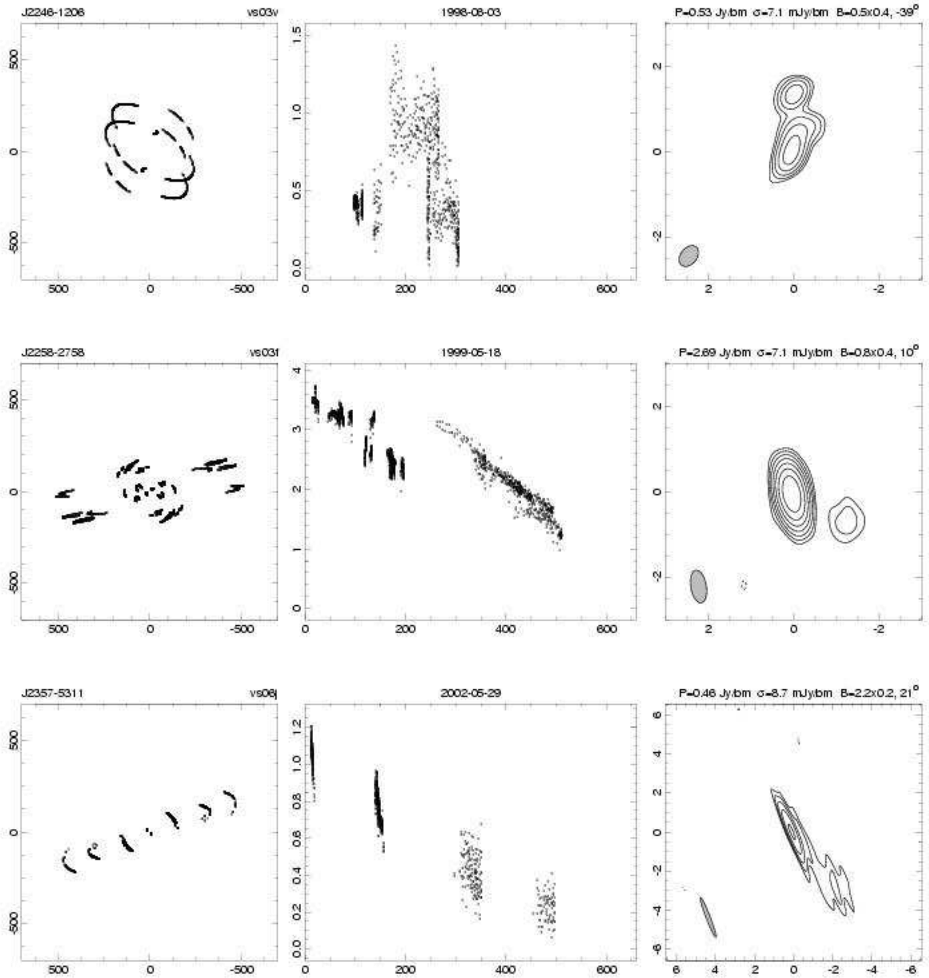

Fig. 1. – *continued*

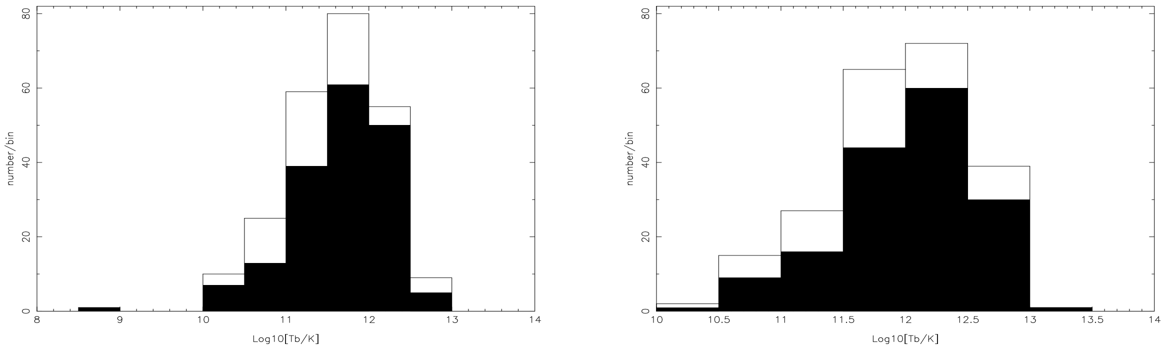

Fig. 2 – Histogram of core brightness temperatures. The left hand plot shows the core brightness temperature in the observer frame for the 239 Survey sources with identified cores binned with $\log_{10}(T_b)$ on the abscissa, and the number per bin as the ordinate. We show the measured T_b where the source was resolvable with an filled bar, otherwise the lower limit to the T_b with open bar. The right hand plot shows the T_b in the source frame for the subset of 222 sources which also have a measured redshift.